

DIRECT SYNTHESIS OF HYDROGEN STORAGE ALLOYS FROM THEIR  
OXIDES

A THESIS SUBMITTED TO  
THE GRADUATE SCHOOL OF NATURAL AND APPLIED SCIENCES  
OF  
MIDDLE EAST TECHNICAL UNIVERSITY

BY

SERDAR TAN

IN PARTIAL FULFILLMENT OF THE REQUIREMENTS  
FOR  
THE DEGREE OF DOCTOR OF PHILOSOPHY  
IN  
METALLURGICAL AND MATERIALS ENGINEERING

FEBRUARY 2011

Approval of the thesis;

**DIRECT SYNTHESIS OF HYDROGEN STORAGE ALLOYS FROM  
THEIR OXIDES**

Submitted by **SERDAR TAN** in partial fulfillment of the requirements for the  
degree of **Doctor of Philosophy in Metallurgical and Materials Engineering**  
**Department, Middle East Technical University** by,

Prof. Dr. Canan Özgen  
Dean, Graduate School of **Natural and Applied Sciences**

Prof. Dr. Tayfur Öztürk  
Head of Department, **Metallurgical and Materials Engineering Dept.**

Prof. Dr. Tayfur Öztürk  
Supervisor, **Metallurgical and Materials Engineering Dept., METU**

Prof. Dr. Kadri Aydınol  
Co-Supervisor, **Metallurgical and Materials Engineering Dept., METU**

**Examining Committee Members:**

Prof. Dr. İnci Eroğlu  
Chemical Engineering Dept., METU

Prof. Dr. Tayfur Öztürk  
Metallurgical and Materials Engineering Dept., METU

Prof. Dr. Dag Noréus  
Materials and Environmental Chemistry Dept., Stockholm Univ.

Prof. Dr. İshak Karakaya  
Metallurgical and Materials Engineering Dept., METU

Prof. Dr. Narin Ünal  
Mechanical Engineering Dept., Akdeniz Univ.

**Date :** 18.02.2011

**I hereby declare that all information in this document has been obtained and presented in accordance with academic rules and ethical conduct. I also declare that, as required by these rules and conduct, I have fully cited and referenced all material and results that are not original to this work.**

Name, Last Name : Serdar Tan

Signature :

## **ABSTRACT**

### **DIRECT SYNTHESIS OF HYDROGEN STORAGE ALLOYS FROM THEIR OXIDES**

Tan, Serdar

Ph.D., Department of Metallurgical and Materials Engineering

Supervisor: Prof. Dr. Tayfur Öztürk

Co-Supervisor: Prof. Dr. Kadri Aydınol

February 2011, 127 pages

The aim of this study is the synthesis of hydrogen storage compounds by electrodeoxidation technique which offers an inexpensive and rapid route to synthesize compounds from oxide mixtures. Within the scope of this study, two hydrogen storage compounds, FeTi and Mg<sub>2</sub>Ni, are aimed to be produced by this technique.

In the first part, effect of sintering conditions on synthesis of FeTi was studied. For this purpose, oxide pellets made out of Fe<sub>2</sub>O<sub>3</sub>-TiO<sub>2</sub> powders were sintered at temperatures between 900 °C – 1300 °C. Experiments showed that by sintering at 1100 °C, Fe<sub>2</sub>TiO<sub>5</sub> forms and particle size remains comparatively small, which improve the reducibility of the oxide pellet.

Experimental studies showed that the reduction of MgO rich MgO-NiO oxide pellet to synthesize Mg<sub>2</sub>Ni occurs only at extreme deoxidation conditions. Pure MgO remains intact after deoxidation. In contrast to these, pure NiO and NiO

rich MgO-NiO mixtures were deoxidized successfully to Ni and MgNi<sub>2</sub>, respectively. Conductivity measurements address the low conductivity of MgO-rich systems as one of the reasons behind those difficulties in reduction.

In the last part, a study was carried out to elucidate the low reducibility of oxides. It is considered that the oxygen permeability becomes important when the reduction-induced volumetric change does not yield fragmentation into solid-state. The approach successfully explains why MgO particles could not be reduced at ordinary deoxidation conditions. The study addresses that Mg layer formed at the surface of MgO particles blocks the oxygen transport between MgO and electrolyte as Mg has low oxygen permeability.

Keywords: Electrodeoxidation, hydrogen storage, metal oxides, Mg<sub>2</sub>Ni, FeTi.

## ÖZ

### **HİDROJEN DEPOLAMA ALAŞIMLARININ OKSİTLERİNDEN DOĞRUDAN SENTEZİ**

Tan, Serdar

Doktora, Metalurji ve Malzeme Mühendisliği Bölümü

Tez Yöneticisi: Prof. Dr. Tayfur Öztürk

Ortak Tez Yöneticisi: Prof. Dr. Kadri Aydınol

Şubat 2011, 127 sayfa

Bu çalışmanın amacı elektrodoksidasyon yöntemi ile hidrojen depolama alaşımlarının üretilmesidir. Günümüzde hidrojen depolama alaşımlarının üretilmesi ergitme ve mekanik alaşımlandırma gibi tekniklerle gerçekleştirilse de bu yöntemler kontrolü zor ve/veya yüksek maliyetli süreçleri içermektedir. Elektrodoksidasyon, oksitleri veya oksit karışımlarını kullanarak metal veya metal alaşımların üretilmesini mümkün kılan bir tekniktir. Çalışma, FeTi ve  $Mg_2Ni$  hidrojen depolama alaşımlarının elektrodoksidasyon ile üretilmesini konu almaktadır.

FeTi üretimi için,  $Fe_2O_3$ - $TiO_2$  oksit peletleri, 900 °C ile 1300°C arasında sinterlenmiş ve sinterleme sıcaklığının indirgenme ve alaşım eldesine etkisi incelenmiştir. Deneyler sonucunda, 1100 °C de yapılan sinterlemenin oksit peletinde FeTi eldesi için uygun kimyasal ve fiziksel koşulları ( $Fe_2TiO_5$  oluşumu, tane boyutunun artmaması gibi) oluşturduğu sonucuna varılmıştır.

Çalışmanın ikinci kısmında,  $Mg_2Ni$  eldesi hedeflenmiştir. Yapılan deneyler  $Mg_2Ni$ 'nin elektrodoksidasyon ile üretiminin oldukça zor olduğunu göstermektedir. Mg-Ni sisteminde olan diğer fazların elde edilmesi için farklı MgO-NiO oranlarında hazırlanmış oksit peletleri de indirgemiş, Ni ve  $MgNi_2$  başarıyla elde edilmistir. Bununla birlikte MgO indirgenmesi ise gerçekleşmemiştir. Yapılan deneylerde MgO miktarının artması ile indirgenme işleminin zorlaştığı gözlemlenmektedir. İletkenlik çalışmaları, MgO'nun düşük iletkenliğinin bu sonuca yol açabileceğine işaret etmektedir.

Çalışmanın son kısmında, elektrodoksidasyon işlemi esnasında katı fazda gerçekleşen hacim değişiminin indirgenme işlemine etkisi incelenmiştir. Geliştirilen bu model ile hacim değişiminin katı halde yarattığı fiziksel değişimlerin (gözenek oluşması, oksit tanelerinin kırılması gibi) indirgenme işleminin gerçekleşmesi için gerekli olduğu gösterilmiştir. Bu yaklaşım kullanılarak yapılan incelemede, MgO indirgenmesi esnasında yüzeyde oluşan Mg tabakasının belirtilen fiziksel değişimleri tolare edebildiği ve Mg tabakasının MgO ile elektrolit arasında oksijen iletimini engelleyebileceği öngörülmektedir.

Anahtar Kelimeler: Elektrodoksidasyon, hidrojen depolama, metal oksitler,  $Mg_2Ni$ , FeTi.

*To the ladies who changed my life: Necla, Jane and Semra*



## ACKNOWLEDGEMENTS

I would like to express my deepest gratitude to my supervisor Prof. Dr. Tayfur Öztürk for his support, encouragement and guidance throughout the study. I am grateful to my co-supervisor, Prof. Dr. Kadri Aydınol for his detailed and constructive comments, and for his important support throughout this work.

I wish to express my sincere thanks to Prof.Dr.Ishak Karakaya for his valuable contributions to the progress of this study. I owe my most sincere gratitude to Prof. Dr. Muharrem Timuçin for his comments and constructive contributions. I would like to appreciate Prof. Dr. Narin Ünal for her understanding and support during my thesis.

I would like to thank to Volkan Kalem for helping me in conductivity measurements. Help of my labmates, Taylan Örs, Eren Şimsek, Hasan Akyıldız, Gülhan Çakmak, Mustafa Yılmaz and Rabia Ölmez Günay are gratefully acknowledged.

I am truly indebted to my parents and my love Semra for their endless support, understanding and belief in me.

## TABLE OF CONTENTS

|  |      |
|--|------|
| ABSTRACT.....  | iv   |
| ÖZ.....  | vi   |
| ACKNOWLEDGEMENTS.....  | ix   |
| TABLE OF CONTENTS.....   | x    |
| LIST OF TABLES.....  | xiii |
| LIST OF FIGURES.....   | xiv  |
| CHAPTER  |      |
| 1. INTRODUCTION.....   | 1    |
| 2. LITERATURE REVIEW.....  | 6    |
| 2.1 Introduction .....   | 6    |
| 2.2 Processing Steps in Electro-reduction.....   | 9    |
| 2.2.1 Preparation of Oxide Pellets.....  | 11   |
| 2.2.2 Selection and Preparation of Electrolyte.....  | 14   |
| 2.2.3 Other Cell Components: Anodes, Crucibles, Reference<br>Electrodes and Auxiliary Parts..... | 16   |
| 2.2.4 Electro-reduction of Oxides and Collection of<br>Product.....                              | 17   |
| 2.3 Electrochemical Reactions in Solid-State Electro-reduction.....                              | 21   |
| 2.3.1 Cathodic Reactions.....  | 21   |
| 2.3.2 Anodic Reactions.....  | 27   |
| 2.3.3 Overall Cell Reactions.....  | 28   |
| 2.4 Three Phase Interline (3PI) Model.....   | 30   |
| 2.5 Factors Affecting the Electro-reduction Process.....   | 35   |
| 2.5.1 Mass Transport of Oxygen in Bulk Oxide.....  | 37   |
| 2.5.2 Oxygen Ionization, Charge Transfer and Structural Changes..                                | 37   |

|   |     |
|---|-----|
| 2.5.3 Pore Diffusion.....   | 41  |
| 2.6 Diffusion of Oxygen in Solid-State and Electronic Conductivity<br>of Oxides.....  | 42  |
| 2.7 Summary.....  | 48  |
| 3. SYNTHESIS OF FeTi FROM MIXED OXIDE PRECURSORS .....  | 50  |
| 3.1 Introduction.....   | 50  |
| 3.2 Materials and Methods.....  | 51  |
| 3.3 Results and Discussion.....   | 53  |
| 3.4 Conclusion.....   | 61  |
| 4. SYNTHESIS OF Mg-Ni COMPOUNDS FROM THEIR OXIDES.....  | 63  |
| 4.1 Introduction.....   | 63  |
| 4.2 Materials and Methods.....  | 65  |
| 4.3 Results and Discussion.....   | 67  |
| 4.4 Conclusion.....   | 79  |
| 5. A COMPERATIVE STUDY FOR ELECTRODEOXIDATION OF NiO,<br>MgO, Fe <sub>2</sub> O <sub>3</sub> AND TiO <sub>2</sub> BASED ON OXYGEN PERMEABILITY..... | 80  |
| 5.1 Introduction.....   | 80  |
| 5.2 Reduction Routes in Electro-deoxidation .....   | 82  |
| 5.3 Oxygen Permeability in Electro-deoxidation Process.....   | 84  |
| 5.4 Examination of Different Oxide Systems .....  | 88  |
| 5.4.1 Deoxidation of NiO.....   | 88  |
| 5.4.2 Deoxidation of MgO.....   | 92  |
| 5.4.3 Deoxidation of Fe <sub>2</sub> O <sub>3</sub> .....   | 95  |
| 5.4.4 Deoxidation of TiO <sub>2</sub> .....   | 100 |
| 5.5 Conclusion.....   | 106 |
| 6. CONCLUSION.....  | 107 |
| REFERENCES.....   | 109 |

## APPENDICES

|                                  |     |
|----------------------------------|-----|
| A. ELECTRODEOXIDTION SET-UP..... | 121 |
| B. PHASE DIAGRAMS.....           | 122 |
| CURRICULUM VITAE.....            | 126 |

## LIST OF TABLES

### TABLES

|           |   |     |
|-----------|---|-----|
| Table 2.1 | Some metals and compounds synthesized by electro-reduction processes and their synthesis conditions.....  | 18  |
| Table 2.2 | Calculated standard oxygen ionization potentials of various oxides in fused calcium chloride melt at 700 °C ( $E_{\text{Na}^+/\text{Na}} = 0$ ) (Chen and Fray, 2001).....  | 22  |
| Table 4.1 | Standard reduction potentials of MgO, NiO and CaO and decomposition potentials of $\text{CaCl}_2$ and NaCl calculated at temperatures of 900°C, 725°C and 600°C. The data in parenthesis refers the potential when the metal is in liquid state. Reduction reactions yielding intermetallics are also shown. ....                   | 69  |
| Table 5.1 | Normalized molar volumes of NiO and Ni at 900 °C. The percent change in volume, when all oxygen is removed, is given in the last column.....  | 89  |
| Table 5.2 | Normalized molar volumes of MgO and Mg calculated from molecular weight and density of materials. Molar volume of Mg is calculated for 600 °C. The percent change in volume, when all oxygen is removed, is given in the last column.....   | 93  |
| Table 5.3 | Normalized molar volumes of $\text{Fe}_2\text{O}_3$ , FeO and Fe. The percent change in volume, when all oxygen is removed, is given in the last column.....  | 97  |
| Table 5.4 | Volume change in solid state for stepwise reduction of $\text{Fe}_2\text{O}_3$ . Note that the value is calculated for 1 mole of reactant.....  | 97  |
| Table 5.5 | Normalized molar volumes of materials observed in deoxidation of $\text{TiO}_2$ . The percent change in volume, when all oxygen is removed, is given in the last column. The molecular weight and density of Ti(O) were calculated by assuming the material has 30at% oxygen. Density of Ti(O) and Ti was calculated for 900°C..... | 102 |
| Table 5.6 | Volume change in solid state for stepwise reduction of $\text{TiO}_2$ . Note that the value is calculated for 1 mole of solid reactant.....   | 102 |

## LIST OF FIGURES

### FIGURES

|            |   |    |
|------------|---|----|
| Figure 1.1 | Flowchart for synthesis of hydrogen storage compounds by three different techniques: electro-reduction, mechanical alloying and melting.....  | 4  |
| Figure 2.1 | A schematic drawing of solid-state electro-reduction processes showing flow of oxygen ions and electrons.....   | 7  |
| Figure 2.2 | Schematic drawings of different electro-reduction processes: (a) FFC Process; (b) OS Process and (c) EMR Process (Abiko et al., 2003).....  | 8  |
| Figure 2.3 | The flowchart of electro-reduction processes.....   | 10 |
| Figure 2.4 | Different types of electrochemical cells used in the electro-reduction processes (Chen et al., 2004).....   | 21 |
| Figure 2.5 | Standard reduction voltage ( $\Delta E^0$ ) of selected oxides: (a) by formation of $O_2$ ; (b) by formation of $CO_2$ . Standard decomposition voltages ( $\Delta E^0$ ) of the selected molten salts are also given in the graphs. ....   | 29 |
| Figure 2.6 | The physical description of 3PI model. The reduction starts from metal-oxide-electrolyte intersection point (a) and propagates through interline where three phases meet (b) and (c). The gray field represents the newly formed metal..... | 32 |
| Figure 2.7 | The propagation of electro-reduction process according to 3PI model (Wang et al., 2008).....  | 32 |
| Figure 2.8 | Deoxidation of a metal oxide pellet. The oxide pellet gradually deoxidizes through (a) to (f). Note that deoxidation proceeds from outside to inside of the pellet (Yan and Fray, 2005).....  | 35 |

|            |  |    |
|------------|--|----|
| Figure 2.9 | Point defects observed in metal oxides in reducing conditions. Black spheres represent metal atoms and gray spheres represent oxygen atoms. (a) reduced cation at interstitial site, (b) reduced cation at cation site, (c) electrons are completely mobile, (d) one electron is trapped at oxygen vacancy and (e) two electrons are trapped in oxygen vacancy.....  | 45 |
| Figure 3.1 | SEM images of oxide powders; (a) $\text{Fe}_2\text{O}_3$ and (b) $\text{TiO}_2$ used in the experiments. Note that $\text{Fe}_2\text{O}_3$ powders are needle-like whereas $\text{TiO}_2$ is in the form of rounded particles.....   | 52 |
| Figure 3.2 | Micrographs of the oxide pellets sintered for 2 hours at (a) 900 °C and (b) 1300 °C. The graphs refer to broken pellets as viewed through the thickness section. (c) is the same as (b) but the section is polished and viewed in back-scattered mode to reveal the two-phase structure. ....  | 54 |
| Figure 3.3 | X-ray diffractograms of the oxide pellets $\text{Fe}_2\text{O}_3$ and $\text{TiO}_2$ mixed in molar proportions of 1: 2 and sintered at (a) 900 °C, (b) 1100 °C. Note the presence of $\text{Fe}_2\text{TiO}_5$ along with $\text{Fe}_2\text{O}_3$ and $\text{TiO}_2$ at 900 °C. Also note that at 1100 °C the sintered pellet has a two-phase structure; $\text{Fe}_2\text{TiO}_5$ and $\text{TiO}_2$ ..... | 55 |
| Figure 3.4 | X-ray diffractograms of the pellets deoxidized at 900 °C for 24 hours at 3.2 V. The diffractograms refer to pellets sintered at (a) 900 °C, and (b) at 1100 °C.....  | 55 |
| Figure 3.5 | SEM image of metallic agglomerate, FeTi, obtained from deoxidation of mixed oxide pellet sintered at 1300 °C.....  | 57 |
| Figure 3.6 | Current-time data collected during deoxidation of the oxide pellet sintered at 1300 °C.....  | 57 |
| Figure 3.7 | X-ray diffractograms of the oxide pellets sintered at 1300 °C and deoxidized in $\text{CaCl}_2$ at 900 °C (3.2V). The diffractograms refer to pellets; (a) in the sintered condition, (b) sintered and immersed into the salt bath for 30 minutes, (c), (d) and (e) refer to sintered pellets electrolyzed for 30 minutes, 6 hours and 24 hours, respectively.....   | 58 |
| Figure 4.1 | SEM images of oxide powders; (a) NiO and (b) MgO used in the experiments. ....   | 66 |

|            |   |    |
|------------|---|----|
| Figure 4.2 | MgO:NiO=1:2 pellet sintered at 1200 °C for 6 hours; (a) X-ray diffractogram, (b) SEM image recorded in back scattered electron mode indicating a two-phase structure; NiO (bright phase) and MgO (gray phase). Black regions are pores..... | 68 |
| Figure 4.3 | Current–time data collected during electrodeoxidation of NiO at 900 °C with 3.2 V. ....   | 71 |
| Figure 4.4 | NiO pellet; X-ray diffractogram of the sample (a) before and (b) after electrodeoxidation, at 900 °C for 24 hours (3.2V). (c) refers to SEM image of the reduced sample. ....   | 71 |
| Figure 4.5 | MgO:NiO=1:2 pellet; (a) X-ray diffractogram and (b) SEM image of powders after electrodeoxidation for 24 h at 900 °C with 3.2 V.....  | 72 |
| Figure 4.6 | MgO:NiO=2:1 pellet; (a) X-Ray diffractogram and (b) SEM image of powders obtained after electrodeoxidation for 24 hours at 725 °C with 3.2 V.....   | 73 |
| Figure 4.7 | Current–time data collected during electrodeoxidation of MgO:NiO=2:1 affected with 5 V at 600 °C.....   | 74 |
| Figure 4.8 | (a) Electrical conductivities of MgO, MgO:NiO = 2:1, MgO:NiO = 1:2 and NiO at room temperature, and (b) conductivity values as a function of temperature up to 600 °C for MgO and MgO:NiO = 2:1. ....                                       | 77 |
| Figure 5.1 | Different deoxidation routes in electrodeoxidation process.....   | 83 |
| Figure 5.2 | The schematic illustration of a metal oxide, $M_xO_y$ particle during deoxidation. Different layers may form during the process.....  | 87 |
| Figure 5.3 | Different cases in deoxidation of oxides: (a) layers are fragmented; (b) no fragmentation in layers .....   | 87 |
| Figure 5.4 | The progress of deoxidation in NiO. Note that reacted layer does not form during process and the metallic Ni are non-blocking.....  | 90 |
| Figure 5.5 | Motion of oxygen ions and oxygen vacancies in deoxidation of NiO. Gray spheres represent oxygen ions and black ones represent Ni atoms.....   | 91 |



|             |   |     |
|-------------|---|-----|
| Figure 5.6  | Deoxidation of MgO. Note that Mg forms a blocking-layer between MgO and electrolyte .....   | 95  |
| Figure 5.7  | The schematic representation for deoxidation of $\text{Fe}_2\text{O}_3$ particle.....   | 98  |
| Figure 5.8  | The progress of deoxidation in $\text{Fe}_2\text{O}_3$ . Note that FeO and Fe are non-blocking.....   | 99  |
| Figure 5.9  | The schematic view to $\text{TiO}_2$ particle during deoxidation. The reacted layer is made out of $\text{CaTiO}_3$ (black nodules) and different sub-oxides of $\text{TiO}_2$ (white nodules). Metallic layer is Ti(O), where metal with less oxygen is shown by lighter color.. | 103 |
| Figure 5.10 | The progress of deoxidation in $\text{TiO}_2$ . Note that multi-phase reacted layer and metallic Ti are non-blocking.....   | 105 |

# CHAPTER 1

## INTRODUCTION

Hydrogen-based technologies have been extensively studied since the carbon based fuels started to form environmental problems in 1970s. The idea behind these technologies base on the use of hydrogen as energy carrier such that hydrogen and oxygen ions are reacted in a fuel cell producing electricity. As hydrogen should be fed to such a system continuously, storing the largest possible amount of hydrogen in the safest way is one of the main challenges in the development of hydrogen-based technologies.

It is known that some metals, e.g. Mg, Ti, La, and their metallic compounds, e.g. FeTi, Mg<sub>2</sub>Ni, LaNi<sub>5</sub>, could react with hydrogen gas and form metal hydrides (Chen and Zhu, 2008). The reversibility of the reaction allows storing extensive amount of hydrogen in the metal and extracting it from the solid metal hydride when necessary. Although the storage capacity of compounds is lower than pure metals, they are considered as better hydrogen storage materials, as they satisfy thermodynamic and kinetic requirements to a higher extent.

With its relatively high capacity (3.6 wt %), Mg<sub>2</sub>Ni is a promising material to store hydrogen, especially for portable applications (Sakintuna et al., 2007). Higher durability in air and higher absorption/desorption rates compared to pure Mg are important advantages of this material. FeTi is another well-known hydrogen storage compound with storage capacity of 1.8 wt % (Yasuda et al. 2009). Although it has some activation problems, the advantage of room temperature hydrogen storage makes it a superior material for stationary hydrogen storage applications.

Extensive usage and commercialization of hydrogen storage compounds depend on their performance, ease of production and the cost. Currently, melting, mechanical alloying, combustion synthesis and reactive milling are popular techniques to synthesize these storage compounds (Zhao and Ma, 2009). In addition, new methods, such as microwave processing, thin film techniques and wet chemistry methods are also investigated by different research groups.

Melting technique is one of the most popular methods in the production of hydrogen storage materials containing transition metals and rare earths. Starting from pure metals, complex compounds could be directly obtained by melting and casting. While it is a simple and well-known method, casted materials are chemically non-homogenous. Thus, after solidification, homogenization and even re-melting processes might be necessary.

For alkaline and alkaline earth metals as well as their alloys, melting techniques are more difficult due to high vapor pressure of these metals, causing loss of material from the molten batch. Due to deviations from the compositions, melting techniques are not preferred to synthesize hydrogen storage compounds based on IA and IIA metals.

Mechanical alloying is a versatile technique to synthesize hydrogen storage materials including compounds containing Mg, Ca, Li etc. (Varin and Czujko, 2002). In this technique, powders of elements are milled by a high-energy ball mill for long durations and a heat treatment step might follow this milling operation. The most significant advantage of this technique is its ability to produce non-equilibrium materials and materials with low crystallinity. However, mechanical alloying, as a process, has very low efficiency. The processing durations could vary from a few hours to a few days and the final product commonly is not in large quantities. There are many variables in the process; duration, ball-to-powder ratio, speed of milling, temperature of milling medium etc. As a result, the reproducibility of mechanical alloying is not very

high. Contamination from balls and container during the milling operation might also create difficulty. Reactive milling is a special type of processing where milling is performed in hydrogen atmosphere. The problems observed in mechanical alloying are also valid in this technique, though reactive milling is a more efficient process in terms of size reduction (Bérube et al., 2007).

For combustion synthesis, elemental powders are mixed together and then pelletized. The ignition agent, placed around the pellet, produces an exothermic reaction when the system is heated up. Sudden increase in the temperature causes reaction of elemental powders in the pellet and the required compound forms in a very short time (Chen et al., 2006). The sudden increase of the temperature makes the process difficult to control. Short processing durations frequently yield a product with extensive compositional variations. The unreacted species may left in the product.

To synthesize hydrogen storage alloys, new techniques have been developed including microwave processing (Li et al., 2010), thin film techniques (Akyıldız and Öztürk, 2010) and wet chemistry methods (Ikeda and Ohmori, 2009). While these techniques are successful to get the required composition, the scale and method of synthesis are far away to adapt those processes for up-scaled production.

In the last decade, different solid-state electro-reduction techniques emerged to obtain metal powders from their oxide, such as Ti from  $\text{TiO}_2$ , Cr from  $\text{Cr}_2\text{O}_3$  and Si from  $\text{SiO}_2$ . They are high temperature electrochemical methods where cathode is the oxide pellet to be reduced, anode is either graphite or an inert material and electrolyte is a molten salt that is able to dissolve some oxygen (Mohandas and Fray, 2004).

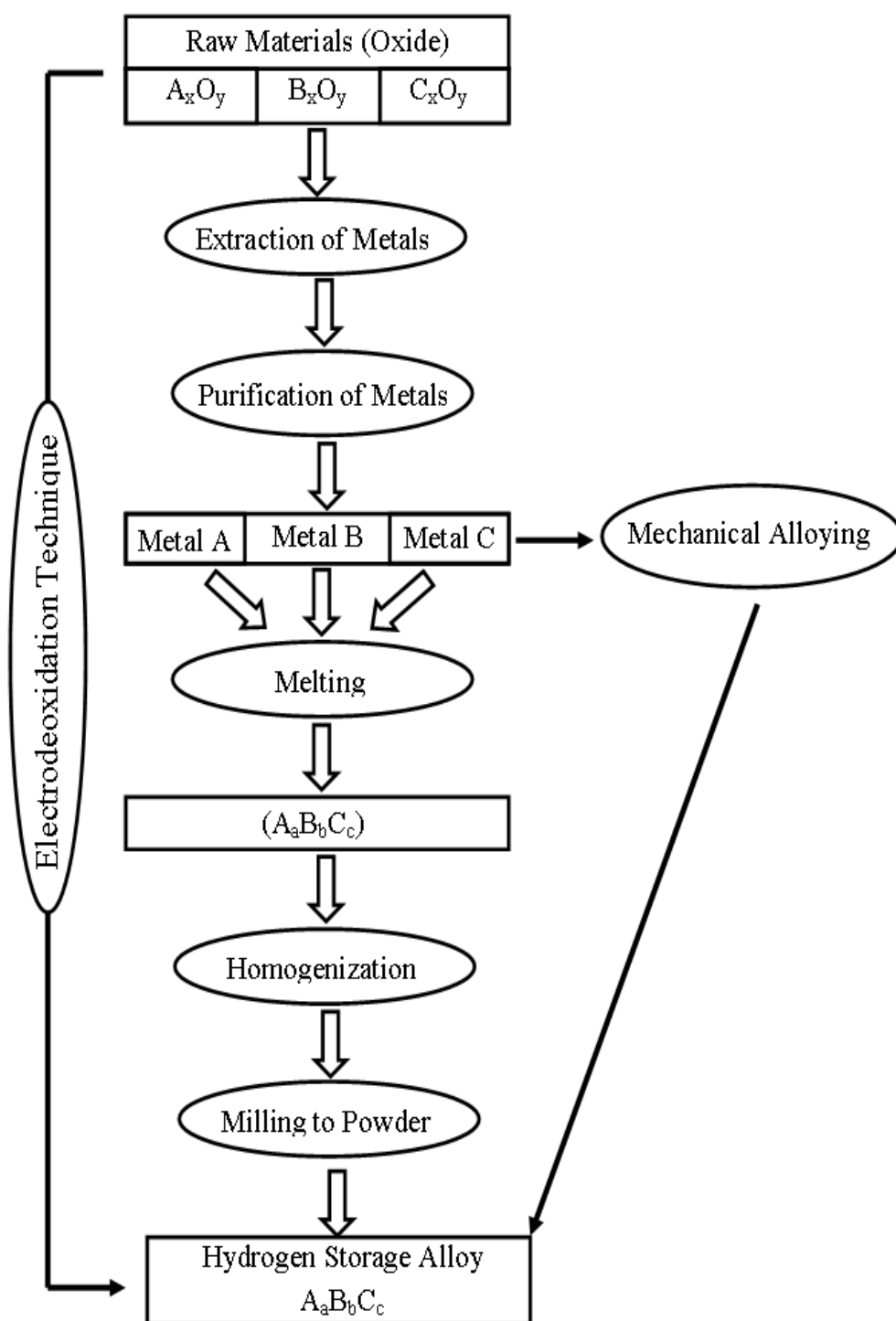


**Figure 1.1** Flowchart for synthesis of hydrogen storage compounds by three different techniques: electro-reduction, mechanical alloying and melting.

In electro-reduction processes, with the application of a constant voltage, oxygen is extracted from the cathode, i.e. oxide pellet, transported through electrolyte and converted to gaseous phase(s) at the anode. Metallic pellet forms at the cathode. This occurs without decomposing the molten salt, as the applied voltage is lower than the decomposition voltage of the molten salt (Chen et al. 2000).

Solid-state electro-reduction techniques are also capable to synthesize alloys from oxide mixtures. The studies mainly focused on synthesis of Ti, Si and Nb based materials. These processes allow compounding of elements with very different melting points, e.g.  $\text{Ni}_2\text{MnGa}$  from  $\text{NiO}$ ,  $\text{MnO}_2$  and  $\text{Ga}_2\text{O}_3$  mixture. Meanwhile, they offer a low-cost way to synthesize compounds as they use oxide powders as raw material. By this way; extraction, alloying and powder processing methods are combined in a single step that could be further developed to continuous production of metallic compounds, see Fig. 1. 1.

This thesis aims to synthesize hydrogen storage compounds by using a solid-state electro-reduction technique. In order to demonstrate this, Mg-Ni and Fe-Ti systems were selected having two important hydrogen storage compounds,  $\text{Mg}_2\text{Ni}$  and  $\text{FeTi}$ .

## CHAPTER 2

### LITERATURE REVIEW

#### 2.1 Introduction

In the last 20 years, solid-state electro-reduction processes were developed to synthesize pure metals from their oxides as well as complex compounds from their oxide mixtures. These techniques are high temperature electrochemical methods by which the oxide cathode is reduced to corresponding metal in a molten salt electrolyte having extensive oxygen solubility (Nagesh and Ramchandran, 2007). They involve oxygen removal in solid-state and offer a great opportunity to synthesize powders of the required compositions.

Electro-reduction of oxide pellets is carried out by applying a constant voltage between the porous oxide pellet and the anode while both are immersed into the molten salt electrolyte, such as  $\text{CaCl}_2$ ,  $\text{BaCl}_2$ , and  $\text{LiCl}$ . The anode could be a graphite piece or an electronically conducting inert material (Sadoway, 2001). With the application of voltage, oxygen is extracted from the oxide powders, transported through the electrolyte and by anodic reactions, it leaves the molten salt medium as  $\text{CO}/\text{CO}_2$  and/or  $\text{O}_2$  depending on the type of the anode used, see Fig. 2.1 (Fray and Chen, 2004). The electrolyte is not consumed during process, as the applied voltage is lower than its decomposition voltage (Chen et al., 2001). It is only used as a medium to transport  $\text{O}^{2-}$  ions from cathode to anode.

Historically, Ward and Hoar's cathodic refining technique is considered as the pioneer work on electro-reduction process (Ward and Hoar, 1961). In this study, liquid copper with impurity X ( $\text{X} = \text{O}, \text{Se}, \text{S}$  or  $\text{Te}$ ) was purified in  $\text{BaCl}_2$ .

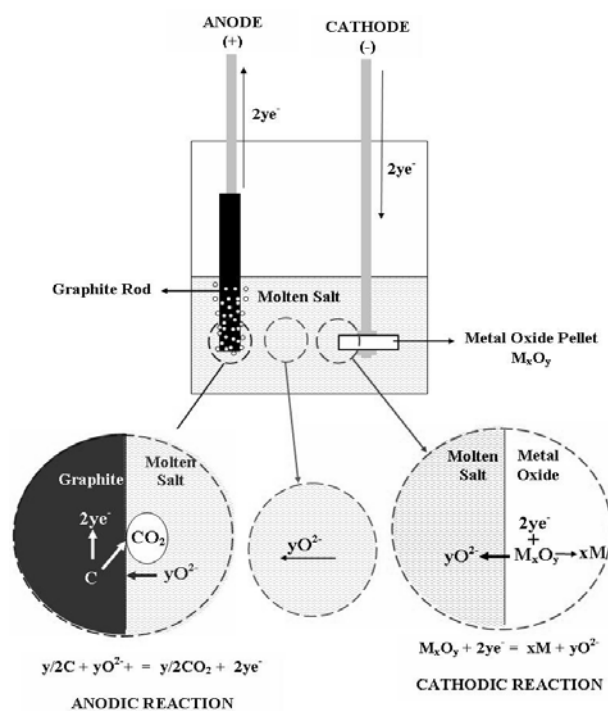


**Figure 2.1** A schematic drawing of solid-state electro-reduction processes showing flow of oxygen ions and electrons.

By decomposing  $BaCl_2$ , the deposited Ba metallothermally reacts with  $[X]_{Cu}$  to form pure Cu and  $BaX$ . In 1990's and 2000's, different studies were carried out to achieve the electro-reduction without  $Cl_2$  gas evolution (Okabe et al., 1992; Ono and Suzuki, 2002). Chen and Fray (2001) reported that electro-refining of liquid Cu could be achieved even if the applied voltage is lower than the decomposition voltage of  $BaCl_2$ .

Okabe and co-workers developed calcium halide flux and Electronically Mediated Reaction (EMR) techniques to remove oxygen from different oxides (Okabe et al., 1992; Okabe et al., 1996). Halide flux technique works by principle of calciothermic reduction of an oxide in calcium saturated molten  $CaCl_2$ . With EMR, Okabe incorporated electrochemistry into the halide flux technique for  $TiO_2$ ,  $Nb_2O_5$  and some rare-earth oxides (Okabe et al., 1993; Hirota et al., 1999; Okabe et al., 1998).



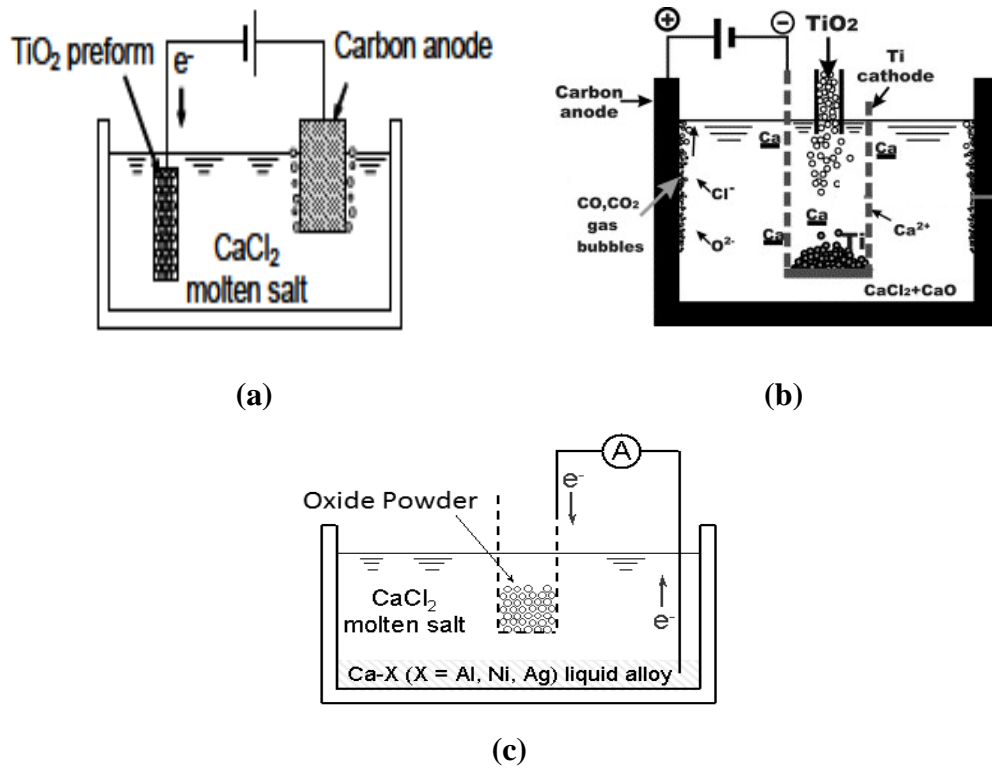


**Figure 2.2** Schematic drawings of different electro-reduction processes: (a) FFC Process; (b) OS Process and (c) EMR Process (Abiko et al., 2003).

Ono and Suzuki (2002) used CaO-CaCl<sub>2</sub> mixtures as electrolyte for in-situ formation of Ca on the oxide cathode. With the application of a voltage between metal oxide cathode and graphite anode, electrolytic reduction of CaO occurs. Then, Ca formed on the oxide powders metallothermally reduces the oxide pellet to the metallic state, see Fig. 2.2 (b).

Chen et al (2000) conducted experiments to remove oxygen from the surface of the thermally oxidized Ti foils in pure CaCl<sub>2</sub> electrolyte. They showed that the oxygen ionization from the oxide scale occurs without calcium deposition and chlorine evolution. As the process includes only transport of oxygen and electrons, but not deposition of metallic calcium, it is called as solid-state electro-deoxidation (Fray, 2001), see Fig 2.2 (a).

As the Kroll Process is an expensive way to produce Ti (Chen et al., 2001), production of pure Ti from  $\text{TiO}_2$  is the main driving force for development of electro-reduction processes in 2000's. After successful pilot-scale production of Ti by FFC Process (Metalysis®), researchers mainly focused on two aspects of electro-reduction: understanding the electrochemical phenomena behind the process and the synthesis of compounds, difficult to obtain by other techniques.

## **2.2 Processing Steps in Electro-reduction**

Electro-reduction involves a series of processing steps to synthesize metal powders from their oxides. These are ceramic processing, high temperature electrochemistry and grinding-separation operations, see Fig. 2.3. In this section, details of these processing steps will be given with a number of examples.

The process uses fine metal oxide powders as raw materials. For the ease of handling, oxide powders are compacted and sintered so that the pellets have certain mechanical strength.

Electro-reduction is carried out in a cell composed of a crucible with electrolyte and two electrodes, i.e. oxide pellet as cathode and a graphite or inert bar as anode. The selection and preparation of electrolyte before deoxidation is crucial for a successful reduction.

The reduction process is conducted at high temperature in an inert atmosphere, usually under argon, by applying a constant voltage between oxide pellet cathode and graphite anode for sufficiently long period of time.

After deoxidation, the final product is a metallic pellet composed of lightly fused metallic powders. Metal powders are obtained simply by soft grinding of the metallic pellet and the removal of residual electrolyte by a suitable solvent.

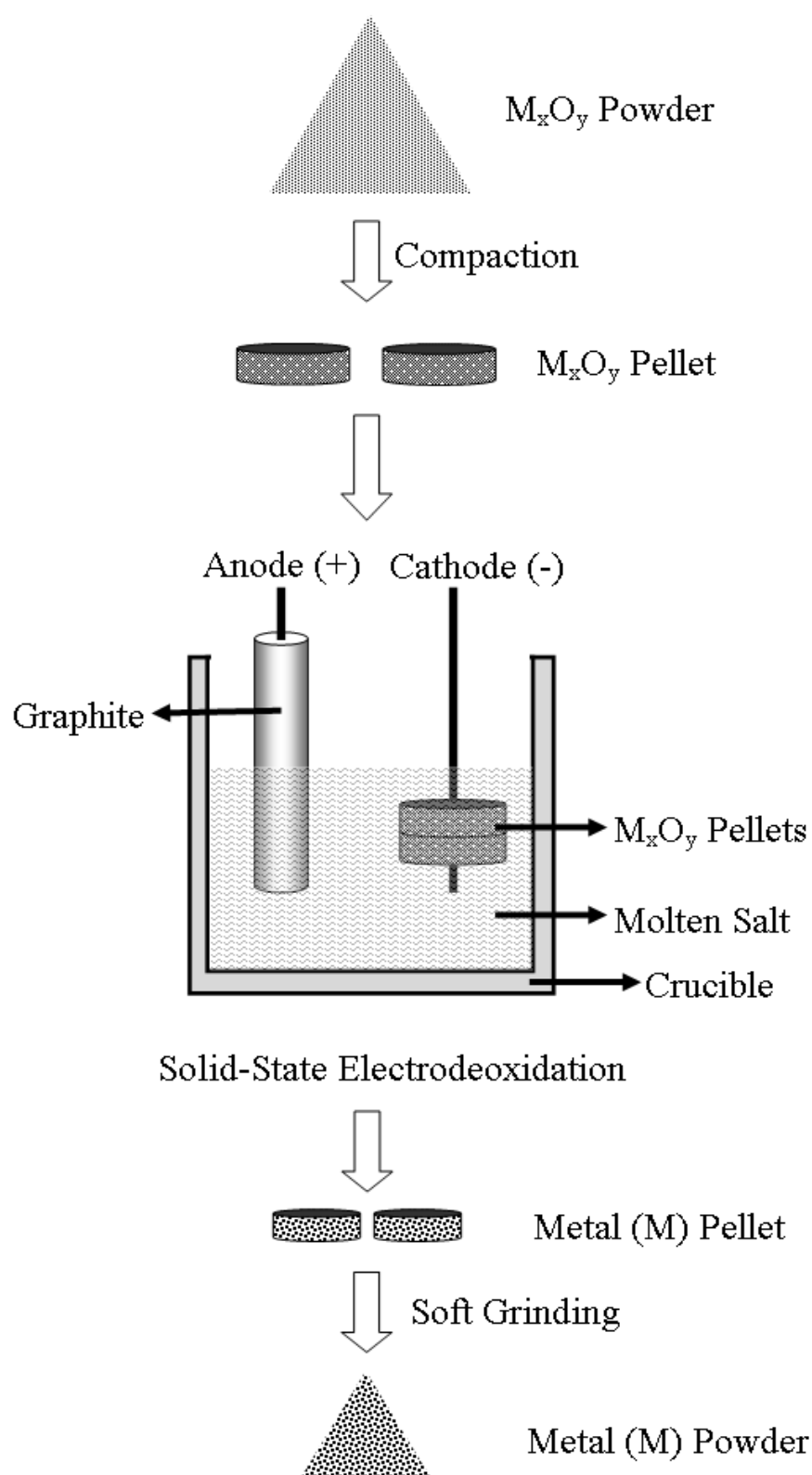


**Figure 2.3** *The flowchart of electro-reduction processes.*

### **2.2.1 Preparation of Oxide Pellets**

To prepare oxide pellets, suitably selected oxide powders are mixed and shaped into pre-forms. Subsequently, these pre-forms are sintered to obtain pellets with reasonable strength, chemistry, porosity and particle size.

The oxide pellet could be made out of a pure oxide (Xu et al., 2005), simply mixed oxides (Wood et al., 2003) or compounded oxides (Qiu et al., 2006). In any case, the overall chemistry of the oxide pellet should give the required metallic composition at the end of electro-reduction (Fenn et al., 2004).

In the most studies, oxide pellets are usually between 10-20 mm in diameter and a few mm in thickness. Yan and Fray (2005) determined that at least one dimension of the oxide pellets should be sufficiently small in order to have an easy penetration of the electrolyte and an easy removal of oxygen ions from the pellets.

The optimization of porosity is necessary as very low porosity of oxide yields limited reduction, while oxide pellets with very high porosities are mechanically instable (Schwandt and Fray, 2005). Oxide pellets with 35-65% porosities are quite common. It is also highly desirable to maximize the amount of open porosity in order to increase the oxide-electrolyte contact area (Sanchez et al., 2007).

All steps of pellet preparation, i.e. selection of oxide powders, mixing, shaping and sintering, should be performed such that they yield oxide pellets with required properties, i.e. dimension, particle size and porosity.

### **Selection of Oxide Powders**

Raw oxide powders should be selected according to their chemistry and particle size. ACS or better grade chemicals are frequently used for lab-scale synthesis of metals and compounds. The use of micron or submicron sized oxide powders in

electro-reduction is preferential for many reasons: high surface area between solid and electrolyte (Yan and Fray, 2009; Yan, 2008); low diffusion path for oxygen in solid (Yan and Fray, 2005) and higher probability of compounding of oxides during sintering (Yong et al., 2006 and Yan et al., 2009).

While fine powders are advantageous, some nano-sized oxides powders, e.g. powders of  $\text{La}_2\text{O}_3$ , are very reactive with moisture and, as a result, must be handled carefully (Zhu et al., 2007). Also, it is difficult to control the sintering parameters for nano-sized oxide powders (Kim et al., 2002). In such cases, the use of coarser powders might be preferential.

### **Production of Porous Oxide Pellets**

Two common methods to form porous oxide pellets are slip casting and compaction. Slip casting involves three consecutive steps: preparation of slurry and its casting, drying and sintering. In compaction, a similar route is followed, i.e. mixing, compaction and sintering.

According to Gordo et al. (2004), the size of oxide powders is critical for the selection of mixing method. For coarse powders, dry mixing for several hours and further compaction is the best technique for preparation of pellets (Qiu et al., 2006 and Wood et al. 2003). For fine powders, Chen et al. (2000) recommends slip casting or wet mixing plus compaction to prepare oxide pellets. The liquid medium helps to distribute fine oxide particles uniformly. In order to mix  $\text{Tb}_4\text{O}_7$  and  $\text{NiO}$  powders, Qiu et al. (2006) preferred anhydrous alcohol stating that water reacts with  $\text{Tb}_4\text{O}_7$ . Jiang et al. (2006) used distilled water to prepare pure  $\text{TiO}_2$  and  $\text{Ca}(\text{OH})_2\text{-TiO}_2$  mixtures, while Sanchez et al. (2007) and Schwandt and Fray (2005) used isopropyl alcohol to make slurries of  $\text{TiO}_2$ . For different  $\text{Nb}_2\text{O}_5$  mixtures, i.e.  $\text{Nb}_2\text{O}_5\text{-SnO}_2$  and  $\text{Nb}_2\text{O}_5\text{-TiO}_2$ , acetone was used by Yan and Fray (2005). Ball mills, multi-axial blenders and ultrasonic mixers are used to distribute oxide powders homogenously in dry and wet mixing (Schwandt and Fray, 2005).

A few percent of binder and/or plasticizer are frequently added to the mixture as a processing aid. Low molecular weight PEG and PVA are the most common (Sanchez et al., 2007; Schwandt et al., 2005). Pore formers, e.g. graphite, polyethylene, polystyrene etc., could be included to obtain pellets with extremely high porosities (Sanchez et al., 2007).

In slip casting, oxide slurries are cast in desired shapes and left to dry (Barsoum, 2002). The solvent evaporates slowly and a solid pre-form is obtained. In fact, uniaxial cold pressing is the most frequently used method to obtain oxide pre-forms in electro-reduction. Compaction pressures could be up to a few hundreds of MPa (Mohandas and Fray, 2009; Yan and Fray, 2005). According to Gordo et al. (2004), the use of very high and very low compaction pressure should be avoided as the former ends up with delamination of pellet, while in the latter there would be difficulties in handling.

Oxide pre-forms are sintered at high temperatures, by which the oxide particles partially fuse to each other and mechanical strength of the pellet increases (Fray, 2001). Sintering is mainly performed between 800 °C – 1200 °C up to 24 hours (Chen et al., 2000; Cox and Fray, 2002). Low heating rates, e.g. 0.1 - 5 °C /min, are preferred so as to maintain the physical integrity of the green compacts (Gordo et al., 2004).

Sintering temperatures should be selected properly as the mixed oxides could react with each other. Qiu et al. (2006) detected that sintering of  $\text{Tb}_4\text{O}_7\text{-Fe}_2\text{O}_3$  pre-forms at 800 °C yields a pellet with two individual oxides, while at 1200 °C, the phases  $\text{Tb}_3\text{Fe}_5\text{O}_{12}$  and  $\text{TbFeO}_3$  form additionally. Sintering can intentionally be performed at high temperatures for compounding the oxide powders. Jiang et al. (2006) sintered  $\text{Ca(OH)}_2\text{-TiO}_2$  pre-form at 1300 °C for 5 h in order to obtain  $\text{CaTiO}_3$  pellet. Ma et al. (2006) sintered  $\text{Fe}_2\text{O}_3\text{-TiO}_2$  pre-form at 1050 °C for 4 h and obtained synthetic ilmenite pellet.

### 2.2.2 Selection and Preparation of Electrolyte

With their high ionic but low electronic conductivities in fused state, alkali and alkaline earth metal salts are preferred as electrolyte in electro-reduction processes (Mishra and Olson, 2005). In order to be used as an electrolyte, a salt should have high stability, high  $O^{2-}$  solubility and low solubility of oxide and/or metal to be worked (Hirota et al., 1999). Non-toxicity and low-cost are other requirements.

$CaCl_2$ ,  $BaCl_2$  and  $LiCl$  are suitable electrolytes for electro-reduction processes with their high decomposition voltages (Chen et al., 2000). Of those,  $CaCl_2$  ( $T_m=772\text{ }^{\circ}C$ ) is the most widely used one, due to its non-toxicity and extensive oxygen solubility, ca. 20 wt %  $CaO$  at  $900\text{ }^{\circ}C$  (Mohandas and Fray, 2004).  $LiCl$  is also used in some deoxidation studies but it does not offer a significant advantage over  $CaCl_2$  (Yan, 2008; Jeong et al., 2008).

According to Chen et al. (2000), other alkaline chlorides, e.g.  $NaCl$  and  $KCl$ , could also be added into  $CaCl_2$  or  $LiCl$  to achieve specific properties, such as lower melting points and lower solubility of metal oxides and/or metals studied.  $NaCl$  is abundant and non-toxic material. It has high stability, i.e.  $-3.21\text{ V}$  at  $900^{\circ}C$ , and has low solubility for oxides. The eutectic composition of  $CaCl_2$ - $NaCl$  ( $T_m=505\text{ }^{\circ}C$ ) is the most frequently used electrolyte which offers lower working temperatures than pure  $CaCl_2$  (Gordo et al., 2004; Wang and Sun, 2006).

If metallothermic reduction is required in the electro-reduction process, oxides could be included into the electrolyte, e.g.  $CaO$  into  $CaCl_2$ ;  $Li_2O$  into  $LiCl$ , (Jeong et al., 2007; Suzuki, 2005). The amount of oxide addition is critical and varies between 0.5 - 15 % mole (Abdelkader et al., 2007).

Metal salts are known to be very hygroscopic. Reactions between metal salts with water result in formation of compounds, such as  $Li_2O$ ,  $Ca(OH)_2$  and

CaOHCl (Mohandas and Fray, 2004). By simply heating to high temperatures without any precaution, a molten salt may contain a few mole percent of these impurities. Chen and Fray (2002) state that presence of unwanted species in the electrolyte causes side reactions in electro-reduction. Thus, formation of these impurities should be minimized by suitable drying procedures. In the best, they should be removed from the molten salt by pre-electrolysis.

According to Chen and Fray (2002), water releases from  $\text{CaCl}_2$  mainly up to 200 °C. Thus, the first step of drying process is heating  $\text{CaCl}_2$  (or  $\text{CaCl}_2 \cdot 2\text{H}_2\text{O}$ ) up to a temperature between 200 °C – 350 °C (Chen and Fray, 2002). Ma et al. (2006) states that heating rates less than 0.5°C/min should be applied under vacuum. The salt is then held at that temperature for several hours. The second step is frequently applied at a temperature between 400 °C – 700 °C. The salt is held at that temperature for a few more hours (Chen and Fray, 2002), while high purity Argon is purged into the drying chamber. After this point, the salt can be either cooled down to room temperature or directly heated up to pre-electrolysis temperature.

For LiCl, a similar procedure is applied (Jeong et al., 2007). Drying of NaCl is simpler as it does not contain chemically bonded water (Yan and Fray, 2005). For drying of mixed electrolytes, the drying procedure is commonly adjusted as if it is pure  $\text{CaCl}_2$  or LiCl.

Before electro-reduction, impurities formed during drying and foreign cations, e.g.  $\text{Mg}^{2+}$ , should be removed from molten salt by pre-electrolysis (Xiao et al., 2006). For this purpose, a graphite anode and a metal cathode wire is immersed into the electrolyte and a constant voltage (2.5 - 3.0 V) is applied between these two for several hours (Wang et al., 2006). The duration of pre-electrolysis depends on the level of residual current measured which varies with temperature, applied voltage and purity of electrolyte (Schwandt and Fray, 2005). The residual current values down to 2 mA/cm<sup>2</sup> are reported.



### **2.2.3 Other Cell Components: Anodes, Crucibles, Reference Electrodes and Auxiliary Parts**

In electro-reduction, anode could be a carbon-based or inert material (Mohandas and Fray, 2004). Carbon-based anodes, i.e. graphite or glassy carbon, offer lower reduction voltages for oxides (Chen et al., 2000). However, they have also some drawbacks, such as formation of CO/CO<sub>2</sub> and carbon dust, back-reactions etc. (Yan and Fray, 2009). These problems could be prevented by the use of inert anodes, such as Pt (Jeong et al., 2007) and SnO<sub>2</sub> (Barnett et al., 2009).

Electro-reduction experiments are conducted in reaction chambers resistant to both heat and corrosive salt vapors. The crucible used in the electro-reduction process could be made out of Ti (Chen and Fray, 2002), stainless steel (Yasuda et al., 2007), graphite (Qui et al., 2005) or an oxide, e.g. Al<sub>2</sub>O<sub>3</sub> (Gordo et al., 2004). For metal crucibles, cathodic protection during electro-reduction is strongly advised (Chen and Fray, 2002). According to Chen et al. (2001), oxide crucibles should be avoided, if very low oxygen content in the metallic pellet is required.

Reference electrodes are often used in voltammetry or in constant voltage deoxidation experiments. For CaCl<sub>2</sub> and CaCl<sub>2</sub>-NaCl, quartz sealed Ag/AgCl reference electrode was found satisfactory (Wu et al., 2008; Gao et al., 2005). A highly inert metal wire, e.g. Pt, Mo, could be used as pseudo-reference electrode (Wang et al. 2006; Qiu et al., 2008). Ti or graphite crucibles can also be set as a pseudo-reference electrode the deoxidation cells (Wang and Li, 2004).

Both oxide pellet and anode should be firmly attached to the current collectors, i.e. wires of Mo, Ni, Kanthal®, stainless steel (Yan and Fray, 2005; Xiao et al. 2006). Meshes of the same metals could be used to sandwich metal oxide pellets to increase the metal-oxide-electrolyte contact (Jiang et al. 2006; Wang et al., 2006). According to Yasuda et al. (2005), metal wires could be wrapped around oxide pellets for the same purpose.

#### 2.2.4 Electro-reduction of Oxides and Collection of Product

Table 2.1 lists the previous studies showing sintering, pre-electrolysis and electro-reduction conditions of different metal oxides. As seen from the table, there are three fundamental parameters in electro-reduction: applied voltage, reduction temperature and the duration of reduction.

The applied voltage is in the range of 2.4-3.3 V for different oxides. According to Qiu et al. (2008), the applied voltage should be high enough to overcome the theoretical reduction voltage of oxide, IR drop, resistance of external connections and possible cathodic and anodic overpotentials. The decomposition voltage of the electrolyte sets the upper limit for the applied voltage.

As given in Table 2.1, electro-reduction is mainly conducted at temperatures between 700-1000 °C. In order to avoid melting, the deoxidation temperature should be lower than melting point of the target metal and/or compound. In synthesis of compounds, reduction temperatures higher than the melting point of the constituent elements could be selected (Wood et al. 2003). Extreme temperatures should be avoided considering the lifetime of the equipments and apparatus.

As electro-reduction processes are not constant current techniques, it is not possible to mention the theoretical time for electro-reduction process. Instead, it is more convenient to calculate the total charge necessary to reduce a metal oxide, i.e.  $Q_t$ , given by Faraday's Law (Ma et al., 2006):

$$Q_t = I \times t = n \times z \times F \quad (2.1)$$

Here,  $I$  is the measured current passing through the cell (A),  $t$  is the duration of deoxidation (s),  $n$  is the number of moles of substance (mol),  $z$  is the electrons transferred per ion and  $F$  is the Faraday's constant (96485.3399 C/mol).

**Table 2.1** *Some metals and compounds synthesized by electro-reduction processes and their synthesis conditions.*

| Metal Oxide  | Target Metal         | Electrolyte                    | Sintering |    | Pre-electrolysis |     |    | Electro-reduction |      |    | Reference                |
|--|----------------------|--------------------------------|-----------|----|------------------|-----|----|-------------------|------|----|--------------------------|
|  |                      |                                | T         | t  | V                | T   | t  | V                 | T    | t  |                          |
| Cr <sub>2</sub> O <sub>3</sub>                                 | Cr                   | CaCl <sub>2</sub> – NaCl (1:1) | 900-1100  | 1  | -                | -   | -  | 2.8 - 3.1         | 900  | 5  | Gordo et al. (2004)      |
| *Nb <sub>2</sub> O <sub>5</sub>                                | Nb                   | LiCl + 4.2 % Li <sub>2</sub> O | -         | -  | -                | -   | -  | 2.5 - 3.4         | 650  | 10 | Jeong et al. (2008)      |
| Nb <sub>2</sub> O <sub>5</sub>                                 | Nb                   | CaCl <sub>2</sub>              | 1000      | 2  | 2.6              | 850 | 10 | 2.4-3.2           | 850  | 12 | Qiu et al. (2008)        |
| SiO <sub>2</sub> (quartz)                                      | Si                   | CaCl <sub>2</sub>              | -         | -  | -                | -   | -  | 2.0 - 2.5         | 850  | 2  | Yasuda et al. (2007)     |
| Ta <sub>2</sub> O <sub>5</sub>                                 | Ta                   | CaCl <sub>2</sub>              | 900       | 2  | 2.7              | 850 | 12 | 3.1               | 850  | 10 | Wu et al. (2007)         |
| <sup>†</sup> Ta <sub>2</sub> O <sub>5</sub>                    | Ta                   | CaCl <sub>2</sub> + 1 % CaO    | 1200      | 3  | 1.3              | 900 | -  | 2.8               | 900  | 8  | Barnett et al. (2009)    |
| *Ta <sub>2</sub> O <sub>5</sub>                                | Ta                   | LiCl + 4.2 % Li <sub>2</sub> O | -         | -  | -                | -   | -  | 2.5 - 3.4         | 650  | 10 | Jeong et al. (2007)      |
| TiO <sub>2</sub>   | Ti                   | CaCl <sub>2</sub>              | 900       | 48 | 2.7              | 950 | 2  | 2.8 - 3.2         | 950  | 12 | Chen et al. (2000)       |
| UO <sub>2</sub>  | U                    | LiCl + 0.5% Li <sub>2</sub> O  | -         | -  | -                | -   | -  | 3.2               | 650  | -  | Sakamura et al. (2006)   |
| ZrO <sub>2</sub>   | Zr                   | CaCl <sub>2</sub> + 1 % CaO    | 600       | -  | 1.3              | 900 | -  | 2.8-3.1           | 1000 | 4  | Abdelkader et al. (2007) |
| Al <sub>2</sub> O <sub>3</sub> -Sc <sub>2</sub> O <sub>3</sub> | Al <sub>3</sub> Sc   | CaCl <sub>2</sub> - NaCl (1:1) | 1400      | 4  | 2.8              | 700 | 10 | 3.2               | 700  | 24 | Liao et al. (2009)       |
| CeO <sub>2</sub> -NiO-CuO                                      | CeNi <sub>4</sub> Cu | LiCl-KCl (eutectic)            | 950       | 4  | 3.0              | 650 | 2  | 3.5               | 650  | 8  | Kang et al. (2010)       |
| FeTiO <sub>3</sub>   | FeTi                 | CaCl <sub>2</sub>              | 900       | 4  | -                | -   | -  | 2.8-3.1           | 900  | 8  | Ma et al. (2006)         |
| Al <sub>2</sub> O <sub>3</sub> -Nb <sub>2</sub> O <sub>5</sub> | Nb <sub>3</sub> Al   | CaCl <sub>2</sub> – NaCl (1:1) | 1000      | 24 | 2.8              | 900 | 10 | 3.1               | 900  | 24 | Yan and Fray (2005)      |
| Nb <sub>2</sub> O <sub>5</sub> -TiO <sub>2</sub>               | NbTi                 | CaCl <sub>2</sub> – NaCl (1:1) | 900       | 24 | 3.0              | 900 | 10 | 2.8 - 3.1         | 950  | 10 | Yan et al. (2005)        |
| Nb <sub>2</sub> O <sub>5</sub> -SnO <sub>2</sub>               | Nb <sub>3</sub> Sn   | CaCl <sub>2</sub> -NaCl        | -         | -  | -                | -   | -  | 3.1               | 935  | 10 | Glowacki et al. (2003)   |

**Table 2.1** (*cont'd*)

| Metal Oxide  | Target Metal                          | Electrolyte                 | Sintering |   | Pre-electrolysis |     |    | Electro-reduction |     |    | References               |
|--|---------------------------------------|-----------------------------|-----------|---|------------------|-----|----|-------------------|-----|----|--------------------------|
|  |                                       |                             | T         | T | V                | T   | t  | V                 | T   | t  |                          |
| Nd <sub>2</sub> O <sub>3</sub> -Co <sub>3</sub> O <sub>4</sub> | NdCo <sub>5</sub>                     | CaCl <sub>2</sub> + 1 % CaO | 1100      | - | -                | -   | -  | 3.1               | 950 | 12 | Abdelkader et al. (2010) |
| NiO-MnO <sub>2</sub> -Ga <sub>2</sub> O <sub>3</sub>           | Ni <sub>2</sub> MnGa                  | CaCl <sub>2</sub>           | 540       | 2 | -                | -   | -  | 3.0               | 950 | 26 | Wood et al. (2003)       |
| Tb <sub>4</sub> O <sub>7</sub> -NiO                            | TbNi <sub>5</sub>                     | CaCl <sub>2</sub>           | 1000      | 2 | 2.6              | 850 | 10 | 2.4 - 3.2         | 850 | 12 | Qiu et al. (2006)        |
| Tb <sub>4</sub> O <sub>7</sub> -Fe <sub>2</sub> O <sub>3</sub> | TbFe <sub>5</sub>                     | CaCl <sub>2</sub>           | 1200      | 2 | 2.6              | 900 | 10 | 2.6 - 3.2         | 900 | 12 | Qiu et al. (2006)        |
| Fe <sub>2</sub> O <sub>3</sub> -TiO <sub>2</sub> -NiO          | TiFe <sub>0.4</sub> Ni <sub>0.6</sub> | CaCl <sub>2</sub>           | 1050      | 4 | -                | -   | -  | 2.8-3.1           | 900 | 8  | Ma et al. (2006)         |
| TiO <sub>2</sub> -NiO  | TiNi                                  | CaCl <sub>2</sub>           | -         | - | 2.6              | 900 | 6  | 3.1               | 900 | 12 | Yong et al. (2006)       |
| ZrO <sub>2</sub> -Cr <sub>2</sub> O <sub>3</sub>               | ZrCr <sub>2</sub>                     | CaCl <sub>2</sub>           | 900       | 2 | 2.6              | 900 | 3  | 3.0               | 900 | 12 | Peng et al. (2009)       |

“T”, “V” and “t” represent temperature in Celsius degree, voltage in Volts and duration in hours, respectively. The electrolyte mixture and additions are given in molar ratio and molar percent respectively. The anode material is graphite otherwise stated.

\*Anode material is platinum

† Anode material is SnO<sub>2</sub>

Electro-reduction processes mainly work at efficiencies between 5 - 60 % depending on the electro-reduction conditions and properties of the pellet (Abdelkader et al., 2007).

An electro-reduction experiment starts with cell assembly. The cell is made out of two electrodes for pre-electrolysis and two electrodes for deoxidation. Different types of cells mentioned in the literature are given in Fig. 2.4. After the assembly, the cell is sealed into the reaction chamber and argon is purged continuously. Before heating up flushing of the chamber with argon is recommended (Mohandas and Fray, 2004). A high temperature furnace is used to heat up the system. The temperature of the molten salt bath is followed continuously during pre-electrolysis and electro-reduction.

Electro-reduction of oxides is carried out just after the pre-electrolysis. After immersing the oxide pellet and anode into the electrolyte, electro-reduction is initiated by applying a constant voltage between these two electrodes.

Upon application of a voltage, current starts to flow. This is due to the transport of oxygen through electrolyte. The current is high initially but diminishes with time (Chen et al., 2000). Deoxidation process is ended up when current cascades down to a low background value which is attributed to the impurities and electronic conductivity of the electrolyte (Alexander et al., 2006). After deoxidation, electrodes are removed from the molten salt and the system is allowed to cooled down to room temperature.

After deoxidation, the pellet contains both product and solidified salt. The salt can be removed either by cleaning the pellet directly or by grinding the pellet to the powders form and further cleaning (Jin et al. 2004). Water is the most common solvent. In order to remove CaO and Ca(OH)<sub>2</sub>, dilute acids, e.g. HCl, CH<sub>3</sub>COOH, can be used (Schwandt and Fray, 2005). Vacuum drying at a temperature lower than 80°C is quite common. Cleaning by ethanol and/or acetone before vacuum drying may also be used.

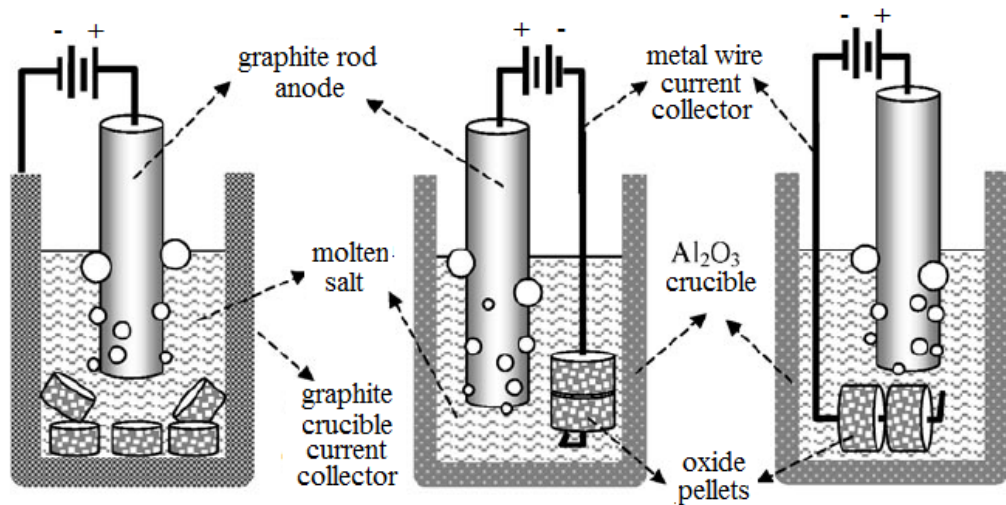
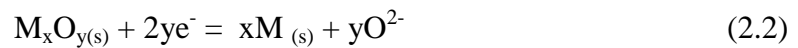


**Figure 2.4** Different types of electrochemical cells used in the electro-reduction processes (Chen et al., 2004).

## 2.3 Electrochemical Reactions in Solid State Electro-reduction

### 2.3.1 Cathodic Reactions

According to Chen et al. (2000), direct ionization of oxygen from the metal oxide,  $M_xO_y$ , or a metal-oxygen solid solution,  $M(O)$ , is possible by following reaction:



Chen and Fray (2001) calculated the oxygen ionization potential for various oxides in pure  $CaCl_2$  melt, Table 2.2. As seen from the table, ionization of oxygen from metal oxides has more positive potential than deposition of metallic Ca from  $Ca^{2+}$ . This demonstrates that direct ionization of oxygen from the oxide pellets is thermodynamically possible without Ca deposition, which is also practically shown by voltammetry, and potentiostatic reduction experiments for various oxides (Dring et al., 2005; Qiu et al., 2005).

**Table 2.2** *Calculated standard oxygen ionization potentials of various oxides in fused calcium chloride melt at 700 °C (  $E_{Na^+/Na} = 0$  ) (Chen and Fray, 2001).*

| Electrode Reaction                      | Potential ( V ) |
|---|-----------------|
| $2PbO(s) + 4e^- = 2O^{2-} + 2Pb$        | 2.082           |
| $SnO_2 + 4e^- = 2O^{2-} + Sn$           | 1.734           |
| $MoO_2 + 4e^- = 2O^{2-} + Mo$           | 1.650           |
| $2/5 Nb_2O_5 + 4e^- = 2O^{2-} + Nb$     | 1.209           |
| $2/3 Cr_2O_3 + 4e^- = 2O^{2-} + 4/3 Cr$ | 1.189           |
| $2/5 Ta_2O_5 + 4e^- = 2O^{2-} + 4/5 Ta$ | 1.038           |
| $TiO_2 + 4e^- = 2O^{2-} + Ti$           | 0.750           |
| $ZrO_2 + 4e^- = 2O^{2-} + Zr$           | 0.349           |
| $2/3 Al_2O_3 + 4e^- = 2O^{2-} + 4/3 Al$ | 0.348           |
| $2MgO + 4e^- = 2O^{2-} + 2Mg$           | 0.143           |
| $2Ca^{2+} + 4e^- = 2Ca$                 | -0.06           |

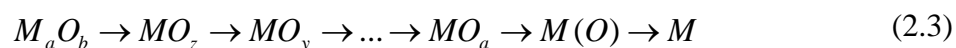
In order to elucidate the real reduction mechanisms at the cathode side, numerous investigations were conducted in the past (Wang and Li, 2004; Wu et al., 2008). The following part gives a summary of possible cathodic mechanisms in electro-reduction process for both pure and multi-component oxide systems.

### **Cathodic Mechanisms in Electro-reduction of Pure Oxides**

The analysis of the partially reduced samples by X-ray diffraction and electron microscopy is the main technique to determine the reduction mechanisms (Qiu et al., 2006; Schwandt and Fray, 2005). Previous studies showed that partially reduced oxide pellets might be composed of different phases: raw metal oxide, sub-oxides, Ca-bearing compounds, pure metals and/or metallic compounds (Jiang et al., 2006; Abdelkader et al., 2007; Okabe et al., 1998; Yan, 2008). The diversity in the chemistry of the partially reduced pellets demonstrates that the

cathodic reduction mechanisms for electro-reduction of pure oxides are more complicated than the reaction given in Eq. 2.2.

It was observed that, in many oxide systems, Ca-bearing compounds form at the start of the deoxidation process (Jiang et al., 2006). Then, oxides and Ca-bearing compounds are reduced by the applied voltage. It was further observed that, in these complex systems, deoxidation mainly proceeds on metal oxide phase. According to Wu et al. (2008), reduction of oxide occurs stepwise in the following order:



Here,  $M_aO_b$  represents stoichiometric oxide with  $b/a > z$ ,  $MO_z$  to  $MO_a$  represent sub-oxides,  $M(O)$  represents metal-oxygen solid solution,  $M$  is the pure metal. Schwandt and Fray (2005) state that Ca-bearing compounds have more negative reduction potential than that of sub-oxides. As a result, they are consumed at the latter stage of the process (Wu et al., 2007).

Alexander et al. (2006) states that the electro-reduction of  $TiO_2$  starts with electrochemical formation of  $CaTiO_3$  and  $Ti_4O_7$  and proceeds by formation of  $Ti_4O_7$ ,  $Ti_3O_5$ ,  $Ti_2O_3$  and  $TiO$ , respectively. Gordo et al. (2004) detected  $CaCr_xO_y$  particles in the partially reduced  $Cr_2O_3$  pellet and speculated that the electro-reduction proceeds either by direct reduction of  $Cr_2O_3$  to  $Cr$  or by stepwise reduction to  $CrO$  and then to metallic  $Cr$ . Similarly, Qiu et al. (2008) states that the reduction of  $Nb_2O_5$  follows the sequence of  $Nb_2O_5$ ,  $NbO_2$ ,  $NbO$  and  $Nb$  in the presence of  $CaNb_2O_6$ ,  $CaNbO_3$  and  $Ca_{0.95}Nb_3O_9$ .

In some systems, Ca-bearing oxides do not form. Voltammetry and potentiostatic reduction studies conducted by Qiu et al. (2005, 2006 and 2006) demonstrate that oxygen removal from  $NiO$  and  $Fe_2O_3$  occurs directly without formation of calcium compounds.

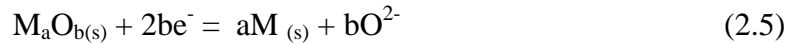
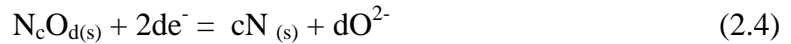


It was found that for some oxide systems, the reduction mainly proceeds on (or with the help of) Ca-bearing compounds. Yasuda et al. (2005) proposed that the reduction of SiO<sub>2</sub> involves presence of calcium by pointing out that CaSiO<sub>3</sub> is highly conducting phase, while pure SiO<sub>2</sub> has very low electrical conductivity, ca. 10<sup>-10</sup> S/cm at 850 °C. Similarly, Yan (2008) examined the reduction of Al<sub>2</sub>O<sub>3</sub> dross. They concluded that although reduction voltage of calcium aluminates, i.e. Ca<sub>12</sub>Al<sub>14</sub>O<sub>33</sub> and Ca<sub>x</sub>Al<sub>2</sub>O<sub>(3-x)</sub>, is higher than that of pure Al<sub>2</sub>O<sub>3</sub>, electro-deoxidation mainly proceeds on those electronically conducting Ca-bearing compounds. Wu et al. (2007) proposes that in the reduction of Ta<sub>2</sub>O<sub>5</sub>, first CaTa<sub>2</sub>O<sub>5</sub> forms and then the reduction proceeds by further reduction of CaTa<sub>2</sub>O<sub>5</sub> to TaO.

### **Cathodic Mechanisms in Electro-reduction for Multi-component Oxides**

Cathodic reactions in deoxidation of multi-component oxides are more complicated than those observed in pure systems. Electro-deoxidation of these oxide pellets involve both reduction and compound formation. In simply mixed and pre-compounded oxides, the preferential reduction of an oxide with more positive reduction potential is expected (Qiu et al., 2006).

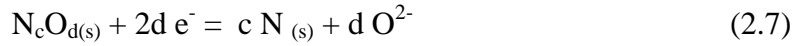
In simply mixed oxides, the most straightforward mechanism in compound formation is reduction of each oxide separately and then formation of the target compound by reaction of pure metals (Yan and Fray, 2005). This is given by:



Here, N<sub>c</sub>O<sub>d</sub> and M<sub>a</sub>O<sub>b</sub> are the individual oxides; M, N are corresponding metals and M<sub>x</sub>N<sub>y</sub> is the compound they formed with x≤a and y≤c.

This mechanism is observed especially when two oxides of similar reduction potentials are reduced together. Liao et al. (2009) states that in  $\text{Al}_2\text{O}_3\text{-Sc}_2\text{O}_3$  pellet, preferential reduction does not occur as theoretical reduction voltages of each oxide is similar, i.e. at  $700^\circ\text{C}$ , 2.80 V and 2.36 V for  $\text{Sc}_2\text{O}_3$  and  $\text{Al}_2\text{O}_3$ , respectively. Yan and Fray (2005) propose that oxides in  $\text{Nb}_2\text{O}_5\text{-TiO}_2$  and  $\text{Nb}_2\text{O}_5\text{-SnO}_2$  mixtures deoxidize individually and corresponding metals react to form NbTi and  $\text{Nb}_3\text{Sn}$  superconductor phases.

Another mechanism frequently observed in the simply mixed oxide systems is the preferential reduction of an oxide from the oxide mixture. In this case, an oxide with more positive reduction potential is reduced first and other oxides are reduced on that metal, given by:

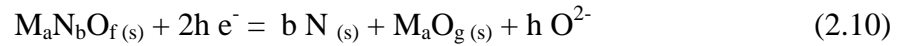


Here,  $\text{N}_c\text{O}_d$  is the oxide with more positive reduction potential,  $\text{M}_a\text{O}_b$  is the oxide with less positive reduction potential; N is the metal of  $\text{N}_c\text{O}_d$ ;  $\text{NM}_z$  and  $\text{NM}_k$  are different compounds of M and N.

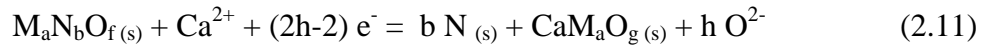
The preferential reduction is observed when two oxides with very different reduction potentials are reduced together. According to Yan (2008), preferential reduction of a metal oxide is beneficial for the reduction of the whole oxide pellet because of the depolarization effect and improvement of electronic conductivity. Previous studies show that in  $\text{Tb}_2\text{O}_3\text{-NiO}$  and  $\text{Tb}_2\text{O}_3\text{-Fe}_2\text{O}_3$  mixtures, reduction of  $\text{Tb}_2\text{O}_3$  and formation of Tb-Ni and Tb-Fe compounds occur nearly 0.2–0.8 V more positive potential than reduction potential of pure  $\text{Tb}_2\text{O}_3$  (Qiu et al., 2006; Qiu et al., 2006). Abdelkader et al. (2010) states that  $\text{NdCd}_5$  is synthesized by cathodic reduction of  $\text{CaNd}_2\text{O}_4$  on metallic Co. Peng et

al. (2009) proposes that reduction of perovskite  $\text{CaZrO}_3$  on metallic Cr is the dominant mechanism for synthesis of  $\text{ZrCr}_2$ .

There are different routes for deoxidation of pre-compounded oxide systems, i.e.  $\text{M}_a\text{N}_b\text{O}_f$ . Previous studies showed that the rule (the more positive the reduction potential of an oxide is, the easier it is reduced) still holds for pre-compounded systems. This simply results in dissociation of the pre-compounded oxide and formation of a metallic phase in deoxidation:



Here,  $\text{M}_a\text{O}_g$  is oxide with less positive reduction potential and N is metal of  $\text{N}_b\text{O}_c$ . It is also proposed by Ma et al. (2006) that  $\text{Ca}^{2+}$  can play a role in dissociation of pre-compounded oxide by formation of a calcite ( $\text{CaM}_a\text{O}_g$ ) and metal phase:



After dissociation, the components deoxidize either separately or by depolarization mechanism. According to Ma et al. (2006), synthesis of FeTi hydrogen storage material from ilmenite, i.e.  $\text{FeTiO}_3$ , occurs by formation of  $\text{CaTiO}_3$  and Fe and subsequent reduction of calcite on Fe phase by depolarization mechanism. For reduction of  $\text{TiNiO}_3$ , the same mechanism works and pure shape memory NiTi alloy could be synthesized in 12 hours at  $900^\circ\text{C}$  (Yong et al., 2006).

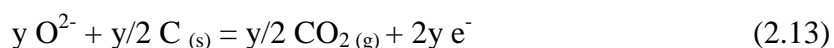
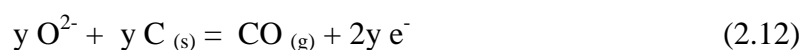
The applied voltage was found to be effective on deoxidation mechanism of multi-component oxides. According to Qiu et al (2006), only NiO is reduced to Ni when 1.8 V is applied between NiO- $\text{Tb}_2\text{O}_3$  pellet and graphite. At applied voltages between 2.4 V and 3.1 V, the reduction initiates by formation of Ni and followed by reduction of  $\text{Tb}_2\text{O}_3$  on Ni particles. Above 3.1 V, simultaneous reduction of NiO and  $\text{Tb}_2\text{O}_3$  occurs. Similarly, in reduction of  $\text{TiNiO}_3$  powders,

only NiO could be reduced to Ni up to 1.8 V while in order to synthesize TiNi, 3.0 V should be applied (Yong et al., 2006).

### 2.3.2 Anodic Reactions

Oxygen ions transported through molten salt electrolyte are removed from the electro-reduction cell by anodic reactions. The gas formed at the anode leaves the molten salt by bubbling. With these reactions, electrons are fed back to the power source through current collector.

According to Schwandt and Fray (2005), oxidation reactions at the anode side involve formations of CO, CO<sub>2</sub> and/or O<sub>2</sub> gases and given by:



Apparently, inert anodes yield only oxygen gas at the anode. In case of graphite anode, both CO and CO<sub>2</sub> could form together (Bhagat et al. 2008; Chen, 2009). Chen et al. (2000) used gas spectrometer to analyze exhaust gas and detected some O<sub>2</sub> together with CO and CO<sub>2</sub>.

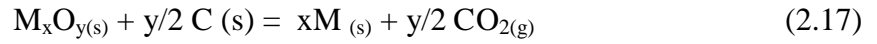
Thermodynamic calculations show that reactions given in Eq. 2.12 - 2.14 are highly favorable at ordinary electro-reduction temperatures, i.e. 600-1000°C (Dring et al., 2005). Fray (2001) states that formation of Cl<sub>2</sub> at the anode by:



This reaction is less favorable than formation of CO, CO<sub>2</sub> and O<sub>2</sub>. As a result, Cl<sub>2</sub> is not observed in electro-reduction processes as long as the applied voltage is less than the decomposition voltage of the electrolyte (Fray and Chen, 2004).

### 2.3.3 Overall Cell Reactions

The overall cell reaction in electro-reduction process is the summation of cathodic and anodic reactions. Qiu et al. (2006) and Sanchez et al. (2007) give the possible overall cell reactions in electro-reduction of an oxide pellet by:

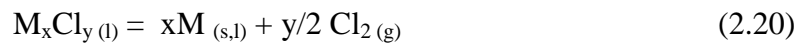


Reaction given in Eq. 2.16 occurs if inert anode is used, while for graphite anode formation of CO and/or CO<sub>2</sub> should be expected. The reduction voltage of an oxide at a specific temperature ( $\Delta E_T$ ) is calculated by using following relations, considering that as both metal oxide and metal are in their pure state:

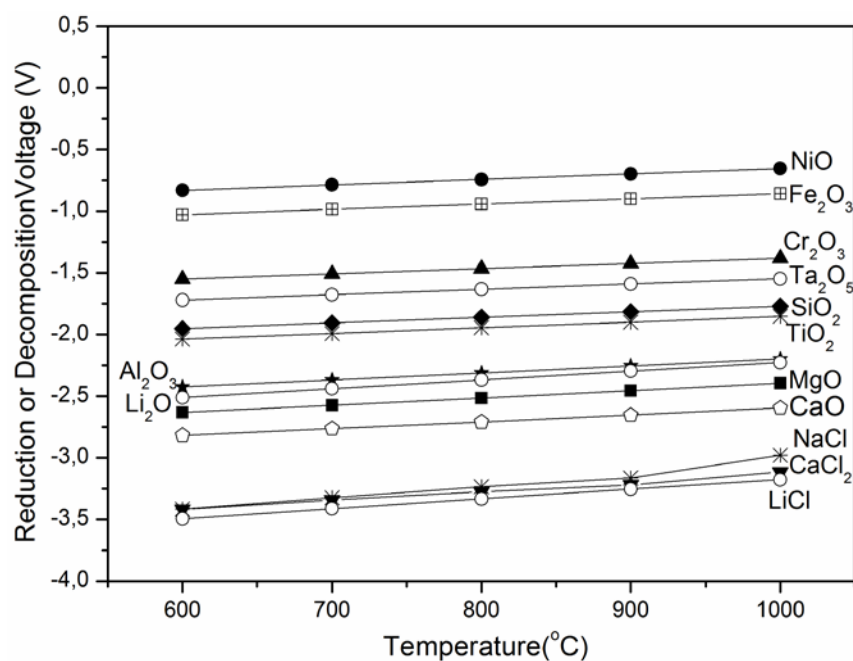
$$\Delta E_T = \Delta E_T^o = -\frac{\Delta G_T^o}{nF} \quad (2.19)$$

Here,  $\Delta E_T^o$  is the standard reduction voltage of metal oxide at temperature T (V);  $\Delta G_T^o$  is the standard Gibbs free energy of overall cell reaction at temperature T (J), n is the number of electrons transferred in the balanced electrochemical reaction and F is Faraday's Constant (96485.3399 C/mol).

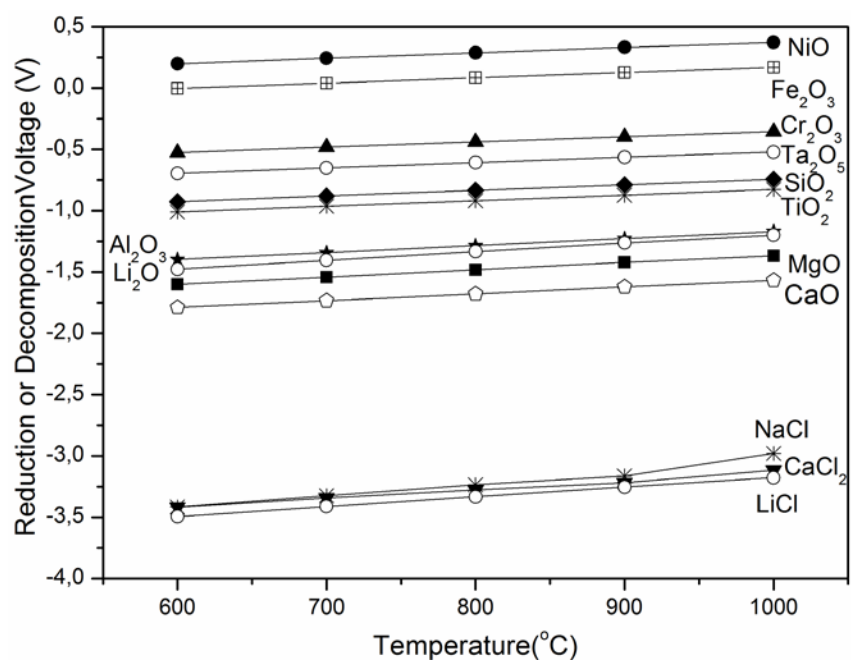
Mohandas and Fray (2004) state that metal chlorides ( $M_xCl_y$ ) are stable up to their decomposition voltages. Above decomposition voltage, they decompose into the alkaline metal (M) and Cl<sub>2</sub> gas by:



Similar to standard reduction potentials of oxides, standard decomposition voltage of metal chlorides could be calculated by using Eq.2.19. Fig. 2.5 shows



(a)



(b)

**Figure 2.5** Standard reduction voltage ( $\Delta E^0$ ) of selected oxides: (a) by formation of  $O_2$ ; (b) by formation of  $CO_2$ . Standard decomposition voltages ( $\Delta E^0$ ) of the selected molten salts are also given in the graphs.

the standard reduction voltages of selected oxides and the standard decomposition voltages of the selected molten salts for a temperature range of 600 °C-1000 °C. Voltage values for reactions, given in Eq. 2.16- 2.18 and Eq. 2.20 could be directly calculated by using F\*A\*C\*T database (F\*A\*C\*T) using Eq. 2.19.

As seen from Fig. 2.5, standard reduction voltages of the selected metal oxides are less than the decomposition voltage of the molten salt electrolytes. Thus, thermodynamically, it is possible to reduce metal oxides to their corresponding metals without decomposing the electrolyte. In order to achieve this, a voltage higher than reduction voltage of the metal oxide should be applied between metal oxide cathode and anode. It should be noted that the use of graphite anode significantly reduces the reduction voltage of the metal oxide compared to the use of an inert anode.

## **2.4 Three Phase Interline (3PI) Model**

The most comprehensive and almost unique approach to explain cathodic events in electro-reduction process is three phases interline (3PI) model developed by Chen and his colleagues (Xiao et al., 2006). According to this model, see Fig. 2.6, reduction occurs and propagates only at metal-oxide-electrolyte interline (Xiao et al., 2007). Oxygen ionizes from oxide and transfers to the electrolyte while electrons transfer from current collector to oxide simultaneously.

Difference in reduction rate of metal oxides could be explained by 3PI model. Some metal oxides, such as  $\text{SiO}_2$ ,  $\text{NiO}$ ,  $\text{Cr}_2\text{O}_3$ , are reduced in a single step process. In these systems, cracks or pores form in the metal due to extensive decrease in the volume of the solid phase (Wang et al., 2008). With penetration of electrolyte through these gaps, electrolyte can reach to new oxide surfaces and deoxidation propagates along those fresh 3PI leaving a metallic skin at the outer surface, see Fig. 2.7.

However, deoxidation of some metal oxides, e.g.  $\text{TiO}_2$ ,  $\text{Nb}_2\text{O}_5$ , necessitates extensive durations. For such oxides, the deoxidation could be a multi-step process. Meanwhile their metals and/or sub-oxides may have significant amount of oxygen solubility. Thus, in these systems, the diffusion of oxygen towards the vicinity of 3PI is quite important (Deng et al., 2005).

Xiao et al. (2007) states that overpotential is the driving force for deoxidation of all metal oxides. The value of total overpotential ( $\eta$ ) can be found by:

$$\eta = E - E_{\text{ext}} - E_{\text{IR}} = \eta_e + \eta_c + \eta_{\text{ohm}} \quad (2.21)$$

Here,  $E$  is the applied voltage (V);  $E_{\text{ext}}$  is the voltage drop due to resistance of external connections (V);  $E_{\text{IR}}$  = voltage drop due to resistance of electrolyte (V);  $\eta_e$  is the overpotential used to govern electro-reduction process (V);  $\eta_c$  is the overpotential used to overcome concentration polarization (V) and  $\eta_{\text{ohm}}$  is the overpotential used to overcome ohmic polarization (V).

Oxygen removal from metal oxide and electro-reduction process is governed by electrochemical component of overpotential ( $\eta_e$ ). However, some of the overpotential is used to overcome ohmic polarization ( $\eta_{\text{ohm}}$ ) which originates from resistance of reduction generated porous metallic skin plus electrolyte within that metallic part. Ohmic polarization increases as reduction proceeds and given by:

$$\eta_{\text{ohm}} = \rho i L \quad (2.22)$$

where,  $L$  is the reduction depth from surface of oxide pellet (cm);  $\rho$  is the summation of the resistivity of porous metal ( $\rho_M$ ) and electrolyte ( $\rho_e$ ) (ohm) and  $i$  is the current density ( $\text{A}/\text{cm}^2$ ).



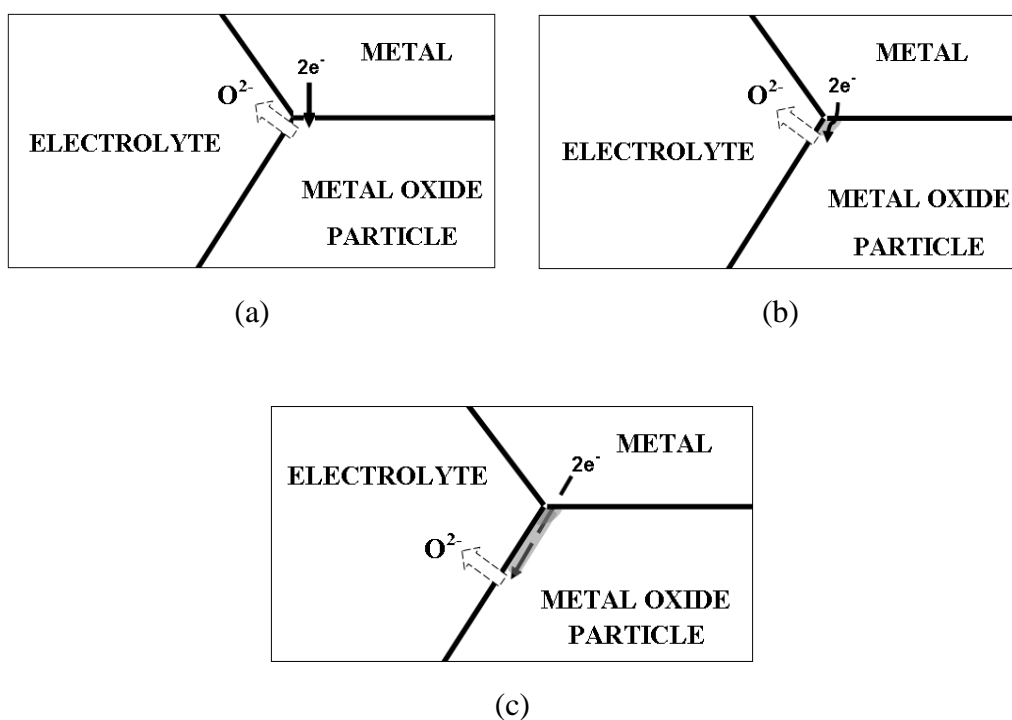


**Figure 2.6** The physical description of 3PI model. The reduction starts from metal-oxide-electrolyte intersection point (a) and propagates through interline where three phases meet (b) and (c). The gray field represents the newly formed metal.

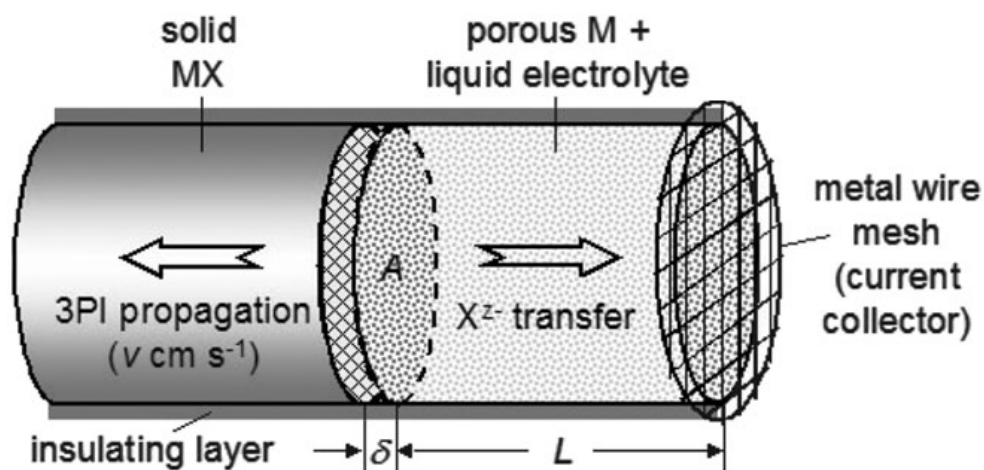


**Figure 2.7** The propagation of electro-reduction process according to 3PI model (Wang et al., 2008).

Some part of the total overpotential is used to overcome the concentration polarization ( $\eta_c$ ), which arises from the difference in concentration of oxygen between bulk of electrolyte and that near to 3PI. According to Deng et al. (2005), its value could be calculated by:

$$\eta_c = \frac{RT}{nF} \ln \left( \frac{C_R^S}{C_R^0} \right) = \frac{RT}{nF} \left[ \ln \left( \frac{i(L + L_o)}{nFD_R C_R^0} + 1 \right) \right] \quad (2.23)$$

Here,  $C_R^S$  is the concentration of  $O^{2-}$  in electrolyte near to 3PI ( $\text{mol/cm}^3$ ),  $C_R^0$  is the concentration of  $O^{2-}$  in the bulk of electrolyte ( $\text{mol/cm}^3$ ),  $L$  is the reduction depth from surface of oxide pellet (cm),  $L_o$  is the effective depth of reduction (cm),  $D_R$  is the diffusion coefficient of  $O^{2-}$  in electrolyte within pores of pellet ( $\text{cm}^2/\text{s}$ ),  $i$  is the cathodic current density ( $\text{A/cm}^2$ ),  $R$  is universal gas constant ( $8.314 \text{ J/mol K}$ ),  $T$  is deoxidation temperature (K),  $n$  is the number of electrons transferred in the balanced electrochemical reaction and  $F$  is Faraday's Constant.

For insulating oxides reduced in single step process, Chen and his colleagues developed an electrochemical approach to calculate the movement rate of 3PI and constructed the relation between overpotential and reduction rate. According to Xiao et al. (2007), at very short times of deoxidation ( $t$ ), the amount of reduction-generated metal is small. As a result,  $\eta_{ohm} \approx 0$ . Then, reduction depth ( $L$ ) at any time ( $t$ ) in a non-porous oxide can be approximated to:

$$L = \sqrt{\left( \frac{1}{b^2} + \frac{2at}{bq} \right)} - \frac{1}{b} \quad (2.24)$$

where, both  $a$  and  $b$  are constants. For longer deoxidation durations,  $\eta_c$  and  $\eta_{ohm}$  increases and reach to constant values, i.e.  $\eta_c^*$  and  $\eta_{ohm}^*$  after a specific time  $t_{min}$  and certain depth  $L_{min}$ . In that case, current density ( $i$ ) and reduction depth ( $L$ ) are approximately given by:

$$i = \frac{\eta_{ohm}^*}{\sqrt{\rho^2 L_{min}^2 + \frac{2\rho\eta_{ohm}^*(t-t_{min})}{q}}} \quad (2.25)$$

$$L = \sqrt{\frac{2\eta_{ohm}^*}{q\rho}(t-t_{min}) + L_{min}^2} \quad (2.26)$$

Here,  $\rho$  is the summation of resistivity of porous metal ( $\rho_M$ ) and electrolyte ( $\rho_e$ ) (ohm) and  $q$  is the charge needed to reduce unit volume of metal oxide ( $C/cm^3$ ).

The equations given above indicate that total current ( $I$ ) decreases with time ( $t$ ) in electro-reduction process. This is actually verified in different studies (Xiao et al., 2006; Chen et al., 2004). Meanwhile, as concentration polarization ( $\eta_c$ ) and ohmic polarization ( $\eta_{ohm}$ ) increases with time in a constant voltage experiment, the reduction rate of oxide sample decreases with time.

3PI model is also used to explain how electro-reduction starts and propagates in porous oxide pellets. Yan and Fray (2005) speculated on and concluded that deoxidation does not occur uniformly, see Fig. 2.8. After formation of Ca-bearing oxides, deoxidation starts from particles touching to the current collector, Fig. 2.8 (a). At that stage, cell current is relatively low due to limited number of sites for oxygen removal.

It was observed that deoxidation propagates faster at the surface but slower through the depth of the porous oxide pellets, see Fig. 2.8 (b) (Jin et al., 2004). With propagation of deoxidation on the surface, more oxygen could be removed from the pellet and current passing through the cell increases (Gordo et al., 2004). When the surface is completely reduced to lower oxides, current reaches a maximum value.

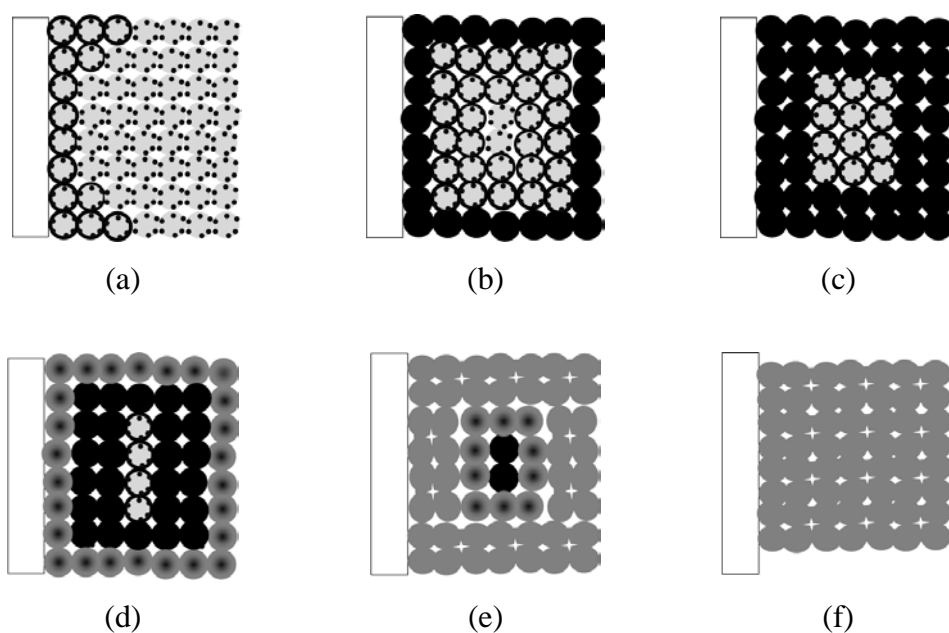


**Figure 2.8** Deoxidation of a metal oxide pellet. The oxide pellet gradually deoxidizes through (a) to (f). Note that deoxidation proceeds from outside to inside of the pellet (Yan and Fray, 2005).

Conversion to metallic state starts from surface of the pellet and propagates towards its center, Fig. 2.8 (a) – (f). As the reduced surface has less porosity and higher mass-transfer resistance to  $O^{2-}$ , concentration and ohmic polarizations increase and current decreases at this stage (Xiao et al. (2007)). For metals with oxygen solubility, slow reduction could also be attributed to slow transport of oxygen in the metal (Fray and Chen, 2004). Depending on the synthesized material and deoxidation temperature, final powders could fuse together, accompanied by shrinkage of the pellet, Fig. 2.8 (f). Final particle sizes up to 10  $\mu\text{m}$  were reported in the literature (Ma et al., 2006).

## 2.5 Factors Affecting the Electro-reduction Process

Assadi (2006) asserts that the final aim of electro-reduction studies is to answer the question: what does determine the reducibility of a metal oxide? It is already known that different oxides have different reducibilities. Some oxides, e.g.

Cr<sub>2</sub>O<sub>3</sub>, NiO, are deoxidized easily (Yasuda et al., 2005; Qiu et al., 2005), while even partial deoxidation of some others, e.g. Al<sub>2</sub>O<sub>3</sub>, B<sub>2</sub>O<sub>3</sub>, is very difficult (Yan, 2008; Ors et al., 2009). The variations and factors affecting electro-reduction can be understood by examination of electro-deoxidation process from different points of view.

Two main properties affect the reducibility of a metal oxide: its reduction voltage and the number of sub-oxides in that metal-oxygen system. The reduction voltage imposes a thermodynamic criterion specific to the oxide and temperature. It is already known that metal oxides with less positive reduction voltage are more difficult to reduce. Meanwhile, previous studies show that oxides with high number of sub-oxides, e.g. TiO<sub>2</sub>, are more difficult to reduce than oxides reduced in a single-step process, such as NiO. It is considered that in multi-step reduction, each reduction step may impose different thermodynamic and kinetic criteria. In that case, all requirements must be satisfied for the progress of deoxidation.

According to Kar and Evans (2006), solid-state phenomena should be included to explain cathodic events in electro-reduction. They consider that electro-reduction occurs in three consecutive steps:

1. Mass transport of oxygen from bulk oxide toward 3PI, if oxide has oxygen solubility.
2. Ionization of oxygen and simultaneous charge transfer from cathode to the electrolyte at 3PI yielding structural changes in the solid state.
3. Diffusion of O<sup>2-</sup> dissolved in the electrolyte through the pores of the pellet.

Different studies validate this sequence stating that they occur in series and the slowest step determines the rate of reduction (Xu et al., 2005; Wang et al., 2006).

### 2.5.1 Mass Transport of Oxygen in Bulk Oxide

In electro-reduction, mass transfer of oxygen occurs as a result of concentration gradient (diffusion) of oxygen and electric field (electromigration) (Wang et al., 2006). According to Chen and Fray (2001), mass transfer of oxygen in solid state is a crucial parameter when the oxide or the synthesized metal has oxygen solubility. Many transition metals-oxygen systems, e.g. Ti-O, Nb-O, Ta-O, Zr-O, and rare earth- oxygen systems, e.g. La-O, Tb-O, Nd-O, fall in this group. Both sub-oxides and metals of those systems have reasonable amount of oxygen solubility. For these oxides, the low deoxidation rate is attributed to slow transport of oxygen in solid state (Chen et al., 2004). In contrast to that, oxygen solubility is very limited for some other metal-oxygen systems, e.g. Al-O, Mg-O, Ni-O, Cr-O. In these systems, oxides are highly stoichiometric and metals have extremely limited oxygen solubility, e.g. ca. 500 ppm for Ni at 900 °C (Park and Altstetter, 1987).

Wang et al. (2006) states that as diffusion coefficient of  $O^{2-}$  in solid Tb ( $10^{-9}$  -  $10^{-10}$   $\text{cm}^2 \text{s}^{-1}$ ) is much lower than that of  $O^{2-}$  in  $\text{CaCl}_2$  ( $6 \times 10^{-8}$  -  $1.5 \times 10^{-7}$   $\text{cm}^2 \text{s}^{-1}$ ), i.e. solid state diffusion is rate determining step in the electro-reduction of  $\text{Tb}_2\text{O}_3$ . In order to minimize this, Yan and Fray (2005) advise to use small oxide powders by decreasing the diffusion path of oxygen in solid phase. According to Wang et al. (2006), diffusion of oxygen in the solid is the rate-determining step especially at high overpotential and low synthesis temperature.

### 2.5.2 Oxygen Ionization, Charge Transfer and Structural Changes

Deoxidation reaction, given in Eq. 2.2, involves many solid-state phenomena: electron transfer from metal to oxide, ionization of oxygen, heterogeneous charge ( $O^{2-}$ ) transfer from oxide to the electrolyte and the formation of a new phase in solid state. According to Wang and Li (2004), charge transfer resistance is one of the most important barrier in deoxidation.

Electronic conductivity of oxide is important such that electron transfer resistance between metal and oxide is related with the electronic conductivities of metal and oxide (Qiu et al., 2005). According to author, both NiO and Cr<sub>2</sub>O<sub>3</sub> are electronic conductors at 900 °C. As a result, electron transfer resistance is small at 3PI. There are many examples pointing out that electronic conductivity is important in electro-reduction. For example, reduction of highly insulating oxide materials, such as TiO<sub>2</sub>, SiO<sub>2</sub>, Al<sub>2</sub>O<sub>3</sub>, proceeds on either sub-oxides or calcium bearing compounds, both of which are known as electronically conducting in some extent (Wu et al., 2007; Schwandt and Fray, 2005; Yan and Fray, 2009). Meanwhile, it was found that in co-presence of Al<sub>2</sub>O<sub>3</sub> and Ca<sub>x</sub>AlO<sub>(3+x)</sub>, reduction occurs via electronically conducting calcium bearing compound although its reduction voltage is less positive than that of Al<sub>2</sub>O<sub>3</sub> (Yan, 2008). Additionally, according to Yan and Fray (2005) presence of electronically conducting phases increases the number of paths for transport of electrons and offer new 3PI for unreduced particles.

Ionized O<sup>2-</sup> ions must pass to electrolyte immediately as there is no place to accommodate O<sup>2-</sup> ions. It was found that charge (O<sup>2-</sup>) transfer is the rate-determining step especially at low overpotential (Wang et al., 2006). Similar to other reactions, activation energy describes how much energy is necessary to transfer O<sup>2-</sup> ions from solid to the electrolyte. In deoxidation studies, charge transfer resistance and activation energy values up to ca. 100 Ω and 200 kJ/ mol were reported, respectively. Two important process parameters affecting charge transfer resistance is temperature and applied voltage. The resistance value decreases with increasing deoxidation temperature. The effect of temperature is more significant at low applied voltages. According to Wang et al. (2006), in reduction of Nb<sub>2</sub>O<sub>5</sub>, increasing deoxidation temperature from 700 °C to 800°C decreases charge transfer resistance values between two to six folds.

Similar to temperature, an inverse relation exists between applied voltage and charge transfer resistance: the higher the voltage applied, the lower the resistance

is. The effect of voltage is significant especially at low temperatures. In deoxidation of Nb<sub>2</sub>O<sub>5</sub>, 5-10 folds decrease is observed in charge transfer resistance value, when the voltage is increased two folds (Wang et al., 2006). In study of Wang and Li (2004), a similar relation is observed for both reduction of TiO<sub>2</sub> to TiO and TiO to Ti. In parallel to the charge transfer resistance, the activation energy also decreases with increasing applied voltage.

AC impedance technique is used to determine charge transfer resistance in electro-reduction experiments. The selection of a suitable equivalent circuit is crucial to obtain the reasonable values. Activation energies for charge transfer can also be calculated from resistance values. According to Wang et al. (2006), charge (O<sup>2-</sup>) transfer resistance ( $R_{ct}$ ), derived from Butler-Volmer equation, is related with activation energy ( $E_a$ ) by following equation:

$$R_{ct} = \frac{BT}{\exp(-\frac{E_a}{RT})} \quad (2.27)$$

Here, B is constant, R is universal gas constant (8.314 J/mol K) and T is deoxidation temperature (K).

By using  $\ln (T/R_{ct})$  vs.  $1/T$  plots, activation energy for O<sup>2-</sup> transfer can be obtained for different applied voltages. It should be noted that if deoxidation occurs stepwise through sub-oxides, each step has its own transfer resistance and activation energy (Wang and Li (2004)). Thus, impedance measurements are frequently conducted at different applied voltages.

Yan and Fray (2005) points out that the large surface area of oxide pellet facilitates the cathodic ionization and charge transfer of oxygen ions at 3PI. This is actually given in Eq. 2.27, such that the constant term B contains surface area term in its denominator. Thus, as surface area increases charge transfer resistance decreases. Physically, this can be explained in a way that as the active surface



area increases, there would be more sites for transfer of  $O^{2-}$  from oxide to electrolyte. High surface area in the oxide pellet is achieved by production of the pellet with open porosity. The smaller the pores and the more open the porous structure are, the higher the surface area of the oxide pellet has (Gordo et al., 2004; Sanchez et. al, 2007).

According to Wang et al. (2006), surfaces where metallic Ca is deposited from the electrolyte form inactive regions for oxygen removal as the presence of metallic calcium prevents oxygen transfer from oxide to the electrolyte. If reduction proceeds on sub-oxides, formation of Ca-bearing oxides at the start of electro-reduction has similar effect, i.e. they block sites for oxygen removal (Schwandt and Fray, 2005). According to Schwandt and Fray (2005), calcium intercalation increases the volume of the oxide. The dimensional increase may lead to shrinkage of some pores and even may results a decrease in the amount of open porosity and total surface area.

Structural changes induced by oxygen removal introduce different factors in electro-reduction. A transformation in crystal structure might be necessary when metal phase forms from oxide. This is also valid when multi-step reduction occurs through sub-oxides. According to Schwandt and Fray, 2005, transformations may necessitate nucleation and growth stages, which could be slow and might affect the rate of reduction. Alexander et al. (2006) states that transformation of  $TiO_2$  to  $Ti_4O_7$ , then  $Ti_3O_5$  and finally  $Ti_2O_3$  is easy, since cooperative mechanisms occur during transformations. However, steps, at which  $CaTi_2O_4$  and  $TiO$  form, are found to be much slower that was attributed to reconstructive changes in the solid. Meanwhile, these atomic rearrangements may end up with the formation of voids when the newly formed material is more densely packed than the consumed one (Sanchez et al., 2007). According to Alexander et al. (2006), more 3PI is created in the formation of  $CaTi_2O_4$  and  $TiO$ , as the electrolyte could reach to fresh oxide surfaces via voids. Apparently, the formation of fresh 3PI increases the deoxidation rate of the oxide pellet.

### 2.5.3 Pore Diffusion

The term, pore diffusion, is used to describe diffusion of oxygen ions into the porous network of metal oxide pellet filled by molten salt electrolyte (Wang and Li, 2004). According to Wang et al. (2006), mass transport of  $O^{2-}$  ions into the electrolyte could be the rate-determining step. Jin et al. (2004) states that the diffusion coefficient of  $O^{2-}$  in pores of  $SiO_2$  (porosity 30-56 %, deoxidized in  $CaCl_2$ ) varies between  $2.8 \times 10^{-6} \text{ cm}^2 \text{ s}^{-1}$  and  $6.8 \times 10^{-6} \text{ cm}^2 \text{ s}^{-1}$  at 900 °C. This is lower than diffusion coefficient of  $O^{2-}$  in bulk  $CaCl_2$ ,  $2.5 \times 10^{-5} \text{ cm}^2 \text{ s}^{-1}$  at the same temperature. According to Wu et al. (2007), pore diffusion is the rate-determining step when the dissolved oxygen ions have difficulty to reach out of the oxide pellet.

For fast removal of  $O^{2-}$  ions from pores to the out of the pellet, the distance travelled by  $O^{2-}$  in the pores of oxide pellet should be minimized. According to Yan and Fray (2005), this distance can be minimized by the use of thin oxide pellet in deoxidation. Yan and Fray (2005) examined  $Nb_2O_5$  pellets with different thicknesses and found that the pellet with 10 mm in thickness contains six-fold more oxygen than pellet with 2 mm thickness has. Wang et al. (2006) proposes that if the thickness of  $Tb_4O_7$  pellet is reduced from 2.0 mm to 1.5 mm, the energy consumed to reduce the whole pellet is nearly halved. Wu et al. (2007) points out that the efficiency and success of electro-reduction is significantly improved when the thickness of oxide pellets is reduced to 1.5 mm or lower. Another way to minimize the distance travelled by  $O^{2-}$  in the pellet is the use of an oxide pellet with coarse pores. Wang et al. (2006) states that the estimated pore diffusion is much higher when the pores are large which form linear paths for oxygen diffusion out of the oxide pellet.

It was reported that the metallic phase at the external surface of the oxide pellet may form a barrier for pore diffusion. According to Kar and Evans (2006), this is true especially if the target metal and/or compound have low melting point. During synthesis of those materials, high temperatures may lead to the growth of

metal particles, see Fig. 2.8. This may hinder the diffusion of  $O^{2-}$  ions by decreasing the number of pores open to external surface of the oxide pellet (Gordo et al., 2004). With the inward growth of metallic layer, pore diffusion decreases with time.

Similarly, formation of Ca-bearing oxides at the beginning of electro-reduction increases the volume of the metal oxide. The dimensional increase may lead to shrinkage of some pores yielding lower pore diffusion (Alexander et al., 2006).

Another factor determining how fast  $O^{2-}$  ions are removed from porous network of oxide pellet is the velocity of  $O^{2-}$  in the electrolyte. According to Honig and Ketelaar (1966), total flux of ions in an electrolyte under the influence of electric field and concentration gradient is given by:

$$V_i \propto J_i = C_i \mu_i E - D_i \frac{\partial C_i}{\partial x} \quad (2.28)$$

where,  $V_i$ ,  $J_i$ ,  $C_i$ ,  $D_i$  and  $\mu_i$  are velocity (cm/s), flux (mol/cm<sup>2</sup> s), concentration (mole/cm<sup>3</sup>), diffusion coefficient (cm<sup>2</sup>/s) and mobility (cm<sup>2</sup>/V s) of ions, respectively;  $E$  is the applied voltage (V) and  $x$  is the distance (cm).

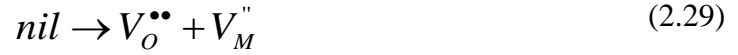
As seen from the Eq. 2.28, higher voltages facilitate oxygen transport in the electrolyte. Similarly, it is known that mobility of charged species in ionic liquids increases as temperature increases (Masset and Guidotti, 2007).

## **2.6 Diffusion of Oxygen in Solid-State and Electronic Conductivity of Oxides**

According to Pirovano et al. (2007) and Kharton et al. (2008), both electronic conductivity and transport of oxygen in metal oxides rely on their defect

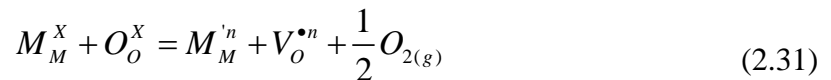
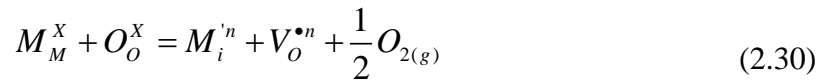
structures. Transport of electrons occurs via favorable energy levels in one-dimensional features in the oxide (Wang et al., 1995). Similarly, oxygen transport is achieved through bulk and/or boundary motion of ions.

Metals with limited number of oxidation states, e.g. Al and Mg, form stoichiometric oxides. As a result, they mainly contain stoichiometric point defects. From variety of types, the most common defect creating vacancy site in oxygen sub-lattice is Schottky type, shown by defect reaction:



Here,  $V_O^{\bullet\bullet}$  oxygen vacancy with relative charge 2+ and  $V_M^{\prime\prime}$  represent oxygen metal vacancy with relative charge 2-, formed in metal oxide (MO). Schottky type defect keeps the original M/O ratio in the metal oxide and does not create new charge carriers.

Non-stoichiometry is deviation from the ideal ratio of metal and oxygen atoms present in the unit cell. Cations in transition metal oxides, e.g.  $Nb_2O_5$ ,  $TiO_2$ ,  $MnO_2$ ,  $V_2O_5$  etc., have many oxidation states, which may change readily. Thus, they possess many sub-oxides and more likely to be non-stoichiometric. Actually, many non-stoichiometric defect reactions are possible in reducing conditions. They are given in Eq. 2.30-2.34 for metal oxide MO:



$$O_o^x = V_o^\bullet + e' + \frac{1}{2} O_{2(g)} \quad (2.33)$$

$$O_o^x = V_o^x + \frac{1}{2} O_{2(g)} \quad (2.34)$$

Here,  $V_o^{\bullet n}$  represents a vacancy in oxygen site with positive relative charge  $n$  ( $0 \leq n \leq 2$ );  $O_o^x$  represents oxygen atom in oxygen site with neutral relative charge;  $M_i^{\bullet n}$  represents interstitially placed metal atom with negative relative charge  $n$  ( $0 \leq n \leq 2$ );  $M_M^{\bullet n}$  represents metal atom in metal site with negative relative charge  $n$  ( $0 \leq n \leq 2$ );  $e$  represents electron and  $n$  is the number of electrons.

As it can be seen from Eq. 2.30 and Eq. 2.31, the oxidation state of metal may decrease by localization of electrons on metal atoms. Oxygen vacancies may also form in the oxygen sub-lattice without reduction of the metal cation, see Eq. 2.32-2.34. It should be noted that the vacant oxygen site, surrounded by positive ions, represents a site with positive charge to which free electrons may be attracted. Thus, Eq. 2.35 and 2.36 may also accompany to the formation of oxygen vacancies ( $V_o^{\bullet n}$ ):

$$V_o^{\bullet\bullet} + e' = V_o^\bullet \quad (2.35)$$

$$V_o^\bullet + e' = V_o^x \quad (2.36)$$

Fig. 2.9 shows different defects formed according to reactions given in Eq. 2.30-2.34.

Lattice diffusion of oxygen is the diffusion of oxygen atoms in the crystal via different mechanisms: vacancy or interstitial (Karen, 2006). In the vacancy mechanism, the motion of oxygen atoms is in the opposite direction that of vacancies. Interstitial mechanism is dominant when dissolved oxygen moves in the metal lattice, e.g. diffusion of oxygen in metallic Ti (Hongyan et al., 2004).

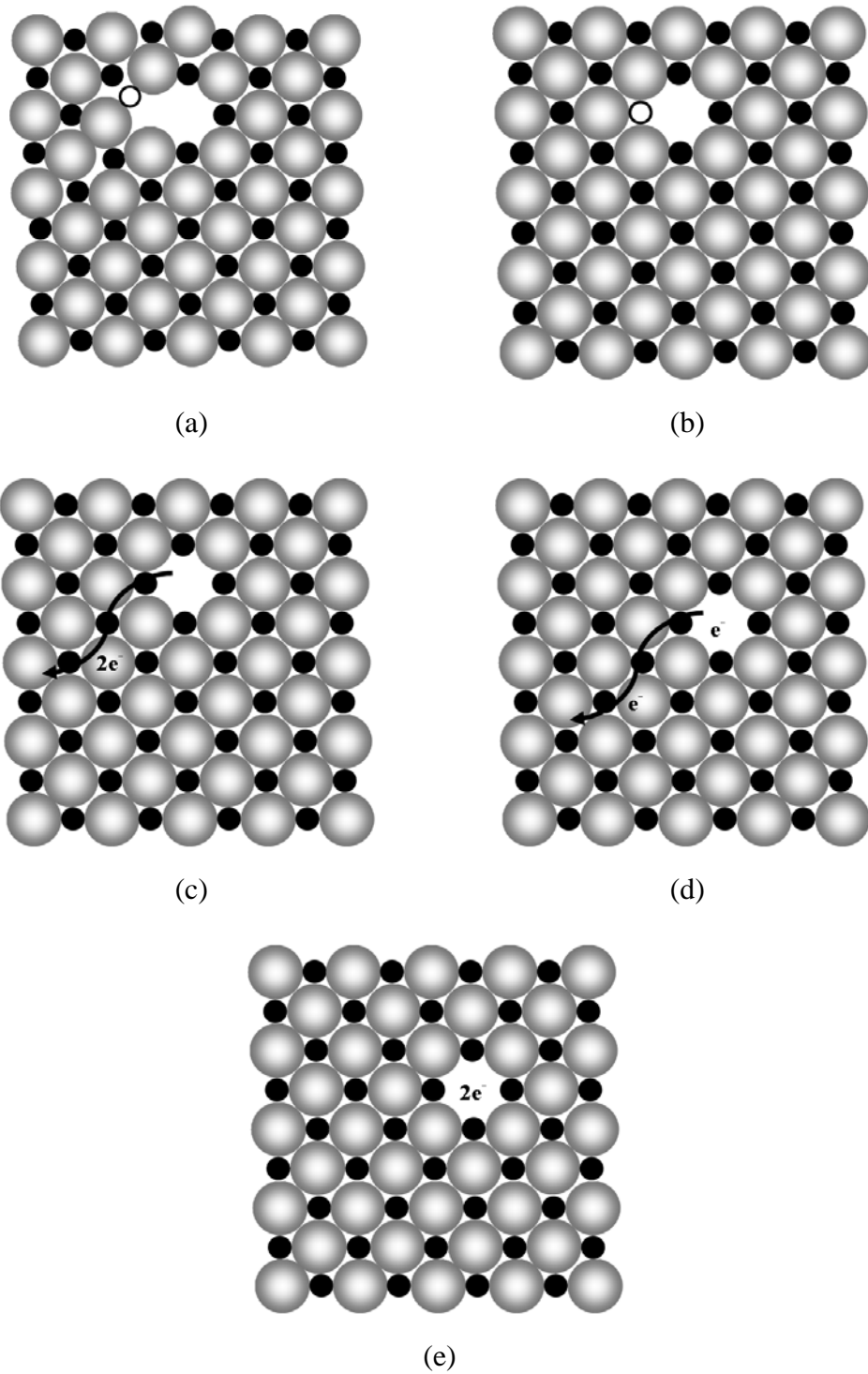


**Figure 2.9** Point defects observed in metal oxides in reducing conditions. Black spheres represent metal atoms and gray spheres represent oxygen atoms. (a) reduced cation at interstitial site, (b) reduced cation at cation site, (c) electrons are completely mobile, (d) one electron is trapped at oxygen vacancy and (e) two electrons are trapped in oxygen vacancy.

Diffusion coefficient (D) is the common term to define the speed of mass transport at different conditions and mechanisms. The higher the value, the faster the transport is. Experimentally, it is given by:

$$D = D_o \exp\left(-\frac{Q_a}{RT}\right) \quad (2.37)$$

where,  $D_o$  is the coefficient of exponential function in diffusion equation ( $\text{cm}^2/\text{s}$ ),  $Q_a$  is the activation energy for diffusion ( $\text{J/mol}$ );  $R$  is the universal gas constant ( $8.314 \text{ J/mol K}$ ) and  $T$  is the temperature (Kelvin degree).

As seen from the Eq. 2.37, an increase in the deoxidation temperature exponentially increases the diffusion coefficient. Additionally, in order to achieve the atomic motion, the activation energy must be overcome. Similar to the activation energy, diffusion coefficient varies with mechanism of transport and material itself. Surface diffusion (at boundaries) is found to be more favorable in some cases (Martin, 2005).

The native charge carriers in an oxide are the cations, anions, electrons, and electron holes. The total conductivity ( $\sigma$ ) is then given by:

$$\sigma = \sigma_a + \sigma_c + \sigma_e + \sigma_h \quad (2.38)$$

where,  $\sigma_a$ ,  $\sigma_c$ ,  $\sigma_e$ ,  $\sigma_h$ , are conductivities originating from transport of anions, cations, electrons and holes, respectively ( $\text{S/cm}$ ).

According to Kofstad and Norby (2007), ionic conductivity ( $\sigma_{\text{ion}}$ ) follows Nernst-Einstein equation for species moving by hoping mechanism:

$$\sigma_{\text{ion}} = \sum_i (z_i e)^2 C_i \frac{D_i}{kT} \quad (2.39)$$

Here,  $z$  is the net charge of ion,  $e$  is the unit charge ( $1.602 \times 10^{-19}$  C);  $C_i$  is the concentrations of ion ( $\text{kg}/\text{cm}^3$ );  $D_i$  is the diffusion coefficient of ion ( $\text{cm}^2/\text{V s}$ );  $k$  is Boltzmann Constant ( $1.3806503 \times 10^{-23} \text{ m}^2 \text{ kg s}^{-2} \text{ K}^{-1}$ ) and  $T$  is the temperature (K). Consequently, the diffusion coefficient, concentration and charge of the ionic specie have significant contribution to the ionic conductivity.

It is known that intrinsic electronic conductivity ( $\sigma_{el}$ ) of an oxide material can be written as:

$$\sigma_{el} = \sigma_e + \sigma_h = C_e e \mu_e + C_h e \mu_h = K \exp\left(-\frac{E_g}{2kT}\right) \quad (2.40)$$

Here,  $\sigma_e$  and  $\sigma_h$ , are conductivities originating from transport of electrons and holes, respectively ( $\text{S}/\text{cm}$ );  $C_i$  is the concentrations of charge carrier ( $\text{unit}/\text{cm}^3$ );  $\mu_i$  is the mobility of charge carrier ( $\text{cm}^2/\text{Volt sec}$ );  $K$  is constant;  $E_g$  is the band gap of the oxide (eV). Apparently, the equation shows that electronic conductivity decreases with increasing band gap.

As given before, in reducing conditions, oxygen and electrons are predominant charge carriers. In that case, total conductivity ( $\sigma$ ) is summation of ionic ( $\sigma_{ion}$ ) and electronic conductivities ( $\sigma_{el}$ ), given by:

$$\sigma = \sigma_{ion} + \sigma_{el} = 2 e [V_O^{2\bullet}] \mu_{V_O} + e C_e \mu_e \quad (2.41)$$

, where,  $[V_O^{2\bullet}]$  is the concentration of doubly charged  $\mu_{V_O}$  mobility of oxygen vacancies;  $C_e$  and  $\mu_e$  is the concentration and mobility of electrons, respectively.

According to Kofstad and Norby (2007), the mobility of electrons is much higher than that of oxygen vacancies thus total conductivity of a non-stoichiometric metal oxide in reducing conditions can be approximated to electronic conductivity of the oxide.



## 2.7 Summary

Solid-state electro-reduction techniques offer a good opportunity to synthesize pure metals as well as multi-component metal alloys. The process itself includes a series of complex phenomena, i.e. removal of oxygen from solid state, transport of oxygen ions through the pores of oxide pellet, transport of oxygen ions in the bulk of electrolyte and anodic reactions.

The success of electro-deoxidation initially depends on the thermodynamic criteria. The applied voltage should be higher than the reduction voltage of the metal oxide to be reduced. However, one should pay attention to phase changes during electro-reduction. Formation of new phases imposes new thermodynamic criteria for electro-reduction. As a result, different reduction routes could be followed in different oxide systems.

There are many factors affecting the success of reduction process even if the thermodynamic criterion is fulfilled. These factors may put some kinetic barrier for electro-reduction of oxides. Practically, the slowest step determines the overall rate of deoxidation. Process parameters, i.e. applied voltage, temperature and time, are used to overcome these kinetic barriers.

The preparation of oxide pellet is crucial for a successful reduction. Highly porous oxide pellets are preferred as they offer more sites for oxygen removal. The use of thin oxide pellets and presence of coarse (linear) pores is helpful to minimize pore diffusion.

Inherent properties of metal oxide, sub-oxides and the final metallic phase are crucial for reducibility of an oxide pellet. The ease of oxygen and electron transport in solid state are two of these properties which favor the deoxidation kinetics. Similarly, extreme distortions in crystal structure by formation of new phases could be helpful in formation of new sites for oxygen removal. On the

other hand, nucleation and growth of new phases might be energy and time consuming. The development of those features in electro-reduction totally depends on the inherent properties of materials present in the pellet during deoxidation.

In summary, electro-deoxidation is not purely electrochemical technique but also involves many solid-state phenomena. Without understanding them, it is rather difficult to optimize processing conditions and obtain the required compound. Although each oxide has its own characteristic properties, some general rules and systematic approaches, e.g. 3PI model, can be put forward to elucidate problems about reducibility.

## CHAPTER 3

### SYNTHESIS OF FeTi FROM MIXED OXIDE PRECURSORS

#### 3.1 Introduction

There has been considerable interest in recent years in the solid-state deoxidation of oxides which would yield alloys and compounds at targeted compositions, e.g. Fray (2001), Suzuki et al. (2004). It is an electrolysis process in molten salt, first developed in the 90's by Fray and co-workers for extraction of Ti from  $\text{TiO}_2$  (Chen et al., 2000). The process makes use of sintered oxide pellet as a starting material, connected to a current collector as the cathode and electrolyzed in a molten salt using a graphite anode. During electrolysis, oxygen in the cathode is ionized, dissolved in the electrolyte and discharged at the anode in the form of CO or  $\text{CO}_2$ . Thus unlike conventional electrolysis where the metal is deposited onto the cathode, here the cathode is gradually de-oxidized leaving the metallic elements behind.

Due to this special nature of the cathode, the preparation of oxide pellet as a cathode material has attracted considerable attention. In the case where the target is pure metal, e.g. Nb (Yan and Fray, 2005), Ta (Hu and Xu, 2006), efforts are mainly concentrated on controlling the porosity of the pellets. Normally, pellets of high porosity are preferred since this is believed to improve the kinetics of deoxidation. In this context, especially in Ti, the formation of  $\text{CaTiO}_3$ , which occurs as a result of reaction of  $\text{TiO}_2$  with the molten salt, has received considerable attention (Jinag et al., 2006). In the case of compounds, an added consideration is the stoichiometry of the product itself. As shown by Qiu et al. (2006), oxides of the same mixture could lead to different products depending on

the sintering conditions. In this study, the target compound,  $\text{TbFe}_2$ , can be obtained when the pellet is sintered at an elevated temperature, i.e. 1200 °C.

The current work deals with the deoxidation of mixed oxides,  $\text{Fe}_2\text{O}_3$  and  $\text{TiO}_2$ , and concentrates on the choice of sintering conditions which would yield FeTi intermetallics. Here, the target composition, FeTi, is a well-known compound that reversibly stores hydrogen at room temperature (Reilly and Wiswall, 1974).

### 3.2 Materials and Methods

Starting materials,  $\text{Fe}_2\text{O}_3$ ,  $\text{TiO}_2$  (Rutile), were of technical grades.  $\text{Fe}_2\text{O}_3$  powders were needle like and  $\text{TiO}_2$  were rounded as given in Fig. 3.1. Both were roughly 1  $\mu\text{m}$  in size but in an agglomerated state. A mixture of  $\text{Fe}_2\text{O}_3$  and  $\text{TiO}_2$  in molar proportions of 1:2 was prepared, i.e. Fe:Ti ratio of 1:1, using a Spex mill at ball-to-powder ratio (B/P) of 1. After 30 minutes of mixing, the mixture was further hand mixed adding some PVA solution and allowed to air dry for 24 hours. The powder mixture was then cold compacted into a cylindrical pellet at a pressure of 110 MPa. These pellets were 18 mm in diameter and 2-3 mm in thickness weighing approximately 2 grams.

Pellets were sintered at elevated temperatures. For this purpose, they were heated up in a tube furnace in air atmosphere to the predetermined temperatures with a heating rate of 5 °C/min. Oxide pellets were held at that temperature for 2 hours.

Electro-deoxidation experiments were conducted in an electrolytic cell. It comprises a stainless steel crucible for holding molten electrolyte and electrodes mounted on a top cover immersible into the electrolyte. There were two pairs of electrodes; one pair was for pre-electrolysis and the other was for deoxidation. The reactor was gas tight, allowing electrolysis to be conducted in an argon atmosphere (99.995 % purity) maintained at a flow rate of 150-250 ml/min.

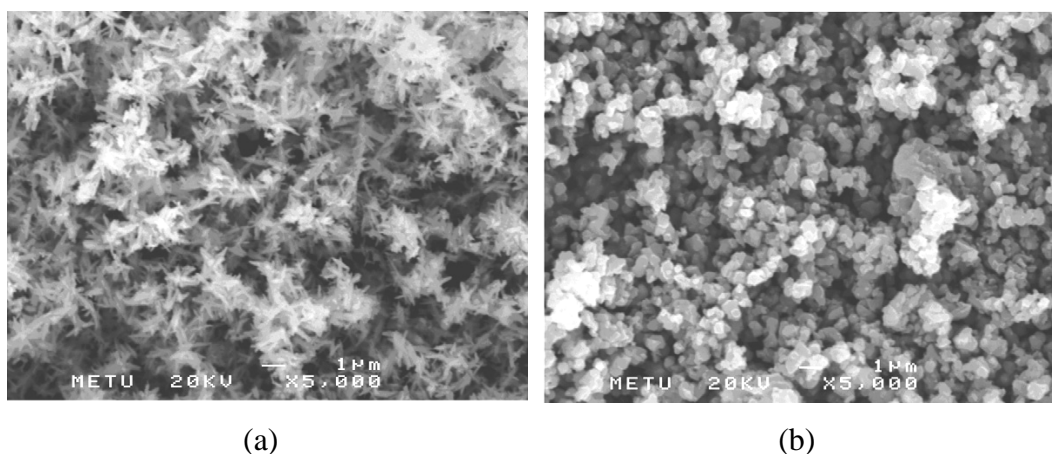


**Figure 3.1** SEM images of oxide powders; (a)  $Fe_2O_3$  and (b)  $TiO_2$  used in the experiments. Note that  $Fe_2O_3$  powders are needle-like whereas  $TiO_2$  is in the form of rounded particles.

1000 g of  $CaCl_2$  was used as electrolyte. This was heated to  $900\text{ }^{\circ}\text{C}$ , i.e. the electrolysis temperature, slowly so as to reduce its moisture content. The electrolyte was further purified by pre-electrolysis using a graphite anode and stainless steel cathode, at a potential of 3.0 V for 6 hours. The current, during the pre-electrolysis following an initial transient rise, decreases gradually over a period of typically 4 hours, finally settling down to a constant value. After pre-electrolysis, these auxiliary electrodes were removed and the electrolysis was initiated by immersing the working electrodes, i.e. oxide pellet (cathode) and a fresh graphite rod (anode) into the molten salt. The electrolysis was carried out at a constant potential of 3.2 V for 24 hours. Current vs. time data were collected by a computer. The temperature of the system was controlled  $\pm 10\text{ }^{\circ}\text{C}$  of the selected temperature.

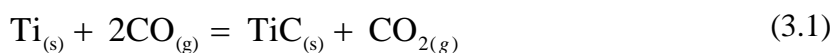
Following electrolysis, the pellet and the graphite were removed from the electrolyte and positioned above the melt. After the system was cooled down to room temperature, the reactor lid was opened and the sample was removed. The sample, which was in the form of a sponge like agglomerate, was washed in hot water and all undissolved material was collected for XRD and SEM analysis.

### 3.3 Results and Discussion

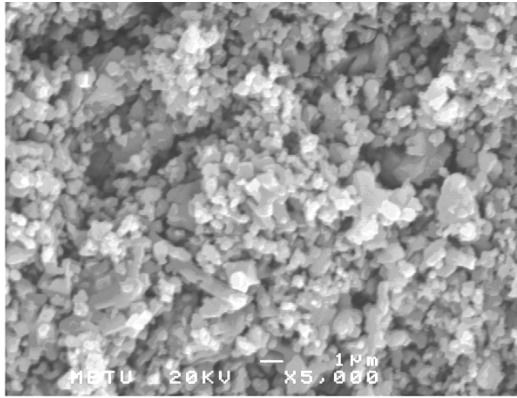
SEM images of pellets sintered at 900 °C and 1300 °C are given in Fig. 3.2. It is seen that the structure which was highly porous at 900 °C (and also at 1100 °C), was quite dense at 1300 °C. The porosity values were approximately 47 % and 45.1 % with sintering at 900 °C and 1100 °C, respectively. Sintering at 1300 °C yielded a porosity value of 17.3 %.

X-Ray diffractograms of the sintered pellets are given in Fig. 3.3. The diffractogram of the sample sintered at 900 °C comprises the initial phases, i.e. Fe<sub>2</sub>O<sub>3</sub> and TiO<sub>2</sub>, as well as a new phase, pseudobrookite (Fe<sub>2</sub>TiO<sub>5</sub>). The formation of this phase via the reaction of TiO<sub>2</sub> with Fe<sub>2</sub>O<sub>3</sub> is expected since the associated Gibbs energy change is negative at the current sintering temperatures (Barin et al., 1973). In pellets sintered at 1100 °C, Fe<sub>2</sub>O<sub>3</sub> is consumed totally by the reaction with the result that the structure is made up of two phases; Fe<sub>2</sub>TiO<sub>5</sub> and TiO<sub>2</sub>, see Fig. 3.3(b). The same was also the case for the pellet sintered at 1300 °C. The two-phase structure is clearly visible in this latter sample, brought out by the back scattered image given in Fig. 3.2 (c).

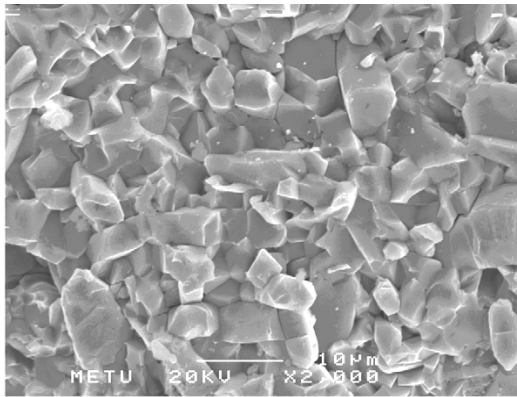
X-ray diffractograms of the pellets after deoxidation are given in Fig. 3.4. It was observed that deoxidation was successful in varying degrees. The greater portion of the pellet sintered at 900 °C after deoxidation was Fe and a Ti bearing compound. The compound was TiC, probably formed at the end of electrolysis, following the reaction:



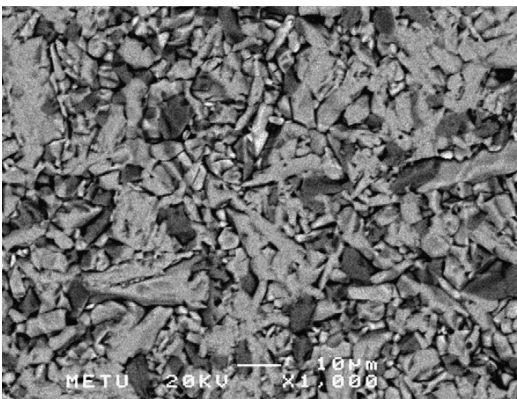
In Eq. 3.1, CO is the anode product (see below) which can accumulate in the cell vessel and could react with Ti reduced from TiO<sub>2</sub> at the cathode. The minor constituents of the sample were Fe<sub>2</sub>Ti and FeTi. Sintering at 900 °C, however, was not successful in yielding the target composition in substantial amounts.



(a)



(b)



(c)

**Figure 3.2** Micrographs of the oxide pellets sintered for 2 hours at (a) 900 °C and (b) 1300 °C. The graphs refer to broken pellets as viewed through the thickness section. (c) is the same as (b) but the section is polished and viewed in back-scattered mode to reveal the two-phase structure.

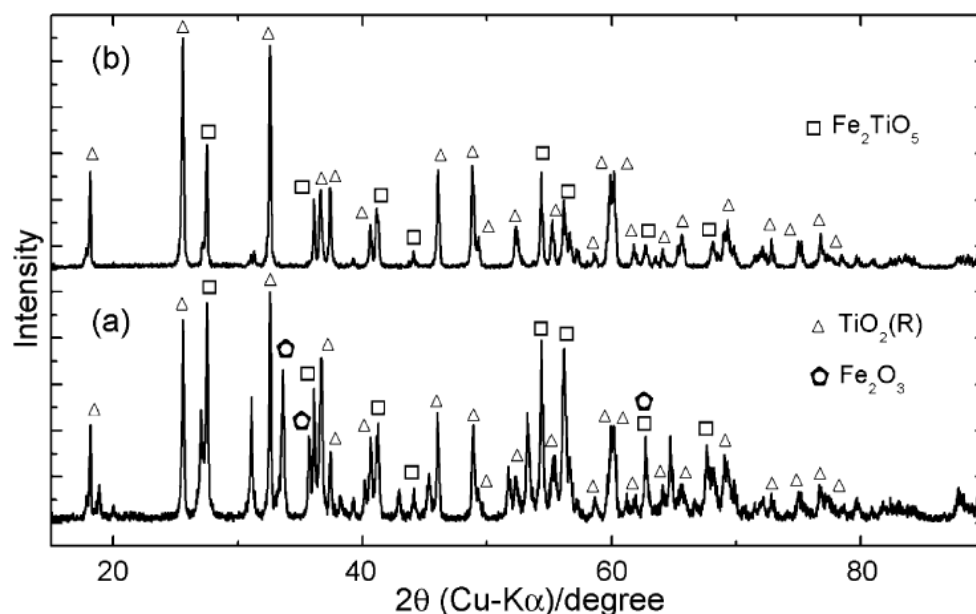


**Figure 3.3** X-ray diffractograms of the oxide pellets  $\text{Fe}_2\text{O}_3$  and  $\text{TiO}_2$  mixed in molar proportions of 1: 2 and sintered at (a) 900 °C, (b) 1100 °C. Note the presence of  $\text{Fe}_2\text{TiO}_5$  along with  $\text{Fe}_2\text{O}_3$  and  $\text{TiO}_2$  at 900 °C. Also note that at 1100 °C the sintered pellet has a two-phase structure;  $\text{Fe}_2\text{TiO}_5$  and  $\text{TiO}_2$ .

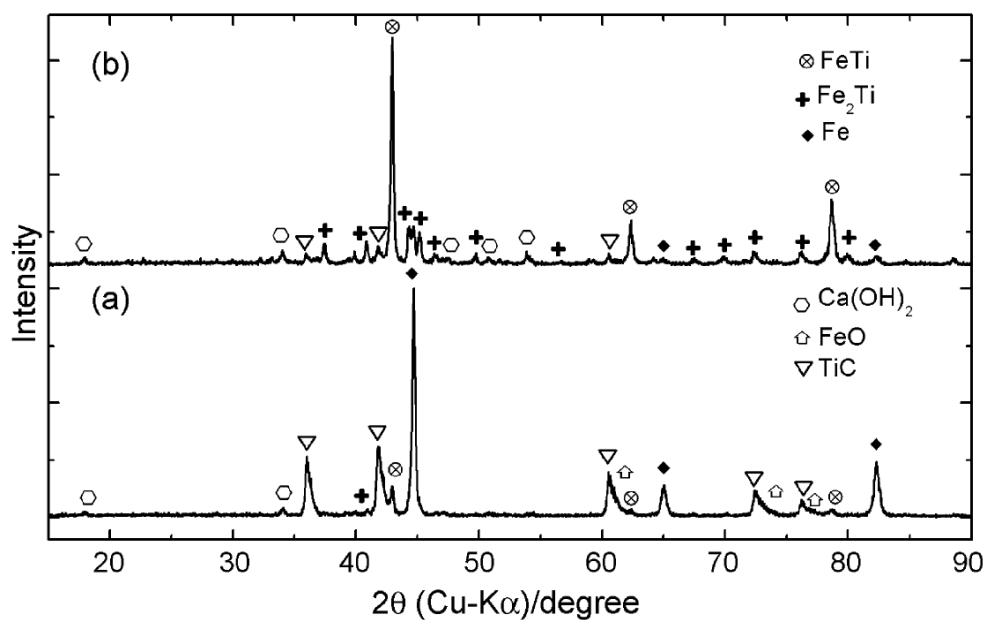


**Figure 3.4** X-ray diffractograms of the pellets deoxidized at 900 °C for 24 hours at 3.2 V. The diffractograms refer to pellets sintered at (a) 900 °C, and (b) at 1100 °C.



The sample sintered at 1100 °C and 1300 °C yielded mainly FeTi, which is the target composition plus Fe<sub>2</sub>Ti as a minor phase. Fe, which was quite dominant at 900 °C, was insignificant in these samples. The same was true for Ti, implying that this element, upon reduction, reacted with the existing phases yielding the target composition FeTi. The SEM image of one such sample is given in Fig. 3.5.

The conditions of sintering reported above for the successful synthesis of FeTi is consistent with that reported in a similar study conducted by Ma et al. (2006). The sintering in this study was carried out at 1050 °C, which yielded a product with X-ray diffractogram very similar to the one reported in Fig. 3.4(b).

To follow the details of electro-deoxidation, samples sintered at 1300 °C were selected for further study. A current – time plot for this sample covering the first 6 hours of electrodeoxidation is given in Fig. 3.6. It is seen that the current, following a rapid rise to a peak value, drops down to a smaller value which then decreases gradually with time. Three positions were selected on this curve for structural examinations and accordingly three samples were prepared. The samples, which were maintained above the salt bath during pre-electrolysis, were then processed sequentially. One sample was immersed into the salt bath, maintained there for 30 minutes and then lifted out. The others were electrolyzed as soon as they were immersed; one for 30 minutes and the other for 6 hours.

The sequence of changes that occurred in the samples during electrolysis can be seen in Fig. 3.7. The X-ray diffractogram shows a systematic change from the sintered condition to that after the 24-hour electrolysis. In the immersed sample, Fe<sub>2</sub>TiO<sub>5</sub> and TiO<sub>2</sub>, that is, the phases in the sintered sample, continue to be the major constituents, but there are also other phases. These are ilmenite (FeTiO<sub>3</sub>), a spinel phase (Fe<sub>2</sub>TiO<sub>4</sub>), and a perovskite phase (CaTiO<sub>3</sub>). After 30 minutes of

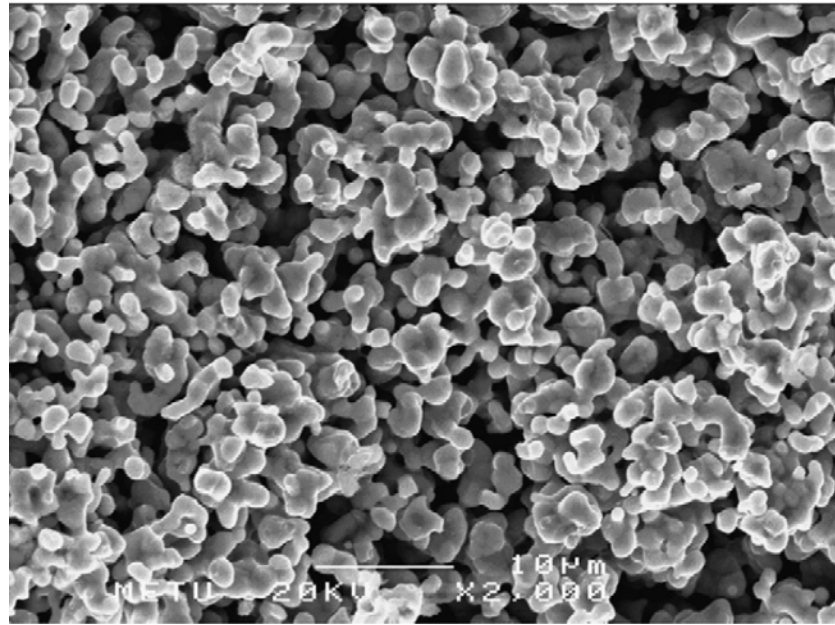


**Figure 3.5** SEM image of metallic agglomerate, FeTi, obtained from deoxidation of mixed oxide pellet sintered at 1300 °C.

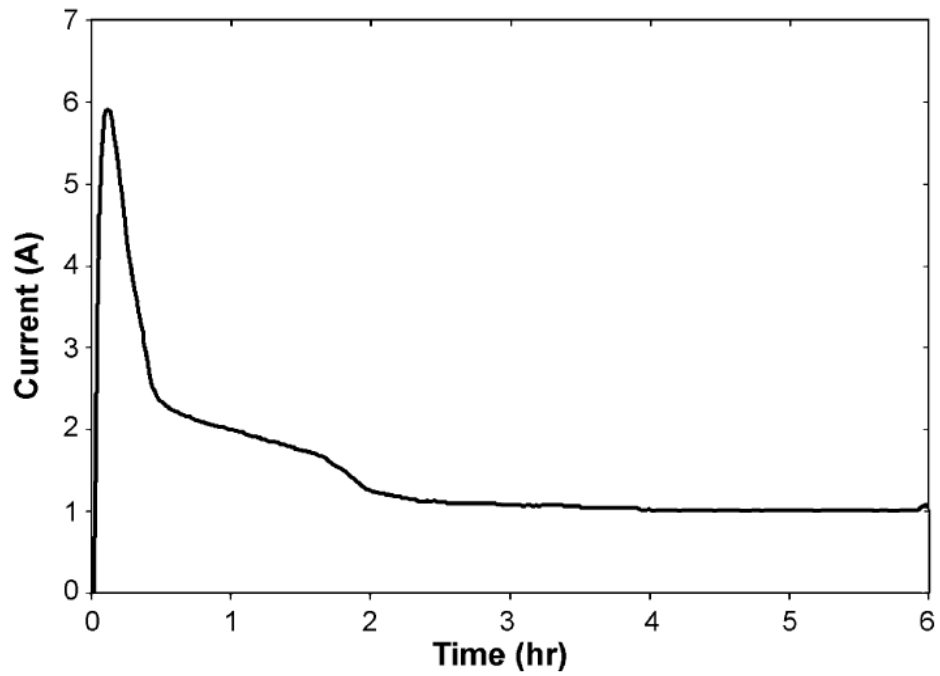


**Figure 3.6** Current –time data collected during deoxidation of the oxide pellet sintered at 1300 °C.

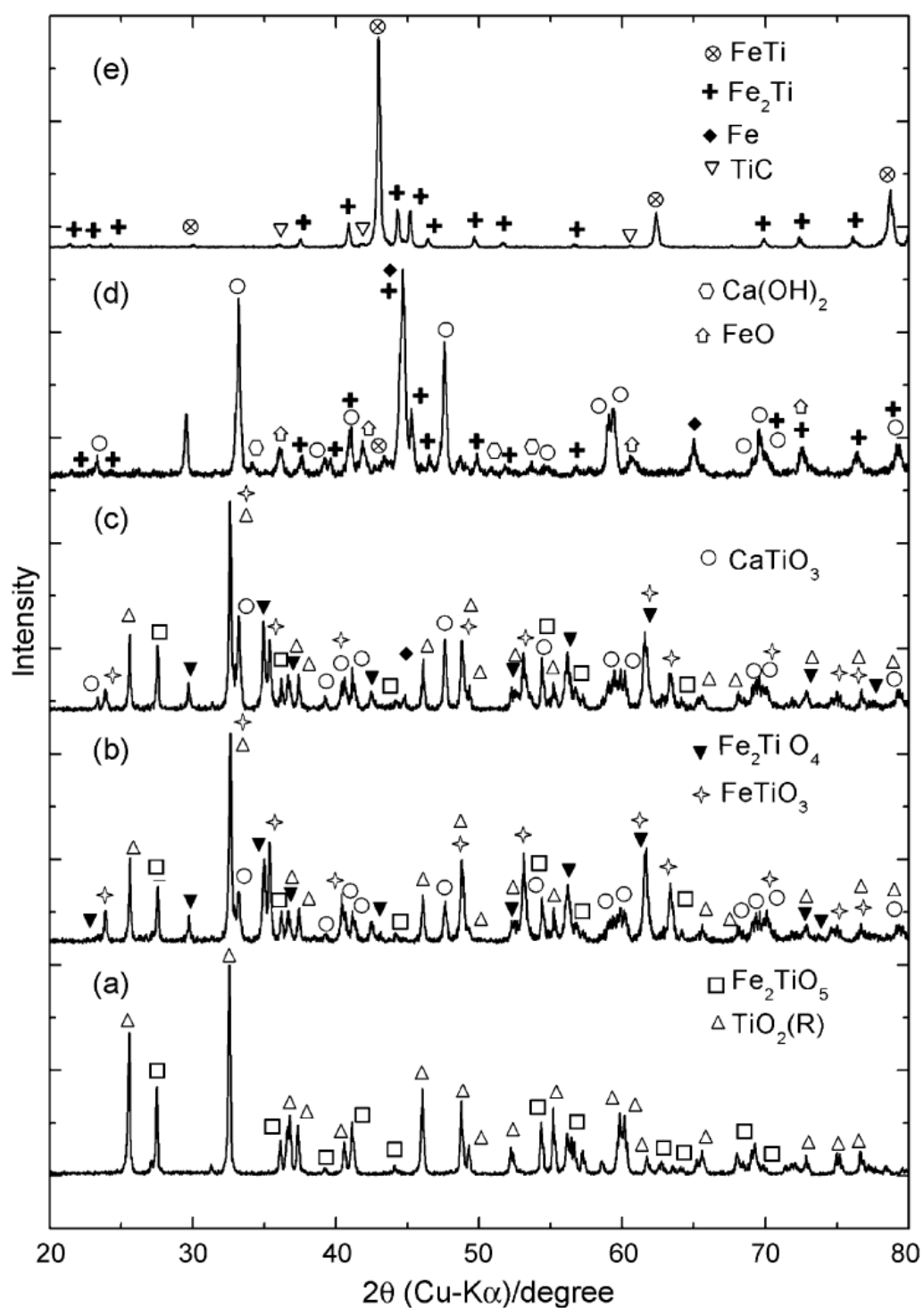
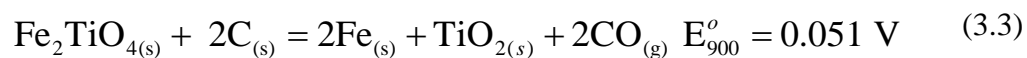
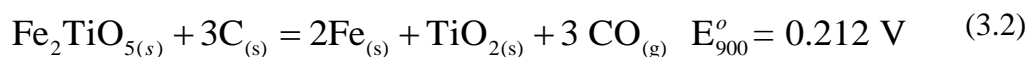


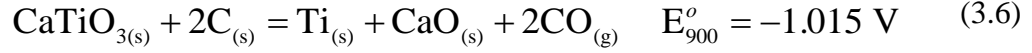
**Figure 3.7** X-ray diffractograms of the oxide pellets sintered at 1300 °C and deoxidized in  $\text{CaCl}_2$  at 900 °C (3.2V). The diffractograms refer to pellets; (a) in the sintered condition, (b) sintered and immersed into the salt bath for 30 minutes, (c), (d) and (e) refer to sintered pellets electrolyzed for 30 minutes, 6 hours and 24 hours respectively.

electrolysis, the phases did not change much, though  $\text{CaTiO}_3$  is much stronger and a metallic phase Fe is already present in the sample. After 6 hours, the  $\text{Fe}_2\text{TiO}_5$  and  $\text{TiO}_2$  are all consumed. Fe is now the dominant phase accompanied by the intermetallic  $\text{Fe}_2\text{Ti}$ . The target composition  $\text{FeTi}$  can be identified in this sample, but it is far from being a major phase. It is interesting to note that  $\text{CaTiO}_3$  continues to be the major phase in this sample. It appears that beyond this, the electrolysis mainly consumes  $\text{CaTiO}_3$  and with the production of Ti as a result, the greater portion of the sample is converted into  $\text{FeTi}$ , see Fig. 3.7 (e).

The observations reported above imply that, from the oxide state to the final composition  $\text{FeTi}$ , electro-reduction follows quite a systematic route. It appears that the oxides are already modified upon immersion into the salt bath even before the electrolysis. Thus a two-phase structure, i.e.  $\text{Fe}_2\text{TiO}_5$  and  $\text{TiO}_2$ , is in part converted into a mixture of phases comprising  $\text{CaTiO}_3$ ,  $\text{FeTiO}_3$  and  $\text{Fe}_2\text{TiO}_4$ . With the progress of electrolysis, as the oxygen is discharged, these complex oxides are consumed and instead the remaining oxygen is tied up in simpler oxides such as  $\text{FeO}$  and  $\text{CaO}$ .

The results of experiments show that Fe is reduced quickly from the iron bearing oxides. In contrast, the reduction of Ti is quite sluggish. After 6 hours of electrolysis, the greater portion of Ti is still tied up in  $\text{CaTiO}_3$ . Using the thermodynamic data, the decomposition voltages of various oxides have been calculated and are listed below with descending order. The values here were determined for the reactions taking place at 900 °C, the anode product being  $\text{CO(g)}$ .





It should be noted that with the reactions given in Eq. 3.2 -3.4, which give rise to Fe, have reduction potentials more positive than those which give rise to Ti, i.e. the reactions given in Eq. 3.5 and 3.6. The early formation of Fe and the persistence of Ti-bearing oxides until the very end of electrolysis are consistent with the above values. It is also worth noting that  $\text{CaTiO}_3$  has a higher decomposition potential than pure  $\text{TiO}_2$  which implies that the reduction process is made difficult by  $\text{CaTiO}_3$  formation.

Electrolysis, with the sequence of changes described above, may be contrasted with the sintering process. While sintering,  $\text{Fe}_2\text{O}_3$  and  $\text{TiO}_2$  are combined into more complex oxides, i.e.  $\text{Fe}_2\text{TiO}_5$ . With electrolysis, the structure first attacked probably by CaO, which probably forms during drying process. The structure is then gradually reduced into simpler oxides yielding first Fe and then Ti. Even though the structure formed by sintering is later disintegrated, it appears that the state, which had evolved during sintering, exercises a considerable effect on the nature of the reduction process. This effect of sintering is most probably related to the length scale of the chemical species in the oxide preforms. At  $900^{\circ}\text{C}$ , the sintered pellet is grossly heterogeneous in that it contains unreacted  $\text{Fe}_2\text{O}_3$  and  $\text{TiO}_2$  phases as well as  $\text{Fe}_2\text{TiO}_5$ . With the porosity of 47%, elements that may form during deoxidation, i.e. Fe and Ti, are not close enough to react with one another. Accordingly deoxidation yields a range of phases, namely Fe, Ti (i.e. TiC see above) as pure elements, and  $\text{Fe}_2\text{Ti}$  and FeTi as intermetallics.

At higher sintering temperatures, the reaction goes to completion. Thus, all  $\text{Fe}_2\text{O}_3$  is consumed and the preform is made up of two phases  $\text{Fe}_2\text{TiO}_5$  and  $\text{TiO}_2$ . The structure, therefore, is more homogenous than that is given above. Even though this structure is modified upon immersion into the salt bath, this modification probably occurs with a length scale that is comparable to the original structure. Thus, upon reduction, elements are close to each other and with diffusion over small distances they react with each other yielding the intermetallics. The result, at the end of electrolysis, is that FeTi makes up the considerable portion of the product.

As a final remark, it should be pointed out that, with the current processing conditions, the phases  $\text{Fe}_2\text{Ti}$  and a small amount of Ti (i.e. TiC) do form in the final product. Since the target composition is FeTi, the formation of these other phases need to be minimized or should be prevented altogether. Following the approach given above, it may be suggested that one method of achieving this, would be to make use of mixed oxides with refined structures, i.e. to employ a processing route that would yield the mixed oxide pellet with as fine a structure as possible. The other route would be to produce a single-phase pellet, namely ilmenite ( $\text{FeTiO}_3$ ).

It appears that the ilmenite approach, with Fe:Ti in 1:1 proportion, would be particularly worthwhile since this would make the electrolysis possible in a variety of sintering conditions. For instance, pellets of increased porosity could be electrolyzed which might accelerate the reduction process, an approach which would create difficulties in the mixed oxide approach.

### **3.4 Conclusions**

In the current work, a study was carried out on the synthesis of FeTi intermetallics from mixed oxide precursors.  $\text{Fe}_2\text{O}_3$  and  $\text{TiO}_2$  mixed in molar proportions of 1:2 were sintered at elevated temperatures ranging from 900 °C to

1300 °C. The sintered oxide was electrolyzed in a molten  $\text{CaCl}_2$  at 900 °C using a graphite anode at a potential of 3.2 V. The study has shown that the use of sintering temperatures close to or above 1100 °C leads to the formation of a two-phase structure,  $\text{Fe}_2\text{TiO}_5$  and  $\text{TiO}_2$ , which successfully yields the target composition FeTi in substantial amounts when electrolyzed. The study further shows that interrupted experiments during the electrolysis and the examination of partially reduced pellets yield considerable information with regard to the sequence of changes that occur during the deoxidation process.

## **CHAPTER 4**

### **SYNTHESIS OF Mg-Ni COMPOUNDS FROM THEIR OXIDES**

#### **4.1 Introduction**

Solid-state electro-reduction of oxides has been an area of intense research during the last decade (Chen et al., 2000; Suzuki, 2005). The method was used not only to extract metals from their oxides (Suzuki et al., 2004) but also to synthesize alloys and compounds from the oxide mixtures (Wang et al., 2006). In this method, pellets of oxide powders used as the cathode were deoxidized by the application of a voltage against graphite without decomposing the electrolyte, a molten salt that is capable of dissolving and transporting oxygen ions. During electrolysis, while oxygen ions are removed from the pellets and transported to the anode to form CO and/or CO<sub>2</sub>, metallic constituents are left behind in the cathode, which via in-situ reactions may yield alloys or compounds. The method has the advantage that when inert anodes are used, the electrolysis leads to oxygen generation rather than CO or CO<sub>2</sub> emission (Seo et al., 2006).

A number of factors affect the ease with which the reduction is achieved in the electrodeoxidation process. It has been reported that, oxides of low reduction voltages, e.g. NiO, Cr<sub>2</sub>O<sub>3</sub>, Fe<sub>2</sub>O<sub>3</sub>, are deoxidized faster than the others, e.g. rare earth oxides (Kang et al., 2009). The ease of reduction is also affected by the oxygen diffusivity in the solid state. Oxides such as TiO<sub>2</sub> and ZrO<sub>2</sub> are reduced relatively easily in the early stages, but as pointed out by Chen et al. (2001), once the metallic state is achieved, the rate slows down, since the diffusion of oxygen



is extremely slow in the metallic lattices. Insulating oxides such as  $\text{SiO}_2$  was also difficult to reduce and required the number of contacting points in the cathode to be increased (Nohira et al., 2003). Here the reduction is claimed to proceed via the propagation of conductor-insulator-electrolyte triple interline (Jin et al., 2004; Xiao et al., 2006). Similarly, the deoxidation of some oxides, such as  $\text{MgO}$  and  $\text{Al}_2\text{O}_3$ , has been found to be complicated due to difficulties in the initial metallization of the oxide pellets as well as due to the fact that the corresponding metals have low melting points (Cox and Fray, 2002).

The reduction of oxide mixtures is often more complicated than their pure counterparts. The mixtures, such as  $\text{Tb}_2\text{O}_3\text{-NiO}$  (Qui et al., 2006),  $\text{Fe}_2\text{O}_3\text{-TiO}_2$  (Tan et al., 2009) and  $\text{TiO}_2\text{-NiO}$  (Yong et al., 2006), have been successfully deoxidized to yield the respective intermetallic compounds, i.e.  $\text{TbNi}_5$ ,  $\text{FeTi}$ , and  $\text{TiNi}$ . The complication often arises because the oxides are reduced at different rates, which may give rise to separate individual phases rather than to the compounds themselves. Yong et al. (2006) reported that the application of a higher voltage may reduce the differences in the reduction rates and could thus promote the compound formation. In this context, the pre-compounding of the oxide mixtures as well as the optimization of the porosity in the pellets could be beneficial to have more complete reduction of the oxides to the required stoichiometry. The reduction of the oxide mixtures also has its advantages. For instance, compounds, such as  $\text{Ni}_2\text{MnGa}$  (Wood et al., 2003) and  $\text{Nb}_3\text{Sn}$  (Yan and Fray, 2005), have been successfully synthesized in the solid state at temperatures higher than the melting points of some of their constituent metals. Also, Qui et al. (2006) points out that the reducibility of the oxide mixture could be improved by fast reduction of one of the oxide phases and the formation of metallic particles in situ may enhance the reduction of the other oxide constituents.

The current work deals with synthesis of  $\text{Mg-Ni}$  compounds and the extraction of pure  $\text{Ni}$  and  $\text{Mg}$  from their oxides. The study is of particular interest since the system involves oxides,  $\text{MgO}$  and  $\text{NiO}$ , which have widely different physical,

such as electrical conductivity and oxygen diffusivity, and thermodynamic properties. Therefore, electro-deoxidation of these oxides, either on their own or as mixtures, is of considerable significance. Moreover,  $\text{Mg}_2\text{Ni}$ , one of the target compounds has a considerable potential as hydrogen storage alloy (Zaluski et al., 1995).

## 4.2 Materials and Methods

Starting materials were NiO (99%, Alfa Aesar) and MgO (99%, Merck) powders. NiO powders were irregular in shape and 1.20  $\mu\text{m}$  in size, Fig. 4.1 (a). MgO particles were much finer, i.e. sub-micron in size, Fig. 4.1 (b). Both powders were in the form of agglomerates with average sizes, measured by a laser diffraction technique, of  $D_{50}$  of 18  $\mu\text{m}$  and 30  $\mu\text{m}$  for NiO and MgO, respectively.

Oxide powders were mixed in fixed proportions corresponding to metallic compositions: Ni,  $\text{MgNi}_2$ ,  $\text{Mg}_2\text{Ni}$  and Mg. The mixing was carried out for 30 minutes in a Spex Mill at ball-to powder ratio (B/P) of 1. The mixtures were further hand mixed with some PVA solution and allowed to air dry for 24 hours. They were then cold-compacted under a force of 5000 N to cylindrical pellets of 15 mm in diameter and 4-7 mm in height. All pellets were heated to 1200  $^{\circ}\text{C}$  with a heating rate of 5  $^{\circ}\text{C}/\text{min}$  and sintered for 6 h.

Deoxidation experiments were conducted in a stainless steel reactor placed in a vertical furnace. The reactor comprises a stainless steel crucible for holding molten salt and has a lid with retractable electrodes immersible into the electrolyte. Two sets of electrodes were available, one set for pre-electrolysis and the other for electro-deoxidation. In both, the anode-to-cathode distance was 25 mm. Anodes were graphite rods, 13 mm of diameter and 100 mm in length, and were connected to a stainless steel current collector. The cathodes were stainless steel wire of 4 mm in diameter, which in the case of working electrode was

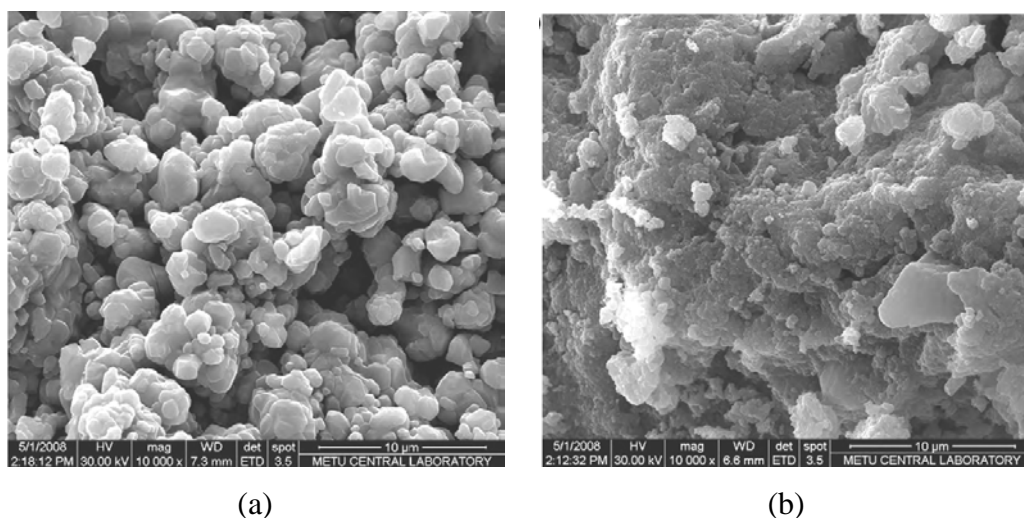


**Figure 4.1** SEM images of oxide powders; (a) NiO and (b) MgO used in the experiments.

connected to the oxide pellet. The reactor was sealed, allowing electrolysis in an argon atmosphere (99.995 % purity) maintained at a flow rate of 150-250 ml/min.

A eutectic mixture of  $\text{CaCl}_2\text{-NaCl}$  was used as the electrolyte, which has a melting point of about 505 °C. 1000 g of electrolyte was used for each experiment. The salt mixture was heated slowly to the electrolysis temperature to reduce its moisture content. The electrolyte was further purified by pre-electrolysis using the auxiliary electrodes at a potential of 3.0 V for a minimum of six hours. Following the pre-electrolysis, the auxiliary electrodes were lifted above the electrolyte, and the electrolysis was initiated by immersing the working electrodes, i.e. oxide pellet (cathode) and a fresh graphite rod (anode) into the salt bath. During electrolysis, current-time data was collected by a computer connected to the power supply.

At the end of each experiment, the electrodes were disconnected from the electrical supply and both the graphite anode and the reduced sample were removed from the electrolyte by positioning them above the melt. After cooling

to room temperature under a continuous flow of argon gas, the reactor lid was opened and the sample with its stainless steel connector was removed. The sample was washed in a hot methanol-ethanol-water mixture and all undissolved material was collected for XRD and SEM analysis.

Volumetric porosities of the oxide pellets after sintering were determined from geometric dimensions and the mass of the pellets, making use of specific density values of the constituent oxides. Phase make-up of the samples was determined via X-ray diffraction. The quantity of phases was determined following Rietveld refinements of the powder diffraction patterns using the software MAUD (Lutterotti et al., 1999).

### **4.3 Results and Discussion**

The oxides following the sintering treatment yielded pellets with porosity values varying between 37-57 %. An X-ray diffractogram of a sintered pellet of mixed oxide  $\text{MgO:NiO} = 1:2$  is given in Fig. 4.2 (a). Since MgO and NiO have the same crystal structure and very similar lattice parameters, diffraction peaks are very close to one another showing considerable overlapping. Still, the peaks of MgO and NiO are differentiated from each other, indicating that the mixed oxides have a two-phase structure rather than a single-phase solid solution. Considering that the sintering was carried out at  $1200^\circ\text{C}$  this is somewhat surprising and could be due to insufficient mixing of the oxides in the Spex Mill ®.

Two phases structure of oxide pellet has been further verified via SEM imaging in backscattered mode. Regions of two different contrasts were apparent, see Fig. 4.2 (b), in compliance with the presence of two-phase structure. Grains in the sintered samples had sizes (mean intercept value) of  $1.9\ \mu\text{m}$  and  $3.2\ \mu\text{m}$  for MgO and NiO respectively.

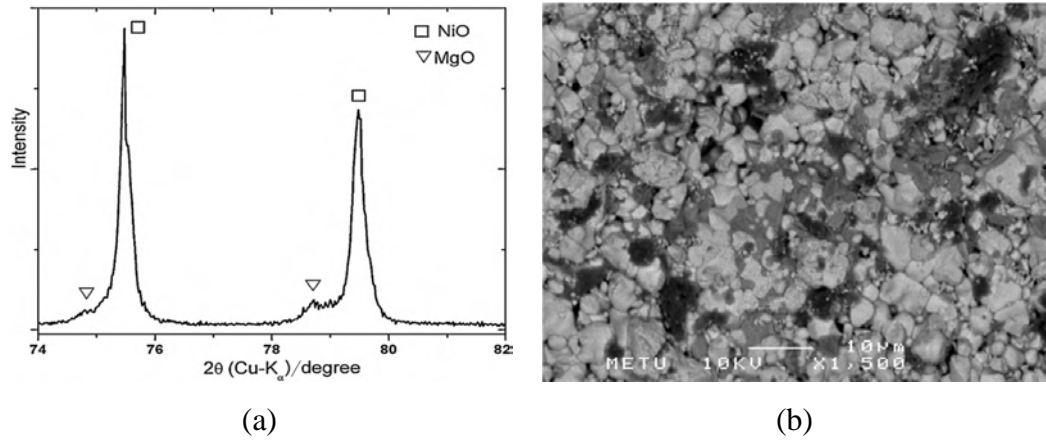


**Figure 4.2** *MgO:NiO=1:2 pellet sintered at 1200 °C for 6 hours; (a) X-ray diffractogram, (b) SEM image recorded in back scattered electron mode indicating a two-phase structure; NiO (bright phase) and MgO (gray phase). Black regions are pores.*

The process of electro-reduction leads to the discharging of oxygen from the cathode leaving the metallic constituents behind. More specifically, under the applied potential, the oxygen is ionized, either directly from the cathode (Chen et al., 2000) or through calcium deposited onto the cathode (Suzuki et al. 2004; Suzuki, 2005), dissolved in the electrolyte and is discharged at the anode (carbon) where it forms CO or CO<sub>2</sub>.

Standard reduction potentials,  $\Delta E^\circ$ , of oxides (MgO and NiO) for both CO and CO<sub>2</sub> evolution and the standard decomposition potentials of electrolyte (CaCl<sub>2</sub> and NaCl) were calculated from the thermodynamic data given in (Barin et al., 1973; Bale et al., 2002) and are shown in Table 4. 1. The potentials calculated for oxides for the case of intermetallic formation, i.e. MgNi<sub>2</sub> and Mg<sub>2</sub>Ni, are also included in the table. Here  $\Delta E^\circ$  values of the overall reactions, in volts, were directly calculated from:

$$\Delta E^\circ = -\frac{\Delta G^\circ}{nF} \quad (4.1)$$

Here  $\Delta G^\circ$  is the standard Gibbs free energy change of the reaction (in Joules) at temperature T, n is the number of electrons transferred in the balanced electrochemical reaction, and F is the Faraday's constant (in C/mol), assuming that the components are in pure state.

The data, given in Table 4.1, indicate that the reduction potential of NiO is positive and therefore it is expected to reduce more easily. The electro-deoxidation of MgO on the other hand requires the application of a relatively high voltages. It should also be noted that at 900 °C, the reactions leading to CO evolution are more favorable whereas at lower temperatures, e.g. 600 °C, the more favorable reactions are those leading to CO<sub>2</sub> evolution.

**Table 4.1** Standard reduction potentials of MgO, NiO and CaO and decomposition potentials of CaCl<sub>2</sub> and NaCl calculated at temperatures of 900°C, 725°C and 600°C. The data in parenthesis refers the potential when the metal is in liquid state. Reduction reactions yielding intermetallics are also shown.

| Reaction  | E° (V)  |         |         |
|---|---------|---------|---------|
|   | 600 °C  | 725 °C  | 900 °C  |
| $NiO_{(s)} + 0.5C_{(s)} = Ni_{(s)} + 0.5CO_{2(g)}$                  | +0.20   | +0.25   | +0.33   |
| $MgO_{(s)} + 2NiO_{(s)} + 3C_{(s)} = MgNi_{2(s)} + 3CO_{(g)}$       | -0.36   | -0.24   | -0.09   |
| $2MgO_{(s)} + 4NiO_{(s)} + 3C_{(s)} = 2MgNi_{2(s)} + 3CO_{2(g)}$    | -0.32   | -0.26   | -0.18   |
| $2MgO_{(s)} + NiO_{(s)} + 3C_{(s)} = Mg_2Ni_{(s,l)} + 3CO_{(g)}$    | -0.98   | -0.86   | (-0.70) |
| $4MgO_{(s)} + 2NiO_{(s)} + 3C_{(s)} = 2Mg_2Ni_{(s,l)} + 3CO_{2(g)}$ | -0.94   | -0.87   | (-0.78) |
| $MgO_{(s)} + C_{(s)} = Mg_{(s,l)} + CO_{(g)}$                       | -1.64   | (-1.52) | (-1.34) |
| $MgO_{(s)} + 0.5C_{(s)} = Mg_{(s,l)} + 0.5CO_{2(g)}$                | -1.60   | (-1.53) | (-1.43) |
| $CaO_{(s)} + C_{(s)} = Ca_{(s,l)} + CO_{(g)}$                       | -1.83   | -1.71   | (-1.52) |
| $CaO_{(s)} + 0.5C_{(s)} = Ca_{(s,l)} + 0.5CO_{2(g)}$                | -1.79   | -1.72   | (-1.63) |
| $NaCl_{(l)} = Na_{(l)} + 0.5Cl_{2(g)}$                              | (-3.37) | (-3.28) | (-3.16) |
| $CaCl_{2(l)} = Ca_{(s,l)} + Cl_{2(g)}$                              | -3.40   | -3.32   | (-3.21) |

The data in Table 4.1 also show that 3.2 V is safely below the decomposition potentials of both  $\text{CaCl}_2$  and  $\text{NaCl}$  at 600 °C and 725 °C. This voltage is quite close to the decomposition potentials of the electrolyte at 900 °C. The decomposition voltage of  $\text{NaCl}$  given in Table 4.1 at 900 °C is slightly less than 3.2 V referring to the pure state. For equimolar solution of  $\text{CaCl}_2$ - $\text{NaCl}$  by using an activity coefficient of  $\text{NaCl}$  as 0.66 (Karakaya and Thompson, 1986), this value is 3.27 V, which is above the applied potential. Furthermore, IR drop, overpotentials make the actual decomposition voltage even greater than 3.27 V.

Current- time curve recorded during deoxidation of  $\text{NiO}$  pellet at 900 °C is given in Fig. 4.3. As seen from the plot, the current shows an initial rise, and over a period of 30 min it settles down to a steady state, which then cascades down to smaller values. After 3 h, the current reduces to a residual value of 0.1 A that continues to drop at a very slow rate until the end of the electrolysis (24 h).

X-ray diffractograms of the  $\text{NiO}$  pellet before and after electro-deoxidation for 24 h at 900 °C are given in Fig. 4.4 (a) and Fig. 4.4 (b). As seen in the diffractograms, the pellet was reduced successfully to pure  $\text{Ni}$ . SEM image of the pellet, given in Fig. 4.4 (c), shows metallic powders in a sintered state, with particle sizes ranging from 5 to 10  $\mu\text{m}$ . Deoxidation of  $\text{NiO}$ , for 24 h at 725 °C and 600 °C, was also successful in yielding pure  $\text{Ni}$ .

The oxide mixture with a target composition of  $\text{MgNi}_2$ , i.e.  $\text{MgO}:\text{NiO} = 1:2$ , was deoxidized at 900 °C. X-ray diffractogram of the product, given in Fig. 4.5 (a), contains metallic constituents, i.e.  $\text{MgNi}_2$  and pure  $\text{Ni}$ , as well as residual  $\text{MgO}$ , indicating that the reduction was not complete. Analysis of XRD pattern showed that the fractions of phases were; 50, 44 and 6 wt % for  $\text{MgNi}_2$ ,  $\text{Ni}$  and  $\text{MgO}$ , respectively. The presence of residual  $\text{MgO}$  (but not  $\text{NiO}$ ) reveals that the reduction of  $\text{NiO}$  proceeded faster than that of  $\text{MgO}$ . SEM image of the product given in Fig. 4.5 (b) shows again a particulate structure, less coarse than that obtained from electrodeoxidation of pure  $\text{NiO}$ .

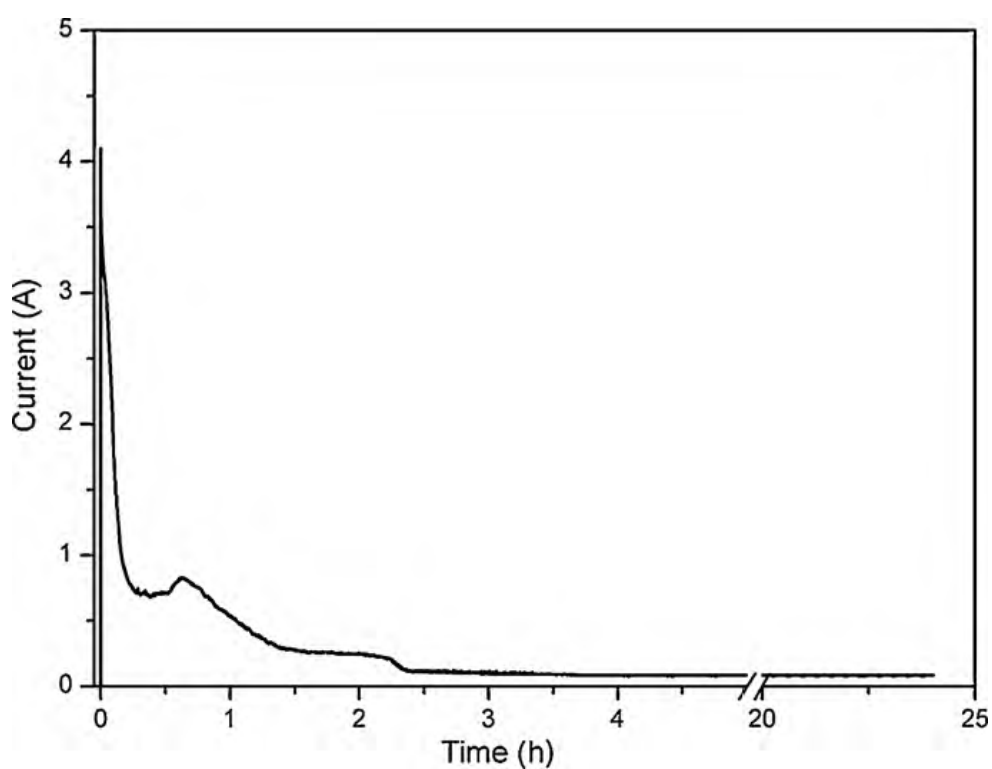


**Figure 4.3** Current–time data collected during electrodeoxidation of NiO at 900 °C with 3.2 V.

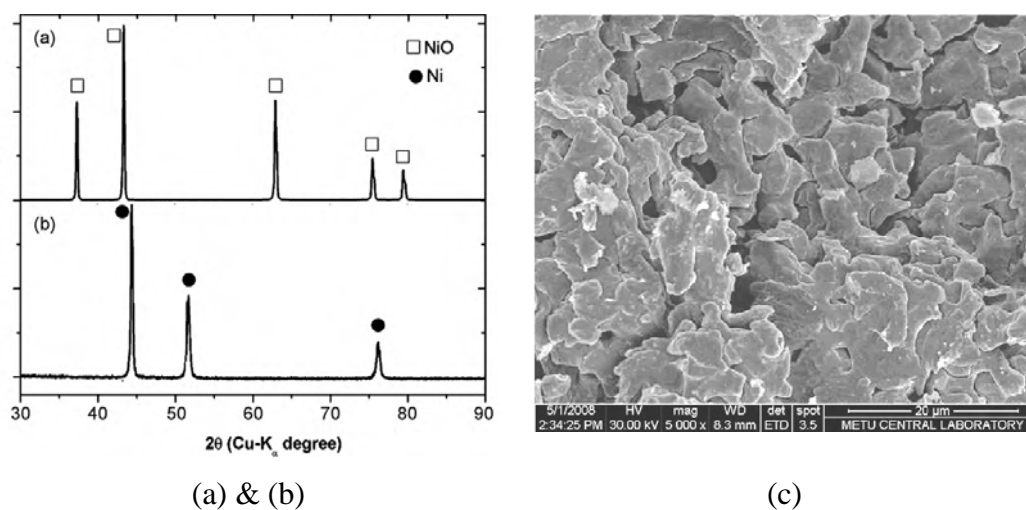


**Figure 4.4** NiO pellet; X-ray diffractogram of the sample (a) before and (b) after electrodeoxidation, at 900 °C for 24 hours (3.2V). (c) refers to SEM image of the reduced sample.



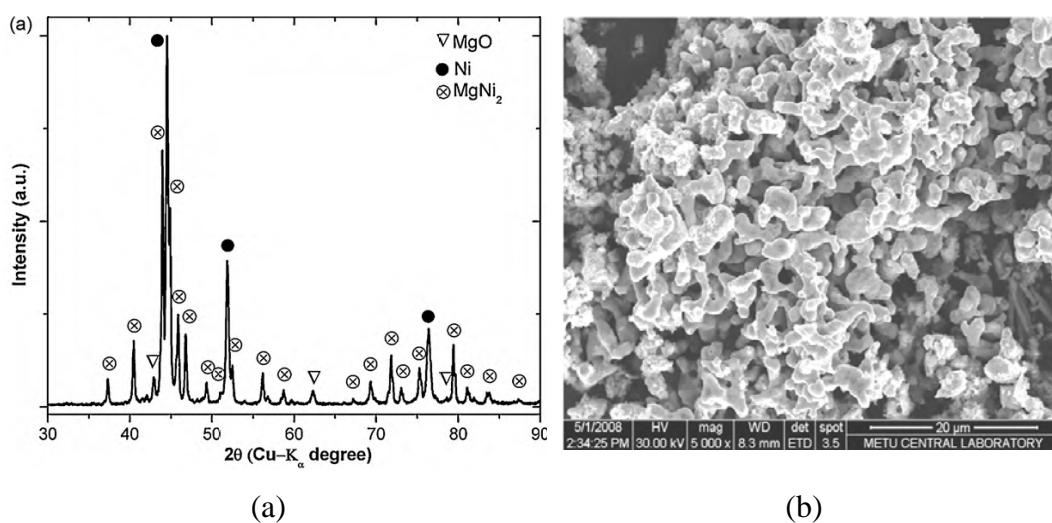


**Figure 4.5**  $MgO:NiO=1:2$  pellet; (a) X-ray diffractogram and (b) SEM image of powders after electrodeoxidation for 24 h at 900 °C with 3.2 V.

Although the oxide mixture  $MgO:NiO=1:2$  after the electrolysis contains a certain fraction of MgO, this fraction is not enough to convert all Ni into  $MgNi_2$ . This implies that a certain fraction of MgO either in partially or fully reduced form was lost from the cathode, probably as a result of dissolution in the electrolyte. This was checked by examining a sample taken from the electrolyte after the electrolysis. The sample was dissolved in water and the resulting residue was analyzed by EDS. The amount of Mg when scaled for 1 kg of electrolyte was approximately 0.09 g. This is nearly 15 % of the total Mg in the cathode.

The mixture  $MgO:NiO=2:1$  could not be electrolyzed at 900 °C, since the target composition  $Mg_2Ni$  is liquid at that temperature. The experiments were therefore carried out at 725 °C, safely below the melting point of  $Mg_2Ni$  (760 °C). As given in Fig. 4.6 (a), the pellet, after 24 hours of electrolysis, contained only a small fraction of metallic phases:  $Mg_2Ni$ ,  $MgNi_2$  and Ni. The rest, i.e. 82 wt % of the sample, was unreduced oxides. The final pellet was easy to grind and SEM image of the pulverized product, given in Fig. 4.6 (b), had a non-metallic

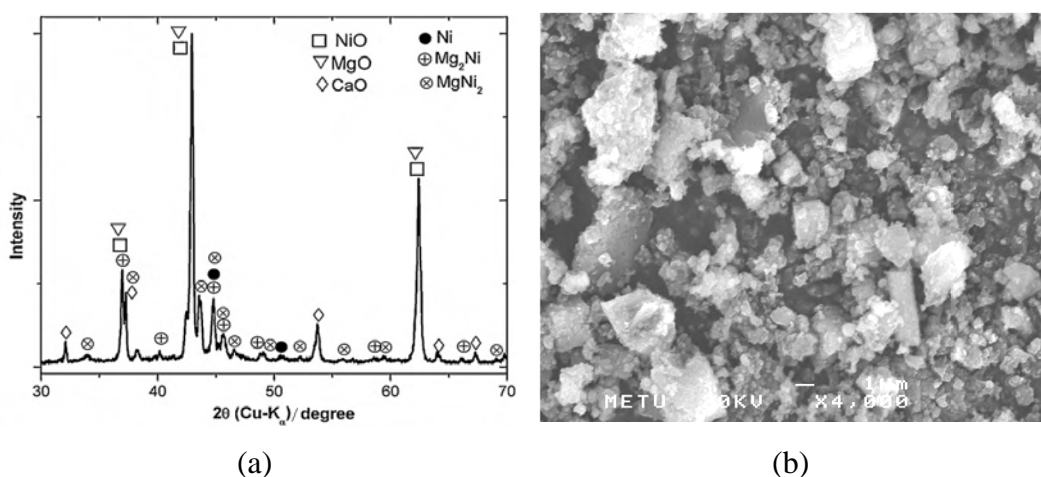


**Figure 4.6**  $MgO:NiO=2:1$  pellet; (a) X-Ray diffractogram and (b) SEM image of powders obtained after electrodeoxidation for 24 hours at 725 °C with 3.2 V.

appearance. For pure MgO, electro-deoxidation was even more difficult. The electrolysis carried out at 600 °C did not lead to any reduction. No trace of Mg could be detected in the sample after 24 hours of electrolysis at 3.2 V.

In attempt to reduce the MgO rich mixtures, separate experiments were carried out at 5 V which is well above the decomposition potential of the electrolyte. Fig. 4.7 shows the current-time plot recorded for  $MgO:NiO = 2:1$  mixture. As seen in the figure, the current fluctuates quite erratically, probably as a result of reactions leading to  $Cl_2$  evolution (Peng et al., 2010). The experiment was quite successful for  $MgO:NiO=2:1$  mixture. The pellet electrolyzed for 24 hours at 600 °C was reduced almost fully to the metallic state. The phases were  $Mg_2Ni$ ,  $MgNi_2$ ,  $Mg(OH)_2$  and a small amount of MgO (5 wt %). The presence of  $Mg(OH)_2$  is probably due to the reaction of metallic Mg with  $H_2O$  used to separate reduced pellet from the salt after electrolysis. The experiment with pure MgO, however, was not as successful. The electrolysis with 5 V at 600 °C yielded only trace amount of  $Mg_2Ca$  and  $Mg(OH)_2$ , both adding up to about 1 wt %, the rest being MgO. Thus, even the application of 5V was not enough to reduce the MgO pellet.

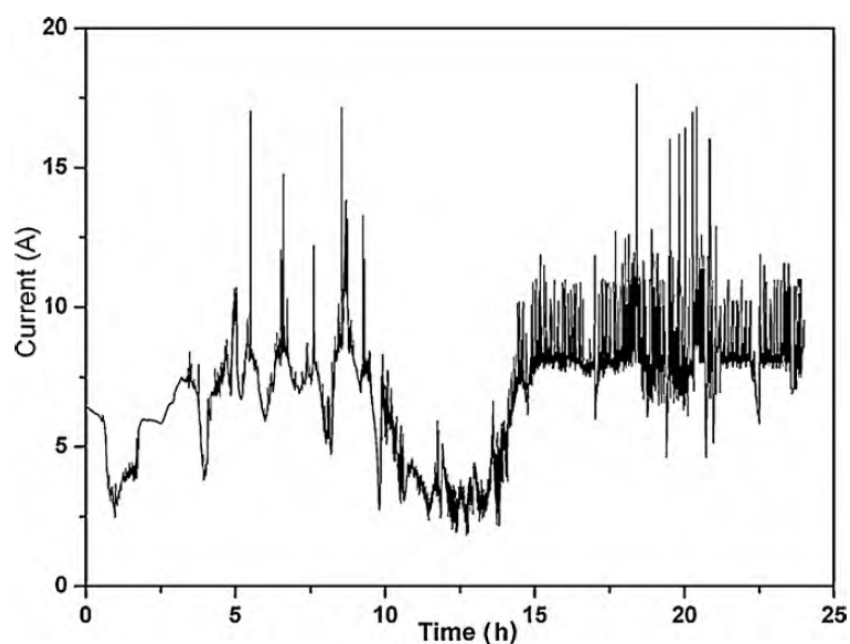


**Figure 4.7** *Current–time data collected during electrodeoxidation of MgO:NiO=2:1 affected with 5V at 600 °C.*

Returning to the results obtained with 3.2 V, it should be pointed out that, of the four metallic phases aimed in the current work, the ease of reduction closely parallels the values of the standard reduction potentials reported in Table 4.1. The reactions in the table were listed according to their reduction potentials (at 725 °C). Accordingly, the reductions become more and more difficult as one moves from Ni rich compositions to Mg rich ones.

The ease of reduction in NiO could be attributed to its low, in fact positive, reduction voltage as well as to the other factors such as its high conductivity (see below). Similar observations were made in a study by Qiu et al. (2005) in which 100-200 micrograms of NiO powders were reduced successfully within a few minutes at 900 °C.

The oxide mixture targeted for MgNi<sub>2</sub> was also reduced relatively easily. Here, the difficulty was in the production of samples with desired stoichiometry since

there was some loss of Mg from the cathode during the electrolysis. Still, the electrolysis of MgO:NiO=1:2 mixture is not unlike that of NiO, i.e. the mixture resulted in a reduction which is nearly complete. Also, as NiO has very low reduction potential, formation of a Ni-rich environment in the pellet probably enhanced the reduction of MgO in the oxide mixture. Similar arguments were put forward by Ma et al. (2006) and Yong et al. (2006) in explaining the enhanced reduction of TiO<sub>2</sub> in the presence of Fe<sub>2</sub>O<sub>3</sub> and NiO.

The loss of Mg during the electrolysis appears to be the major obstacle for the desired quantity of compound formation. Conditions in the pellet should be such that Mg upon reduction should react with Ni, which had been reduced earlier in the process, forming the targeted compound. Circumstances that favor compound formation are well documented in the earlier studies. One approach is to carry out the electrolysis under high potential. In such conditions as explained by Yong et al. (2006), the differences in the reduction rate of the oxides are diminished and all elements are extracted in the same time scale, which would allow them to react with one another resulting in the compound formation. The other approach is the solutionizing of the oxide mixture itself (Qiu et al., 2006; Qiu et al., 2005). In this case, the metallic species being present in the same oxide phase are close to each other, which upon reduction could react easily with one another. The latter approach would be particularly suitable for the current system since the oxides NiO and MgO have complete solid solubility. Thus, it is possible to form MgO and NiO in a single-phase structure in which Mg:Ni ratio can be adjusted to any preselected value.

Current experiments show that the reduction of MgO via electro-deoxidation is an extremely difficult task. This is true for the mixture targeted for Mg<sub>2</sub>Ni as well as that for the pure Mg. For instance, after 24 hours of electrolysis of MgO:NiO=2:1 mixture yielded only a small fraction of metallic phases, four-fifths of the pellet still remained as oxides. This implies that the phases in the oxide mixture do not behave independently. If they were, NiO could have been

reduced to pure Ni totally, leaving behind MgO. In a pellet with porosity in the order of 40% or so, this situation could be partially attributed to the insufficient conductivity of the pellet.

To check this, the electrical conductivities of the oxide pellets were measured with a two-probe technique. The results, given in Fig. 4.8 (a), verify that the conductivity of MgO differs drastically from that of NiO. The value for MgO at room temperature is close to  $10^{-14} \text{ ohm}^{-1} \text{ cm}^{-1}$ , i.e. five orders of magnitude less than that of NiO. It is also interesting that the conductivities of the mixtures are also quite different. While NiO rich mixture, i.e. MgO:NiO=1:2 has a value intermediate between those of MgO and NiO, the same does not hold true for MgO:NiO=2:1. This mixture has almost the same conductivity as pure MgO.

Clearly, in mixtures corresponding to Ni and MgNi<sub>2</sub>, NiO is the continuous phase with the result that conductivity of the pellet is close to that of NiO. Thus, the pellet in such mixtures benefits from the high conductivity of the host phase. In MgO:NiO=2:1 mixture, it appears that MgO is the continuous phase and the presence of NiO which occurs as isolated islands, does not exert a pronounced influence on the conductivity. Thus, the conductivity of the MgO rich mixture does not differ significantly from that of pure MgO.

It should be mentioned that conductivities measured for MgO and the MgO rich mixture are not unlike those expected for other insulating oxides such as ZrO<sub>2</sub> and SiO<sub>2</sub>. The latter oxide, for instance, was reduced quite successfully by increasing the number of contacting points in the cathode (Nohira et al., 2003). Chen and co-workers (Jin et al., 2004; Xiao et al., 2006) formalized this by three-phase interline model according to which the reduction proceeds along conductor/insulator/electrolyte interlines into the insulator oxides. Obviously, this mechanism was not operative in the current samples as experiments carried out by pellets sandwiched between two metallic plates did not lead to noticeable improvements.

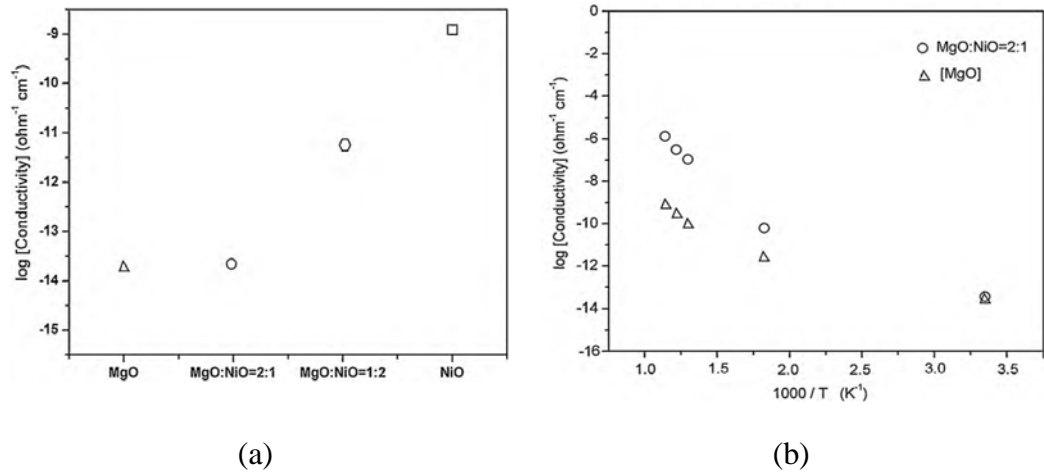


**Figure 4.8** (a) Electrical conductivities of MgO, MgO:NiO = 2:1, MgO:NiO = 1:2 and NiO at room temperature, and (b) conductivity values as a function of temperature up to 600 °C for MgO and MgO:NiO = 2:1.

It is apparent that the oxides in the current system, both MgO and NiO, differ from most of the other oxides in the details of their electro-deoxidation. Electroreduction of oxides, such as TiO<sub>2</sub> (Dring et al., 2006), Nb<sub>2</sub>O<sub>5</sub> (Wu et al., 2008) and B<sub>2</sub>O<sub>3</sub> (Ors et al., 2009), Cr<sub>2</sub>O<sub>3</sub> (Hyslop et al., 2010) and Ta<sub>2</sub>O<sub>5</sub> (Song et al., 2010), involve the formation of intermediate phases which, in the respective order, are CaTiO<sub>3</sub>, CaNbO<sub>3</sub>, CaB<sub>2</sub>O<sub>4</sub>, CaCr<sub>2</sub>O<sub>4</sub>, CaCr<sub>2</sub>O<sub>4</sub> and calcium tantalates. Thus, the reduction in these oxides is not a direct process but occurs through these intermediaries. This is also true for ZrO<sub>2</sub> and SiO<sub>2</sub> where as mentioned by Peng et al. (2008) and Yasuda et al. (2007), CaZrO<sub>3</sub> and CaSiO<sub>3</sub> do form during their electrodeoxidation. The electroreduction of Al<sub>2</sub>O<sub>3</sub> to Al (Xie et al., 2009), as has recently been reported by Yan and Fray (2009), similarly, involves the formation of calcium aluminates. Thus, in the three-phase interline where the reduction proceeds, it is not the starting oxide but the intermediate phase, which is in contact with the conductor and the electrolyte. Thus, the formation of intermediate phases such as CaSiO<sub>3</sub>, CaZrO<sub>3</sub> or calcium aluminates is expected to alter the conditions for electroreduction including the local conductivity of the pellet. MgO (and also NiO) in contrast do not form such

intermediate phases. Therefore, the insulating nature of MgO is not altered during the electrolysis.

Values of conductivity reported above refer to oxides at room temperature. Since the electrolysis was carried out at elevated temperatures, the applicable values are much higher than those reported above. Conductivities of MgO and MgO:NiO=2:1 mixtures were measured at temperatures up to 600 °C and are reported in Fig. 4.8 (b). The conductivity of MgO rises to  $10^{-9} \text{ ohm}^{-1}\text{cm}^{-1}$ , and that of MgO:NiO=2:1 to  $10^{-6} \text{ ohm}^{-1} \text{ cm}^{-1}$  at 600 °C. The values measured for MgO are comparable with those reported by Lewis and Wright (1968). The conductivity of NiO on its own was not measured in this study, but the reported values are as high as  $10^{-2} \text{ ohm}^{-1} \text{ cm}^{-1}$  at 600 °C (Mitoff, 1961). Since NiO can be electrodeoxidized quite successfully at this temperature, the value of  $10^{-2} \text{ ohm}^{-1} \text{ cm}^{-1}$  can be taken as a rough measure of the required conductivity. Then, to reach this value in MgO, using the temperature dependence of conductivity given by Lewis and Wright (1968), the required temperature needs to be as high as 1500 °C.

Electrolysis at elevated temperatures may be employed for Mg compounds of high melting points but for the current compositions of Mg<sub>2</sub>Ni and pure Mg, which have the melting points of 760 °C and 650 °C, this approach would not be relevant. Clearly, for successful electro-reduction of MgO rich mixtures, it would be desirable to find processing techniques that would render pellets with an acceptable conductivity. Evidently, any processing techniques that would disrupt the continuity of MgO phase would be helpful in this respect. But to increase the conductivity to its highest possible level, it is necessary to develop carefully tailored microstructures in the oxide pellets. One possibility, which might be relevant for MgO:NiO=2:1, would be to make NiO the host phase, i.e. NiO, though small in its proportions, could be distributed in a manner that could preserve its connectivity while enveloping each and all MgO particles.

#### 4.4 Conclusion

A study was carried out on the synthesis of Mg-Ni compounds as well as pure Ni and Mg from their oxides using the method of electro-deoxidation. The oxides were in the form of discrete phases, NiO and MgO, 3.2  $\mu\text{m}$  and 1.9  $\mu\text{m}$  in size respectively, suitably proportioned to yield Ni,  $\text{MgNi}_2$ ,  $\text{Mg}_2\text{Ni}$  and Mg. The oxides were electrolyzed in a eutectic mixture of  $\text{CaCl}_2$ -NaCl solution maintained at a constant temperature (900  $^\circ\text{C}$  - 600  $^\circ\text{C}$ ), using a graphite anode at an applied voltage of 3.2 V.

The following can be concluded from the current study:

- i) NiO with positive reduction potential can be reduced quite successfully to a metallic state at temperatures studied in this work. The oxide mixture  $\text{MgO:NiO}=1:2$  can also be deoxidized to a metallic state comprising the phases  $\text{MgNi}_2$  and Ni.
- ii) MgO rich mixtures are difficult to reduce via electro-deoxidation. The mixture  $\text{MgO:NiO}=2:1$  can be reduced to metallic phases only in small proportions. Difficulties in the reduction of MgO and MgO rich mixtures are attributed to low conductivity of MgO.

Further, the low conductivity of the latter compositions is due to MgO being the continuous phase. It is therefore suggested that the conductivity and thus the reducibility of the oxide mixtures would be improved if NiO could be made the host phase.



## **CHAPTER 5**

### **A COMPERATIVE STUDY FOR ELECTRODEOXIDATION OF NiO, MgO, Fe<sub>2</sub>O<sub>3</sub> AND TiO<sub>2</sub> BASED ON OXYGEN PERMEABILITY**

#### **5.1 Introduction**

Electro-reduction techniques provide a simple and cost effective route for synthesis of transition metals, e.g. Ti, Cr, Ni and Nb, and rare-earths, e.g. Tb and U, from their oxides (Chen et al., 2000, Chen et al., 2004; Qiu et al., 2005; Wang and Sun, 2006; Wang et al., 2006; Hur et al., 2003). Many compounds, such as LaNi<sub>5</sub>, FeTi, NiTi and NdCo<sub>5</sub>, were also successfully obtained by electro-reduction of oxide mixtures (Zhu et al., 2007; Tan et al., 2009; Jackson et al., 2008; Abdelkader et al., 2010).

As shown in the previous chapters, reducibility of metal oxides do vary quite considerably. Some oxides are deoxidized very easily, e.g. NiO, Fe<sub>2</sub>O<sub>3</sub>, while for some others, e.g. TiO<sub>2</sub>, MgO, deoxidation is rather difficult to proceed or it halts completely after a while. As the applied voltage is always higher than reduction voltage of oxides, the difficulty in deoxidation is mainly attributed to slow reduction of oxide pellets (Yan and Fray, 2009; Tripathy et al., 2007).

There might be many reasons for slow reduction of oxides. Wang and Li (2004) state that the diffusion of oxygen in solid state, ionization of oxygen charge transfer to electrolyte and pore diffusion of oxygen ions within electrolyte may put kinetic barriers for the electro-reduction process. Any condition that retards

the oxygen transport from oxide pellet to anode decreases the deoxidation rate. In order to avoid this, the properties of pellet, e.g. particle size, porosity and thickness, as well as experimental conditions, i.e. temperature and voltage, should be optimized (Yan and Fray, 2005; Mohandas and Fray, 2004). According to Alexander et al. (2006), both nucleation and growth of the newly formed phase are also critical for the rate of the deoxidation process.

In order to explain the deoxidation of metal oxides, different models were proposed in recent years. Three-Phase Interline (3PI) model looks at the electro-deoxidation of metal oxides from electrochemistry point of view (Xiao et al., 2006). It allows calculation of deoxidation rate for an insulating metal oxide, e.g.  $\text{SiO}_2$ . The model successfully shows how the applied voltage, time and overpotential are correlated and affect the deoxidation process (Wang et al., 2008).

Yan and Fray (2005) developed a conceptual model to show how the deoxidation initiates and propagates in a porous metal oxides pellet. Based on experimental results and 3PI model, this model is helpful to demonstrate and predict kinetics of electro-reduction process by examining products obtained from interrupted deoxidation experiments. A similar approach was also used to determine the deoxidation pathway of  $\text{Fe}_2\text{O}_3$ - $\text{TiO}_2$  mixtures, see Chapter 3.

Assadi (2006) developed a phase-field model in order to estimate how deoxidation starts and proceeds in a non-porous metallic pellets. In this 2D model, it was stated that the rate of deoxidation depends on diffusion of oxygen in solid state. Kar and Evans (2008) developed a shrinking core model in order to explain propagation of deoxidation in  $\text{TiO}_2$  pellet. This model emphasizes on oxygen diffusion in sub-oxides, considering that they are neighbors of each other, i.e. connected series, in the oxide particle.

In this chapter, a study was carried out to look at electro-deoxidation of a metal oxide particle in contact with a molten salt electrolyte. The approach emphasizes the importance of oxygen permeability for propagation of deoxidation. Reduction of oxides, namely NiO, MgO, Fe<sub>2</sub>O<sub>3</sub> and TiO<sub>2</sub>, by electro-deoxidation was examined from this point of view.

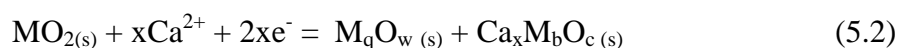
## 5.2 Reduction Routes in Electro-deoxidation

Relative stabilities of phases in electro-deoxidation process are shown in Fig. 5.1. As seen from the figure, the initial oxide is thermodynamically more stable than metal to be produced. Ca-bearing oxides, see Fig. 5.1, are known to be more stable than the initial metal oxide and its sub-oxides (Alexander et al., 2006).

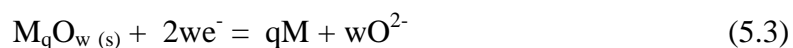
Formation of sub-oxides and Ca-bearing compounds, however, depends on the metal oxide to be reduced. Fig. 5.1 shows possible routes of electro-deoxidation, i.e. R<sub>1</sub>, R<sub>2</sub>, R<sub>3</sub> and R<sub>4</sub>. Synthesis of pure metal could take place directly in a single-step process, i.e. via R<sub>1</sub>. For an oxide, e.g. MO, the cathodic reaction is:



In deoxidation of some oxides, initial oxide may decompose into a sub-oxide and a Ca-bearing compound as given by R<sub>2</sub> in Fig. 5.1. In this case, some of the electrons gathered from current collector are used to convert the initial oxide, MO<sub>2</sub>, to Ca-bearing compound by following reaction:



Here, Ca<sub>x</sub>M<sub>b</sub>O<sub>c</sub> is Ca-bearing compound and M<sub>q</sub>O<sub>w</sub> is a sub-oxide. While Ca-bearing phase forms, the sub-oxide, i.e. M<sub>q</sub>O<sub>w</sub>, is reduced simultaneously by:



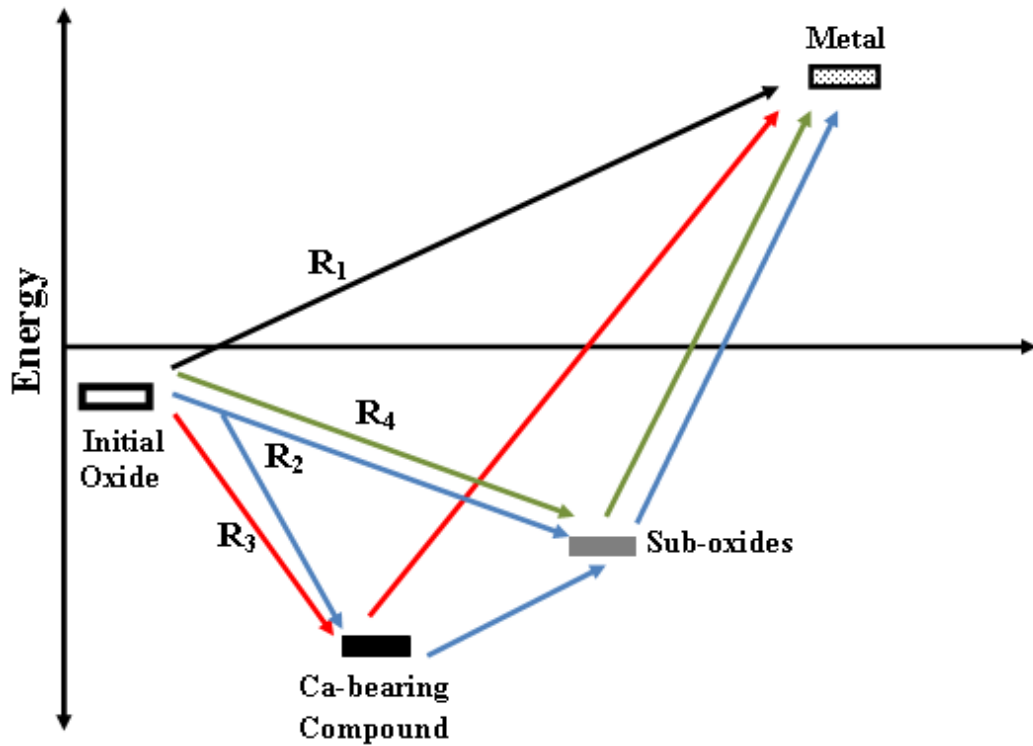


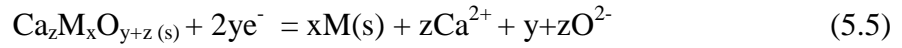
**Figure 5.1** Different deoxidation routes in electrodeoxidation process.

It is worth noting that Ca-bearing compounds are more stable than sub-oxides and they are consumed only in the later stages of deoxidation, see Chapter 3. This is already illustrated in Fig 5.1 where Ca-bearing oxides are shown to decompose into sub-oxides.

A third route in electro-deoxidation may follow  $R_3$  in Fig. 5.1. Here, only Ca-bearing compound forms by a chemical reaction given by:



The reaction given in Eq. 5.4 is thermodynamically favorable for many oxide systems (Yan, 2008). Subsequent to the formation of Ca-bearing compound, its reduction to pure metal may occur by:



It is known that  $\text{Al}_2\text{O}_3$  is reduced in this way (Yan and Fray, 2009).

The fourth route,  $R_4$ , involves stepwise reduction of an oxide through its sub-oxides, see Fig. 5.1. Here, Ca-bearing compounds do not form as they are thermodynamically unstable at reduction conditions or Ca-M-O system does not involve those compounds at all. Previous studies show that reduction of  $\text{Fe}_2\text{O}_3$  occurs in this way (Li et al., 2009).

### 5.3 Oxygen Permeability in Electro-deoxidation Process

Fig. 5.2 shows a schematic drawing of a single oxide particle ( $\text{M}_x\text{O}_y$ ) in contact with electrolyte from its one side and well attached to the current collector from other side. The directions of oxygen and electron flow are also indicated in the figure. Electrons transferred from current collector are transported to reduction front. Similarly, there is a net oxygen flow out of the oxide particle.

The approach presented here is similar to 3PI model stating that oxygen flow occurs from pellet to the electrolyte. However, it differs from 3PI model such that the oxide is electronically conducting while in 3PI model the electron transfer is achieved only by a metallic conductor. In case of non-conducting oxides, the presence of a metallic conductor at solid-electrolyte interface delivering electrons from current conductor, such as a metallic wire, is beneficial. However, Fig. 5.2 offers a simple way to explain the development of deoxidation in an oxide particle and as a result preferred in this study.

In Fig. 5.2, it is considered that the initial reaction of metal oxide results in the formation of a reacted layer at the oxide-electrolyte interface. The chemistry of the reacted layer depends on the deoxidation route followed in reduction process, see Fig. 5.1. It can be made out of only sub-oxides or can be mixture of Ca-

bearing compound plus sub-oxides. Reduction of the reacted layer yields the target metal at the outermost surface of the oxide particle. These layers are separated by boundaries numbered from 1 to 3 in Fig. 5.2.

For such an oxide particle, the progress of deoxidation depends on two processes: conversion of oxide ( $M_xO_y$ ) to the reacted layer, as given in Eq. 5.2 and 5.4, and conversion of the reacted layer to the target metal (M), given by Eq. 5.3 and 5.5. The conversion reactions occur by transport of oxygen. If the layer has a contact with electrolyte, the oxygen removal occurs directly from solid to electrolyte. If the solid phase does not have a contact with electrolyte, the oxygen is transferred to the adjacent solid layer towards electrolyte.

The direct removal of oxygen ions from solid to the electrolyte occurs when there is a contact between the reactant solid phase and the electrolyte. For example, in order to convert the metal oxide to the reacted layer, both previously converted metal and reacted layer must be fragmented. The fragmentation can be induced by volume incompatibilities between initial and final phases. Thus, there should be extensive difference between normalized molar volumes of target metal, reacted layer and metal oxide. The molar volume:

$$V_m = \frac{MW}{\rho} \quad (5.6)$$

Here, MW is the molecular weight of material (g/mol),  $\rho$  is density of material ( $\text{g/cm}^3$ ) and  $V_m$  is the molar volume of the material ( $\text{cm}^3/\text{mol}$ ). This quantity is normalized with respect to a mole of metal atom.

If there is an extensive change in normalized molar volume during deoxidation, the product phase loses its physical integrity and breaks into pieces. By this way, the electrolyte could penetrate into solid phase and reactions given in Eq. 5.2-5.5

can proceed occur. If this is not achieved, deoxidation process slows down or may stop altogether.

A similar argument on porous structure of product was developed by Chen et al. (2000). The fragmentation of solid is the basis of 3PI model as the formation of new 3PI relies on the penetration of electrolyte (Wang et al., 2008). Alexander et al. (2006) discussed the volume change in reduction of  $\text{TiO}_2$  and stated that the volume change in the solid is critical for the progress of deoxidation. Recently, Li et al. (2010) stated that the change in molar volume must lead to shrinkage of solid while in volume expansion or limited shrinkage, deoxidation may retard.

For deoxidation to proceed without fragmentation, the oxygen must be transferred to the adjacent layer. Then, this adjacent layer must have sufficiently high oxygen permeability so that the oxygen transport and electrodeoxidation occurs. The permeability of oxygen,  $P$ , can be defined by:

$$P = S \times D \quad (5.7)$$

Here,  $S$  is the solubility and  $D$  is the diffusivity of oxygen in solid.

If oxygen permeability of a layer is low, then deoxidation process slows down. Deoxidation may halt completely due to extremely low oxygen permeability of a layer. In a successful deoxidation, oxygen is transported through layers. Once the oxygen reaches to the boundary where solid is in contact with electrolyte, it is transferred to liquid by electrochemical reaction.

Two extreme cases for deoxidation are illustrated in Fig. 5.3. Fig 5.3(a) represents the case in which normalized molar volumes of all layers are different from each other. This results with the fragmentation of each layer through which the electrolyte could penetrate. Thus, the conversion from oxide ( $\text{M}_x\text{O}_y$ ) to reacted layer and conversion from reacted layer to target metal ( $\text{M}$ ) occur one after the other.

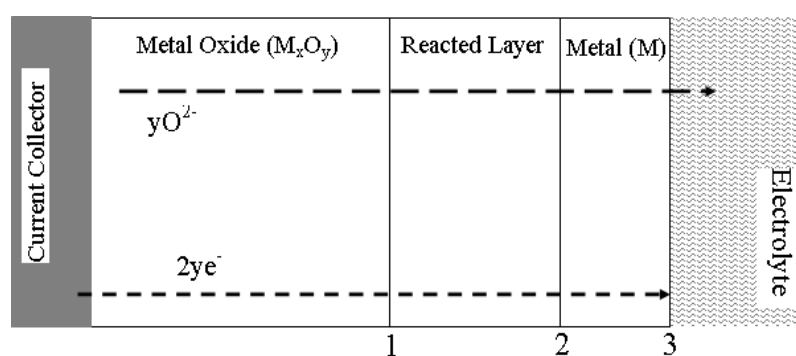
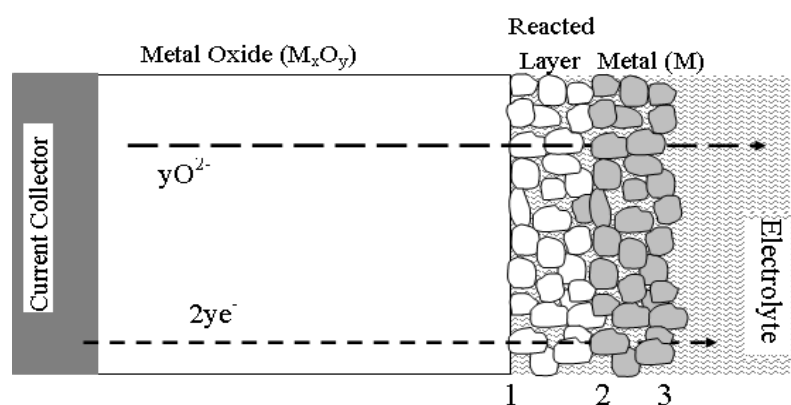
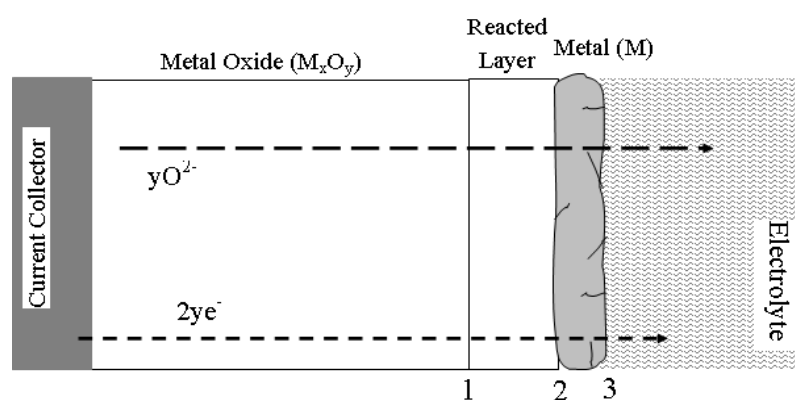


**Figure 5.2** The schematic illustration of a metal oxide,  $M_xO_y$  particle during deoxidation. Different layers may form during the process.



(a)



(b)

**Figure 5.3** Different cases in deoxidation of oxides: (a) layers are fragmented; (b) no fragmentation in layers.



Fig 5.3(b) represents the case in which both reacted and metal layers are in place without fragmentation. In this case, the normalized molar volumes of metal, reacted layer and metal oxide are nearly the same or the difference could be compensated by the system. The physical integrity of the system allows transport of oxygen ions only from one layer to another. However, the success of deoxidation depends on the oxygen permeability of each layer. If oxygen ions move through each layer successfully, the deoxidation occurs at metal/electrolyte interface, i.e. boundary number 3.

## 5.4 Examination of Different Oxide Systems

While Fig. 5.1. and Fig. 5.3 give a general view on deoxidation, it is useful to examine different oxide systems, i.e. NiO, MgO, Fe<sub>2</sub>O<sub>3</sub> and TiO<sub>2</sub>.

### 5.4.1 Deoxidation of NiO

As reported in Chapter 4, NiO was successfully deoxidized to Ni at 900 °C by applying 3.2V. After 24 h of deoxidation, XRD of the product has only Ni peaks showing complete deoxidation, see Fig. 4.4. SEM analysis showed that the Ni particles are fused together forming particles up to 10 µm in size. In current-time plot recorded during deoxidation, Fig. 4.3, the current cascade down to 0.1 A within 3 h. This implies that the reduction is fast and completes in a duration much shorter than 24 h. Previous studies do confirm this fast reduction of NiO at ordinary deoxidation temperatures, i.e. 850-950 °C (Jackson et al., 2010).

Easy reduction of NiO is the result of different properties of the oxide. The reduction voltage of NiO is +0.22 V and +0.33 V at 600 °C and 900 °C, respectively, see Table 4.1. The conductivity of NiO pellet is high, 10<sup>-9</sup> ohm<sup>-1</sup> cm<sup>-1</sup> at room temperature, see Chapter 4. It is known that the conductivity increases further with increase in temperature (Antolini, 1992). There is no sub-oxide of NiO. Also, it is difficult to substitute Ca<sup>2+</sup> ion in NiO ( $r_{Ca}^{2+} = 1.0 \text{ \AA}$   $r_{Ni}^{2+} = 0.7 \text{ \AA}$ ) (Barsoum, 2002).

The characteristics of NiO reported above imply that the reduction of NiO occurs by route R1, Fig 5.1. The reduction occurs in a single step process without formation of Ca-bearing compounds. This is parallel to what was observed in previous studies (Qiu et al., 2005). Sub-oxides and Ca-bearing compounds do not form in the oxide pellet during deoxidation of NiO meaning that the reacted layer does not form. Thus, the applicable cathodic reaction has the form:

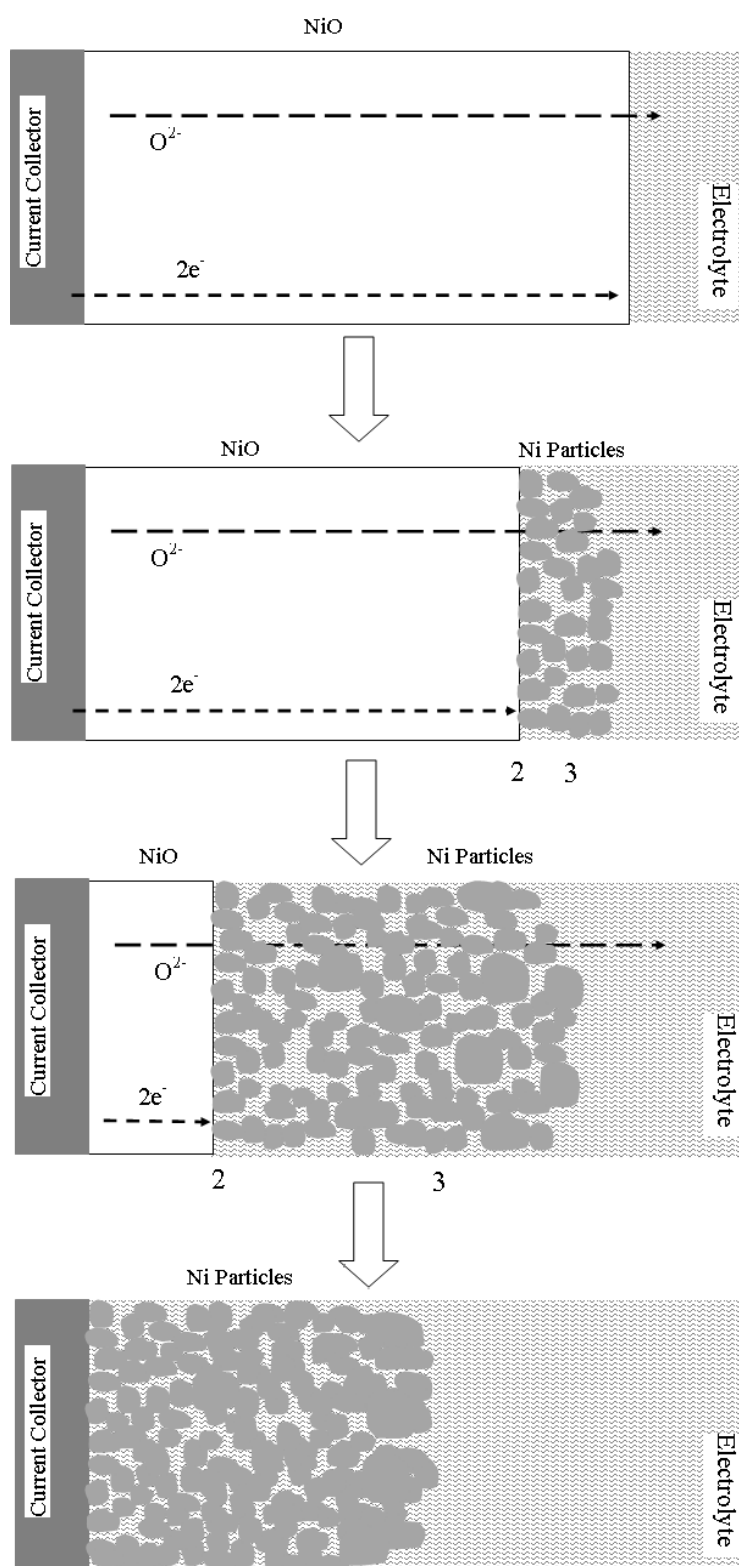


Table 5.1 shows normalized molar volumes of NiO and Ni. As seen from the table, molar volume of Ni is ca. 37 % smaller than that of NiO, i.e. there is considerable shrinkage during deoxidation. This implies that the deoxidized parts fragments into pieces. Oxygen removal from NiO occurs via oxygen transport between oxide and electrolyte.

**Table 5.1** *Normalized molar volumes of NiO and Ni at 900 °C. The percent change in volume, when all oxygen is removed, is given in the last column.*

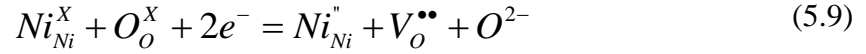
| <b>Material</b> | <b>Molecular Weight<br/>(g/mol)</b> | <b>Density<br/>(g/cm<sup>3</sup>)</b> | <b>Normalized<br/>Molar Volume<br/>(cm<sup>3</sup>/mol Ni)</b> | <b>%<br/>Change</b> |
|-----------------|-------------------------------------|---------------------------------------|--|---------------------|
| NiO             | 74.69                               | 6.67                                  | 11.20  | - 36.33             |
| Ni              | 58.69                               | 8.23                                  | 7.13   | -                   |

The progress of deoxidation in NiO particle is schematically shown in Fig. 5.4. Here, metallic Ni forms in front of NiO as a porous non-blocking layer, allowing transport of electrolyte. As the electrolyte can reach to NiO surface, reduction can proceed by Eq. 5.8.



**Figure 5.4** The progress of deoxidation in NiO. Note that reacted layer does not form during process and the metallic Ni is non-blocking.

It is worth to examine the deoxidation of NiO from atomistic point of view. In deoxidation of NiO, oxygen is removed from the surface of the oxide particle continuously. This is schematically shown in Fig. 5.5. The removal of oxygen ions result in formation of oxygen vacancies in the oxygen sub-lattice. The defect reaction representing the oxygen removal form NiO lattice is given by:



In fact, this is equal to the deoxidation reaction given in Eq. 5.8. Here,  $Ni_{Ni}^X$  and  $O_O^X$  represents Ni atom in nickel site and oxygen atom in oxygen site, respectively;  $V_O^{\bullet\bullet}$  is oxygen vacancy with relative charge 2+ and  $Ni_{Ni}''$  represents nickel atom with relative charge 2-.

As seen from the equation, the reduction reaction creates a metallic Ni at Ni site and a neutral oxygen vacancy in oxygen sub-lattice. The formed oxygen ion is transferred to molten salt through NiO/electrolyte interface.

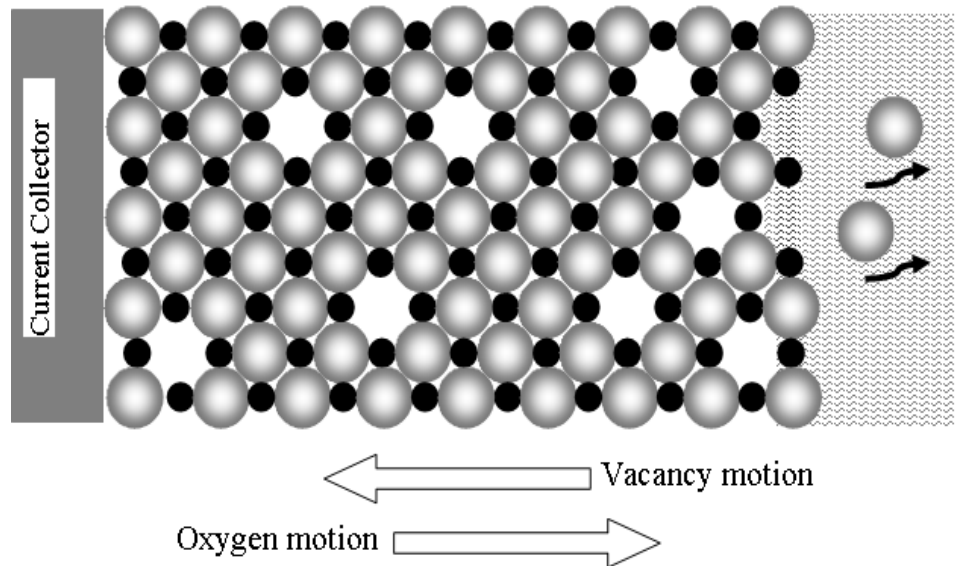


**Figure 5.5** Motion of oxygen ions and oxygen vacancies in deoxidation of NiO. Gray spheres represent oxygen ions and black ones represent Ni atoms.

The reaction given in Eq. 5.9 implies that NiO/electrolyte interface behaves as a source for oxygen vacancies. As a result, it is considered that the vacancy mechanism dominates for the transport of oxygen in NiO although both interstitial and vacancy mechanisms were proposed for oxygen diffusion in NiO (Keeffe and Moore, 1961). The motion of oxygen ions and vacancies are in opposite directions in NiO, Fig. 5.5. Reported diffusion coefficient value for oxygen in NiO lattice is between  $10^{-10}$ - $10^{-15}$  m<sup>2</sup>/s at 900°C (Keeffe and Moore, 1961; Dubois et al. 2006).

Reactions given in Eq. 5.9 and Fig. 5.5 means that the formation and motion of vacancies creates an oxygen gradient in NiO particle, i.e. the closer to the NiO/electrolyte interface, the lower the oxygen concentration is. This gradient results in a gradual volume change in the solid lattice. Once the shrinkage reaches to a critical value, system could not tolerate it and a part of NiO accommodating reduced Ni separates from the main lattice by fragmentation. Thus, oxide surface continuously breaks-up leaving pieces while electrolyte penetrates through them. As a result, neither Ni nor oxygen deficient NiO surface do not behave as a blocking layer in reduction of NiO.

#### **5.4.2 Deoxidation of MgO**

Experimental results show that the reduction of MgO is quite difficult. As given in Chapter 4, the attempt to reduce pure MgO in CaCl<sub>2</sub>-NaCl eutectic was not successful at 600 °C. It was found that oxide pellets remain intact after deoxidation for 24 hours. A similar result was obtained when the reduction is conducted in CaO added electrolyte (Cox and Fray, 2002).

The difficulty in deoxidation of MgO could be attributed to several reasons. The reduction voltage of MgO is - 1.64 V at 600 °C. This is much higher than the voltage necessary to reduce many oxide systems, see Fig. 2.5. The high reduction voltage puts an important barrier for deoxidation of MgO leaving little overpotential to overcome different polarizations, see 3PI model in Chapter 2.

It is also shown in Chapter 4 that sintered MgO pellets exhibit quite low conductivity both at room temperature and at 600 °C,  $10^{-14}$ – $10^{-9}$  ohm<sup>-1</sup> cm<sup>-1</sup>, respectively. In fact, MgO is known as an insulating oxide (Stankic et al., 2005).

There are also other factors which may limit the deoxidation of MgO. As the melting point of Mg is 650 °C, the reduction temperature should be kept around 600 °C. Cox and Fray (2002) state that there might be mass transport limitation for oxygen in both solid and liquid state due to low deoxidation temperature.

The reduction route for MgO has not been reported yet. However, structurally MgO is very similar to NiO: it has rock-salt structure, it does not have a sub-oxide and Ca<sup>2+</sup> does not incorporate into MgO lattice. As a result, the reduction of MgO is expected to occur similar to that of NiO, i.e. in single step process without formation of the reacted layer.

Table 5.2 shows normalized molar volumes of MgO and Mg. It can be seen that with deoxidation of MgO, 35 % expansion in the volume occurs at 600 °C. This is opposite to what was mentioned for reduction of NiO. It is considered that 35 % of volumetric expansion in metallic magnesium results in very limited fragmentation or it can be accommodated without the fragmentation of Mg layer.

**Table 5.2** *Normalized molar volumes of MgO and Mg calculated from molecular weight and density of materials. Molar volume of Mg is calculated for 600 °C. The percent change in volume, when all oxygen is removed, is given in the last column.*

| Material | Molecular Weight<br>(g/mol) | Density<br>(g/cm <sup>3</sup> ) | Normalized<br>Molar Volume<br>(cm <sup>3</sup> /mol Mg) | %<br>Change |
|----------|-----------------------------|---------------------------------|---|-------------|
| MgO      | 40.30                       | 3.58                            | 11.26   | + 34.9      |
| Mg       | 24.31                       | 1.60                            | 15.19   | -           |

Once it is formed, Mg layer may maintain its volume, introducing significant amount of local stress to its surrounding, or it may expand out of the oxide particle. In any case, magnesium layer is expected to form between oxide and electrolyte with very limited fragmentation, see Fig. 5.6.

The physical integrity of Mg layer has an important consequence: the deoxidation could not proceed through oxide/electrolyte interface. The expanded, but non-fragmented, Mg layer prevents the penetration of electrolyte and the formation of new oxide-electrolyte contacts. In a recent study, Li et al. (2010) reached the same conclusion for MgO by stating that the volume expansion is the main reason in MgO system yielding failure of deoxidation.

For deoxidation to proceed in MgO, oxygen must transfer to Mg layer, transport through it and finally leave from the solid at Mg/electrolyte interface. In this case, the deoxidation can be given by two reactions in series:



, which sum up to give:



Apparently, oxygen permeability in Mg is critical. It is known that the solubility of oxygen in Mg is extremely small, i.e. in the order of ten ppm (Kofstad, 1972). Consequently, the amount of oxygen that could be transported through Mg is very limited. Meanwhile, the diffusion of oxygen in Mg is expected to be extremely slow, as for hcp metals, the activation energy for oxygen diffusion is as high as 350 kJ/mol (Khanna, 2002). Thus, the permeability of oxygen in magnesium must be extremely low. As a result of fairly low oxygen permeability in Mg, the deoxidation does not proceed but halts completely.

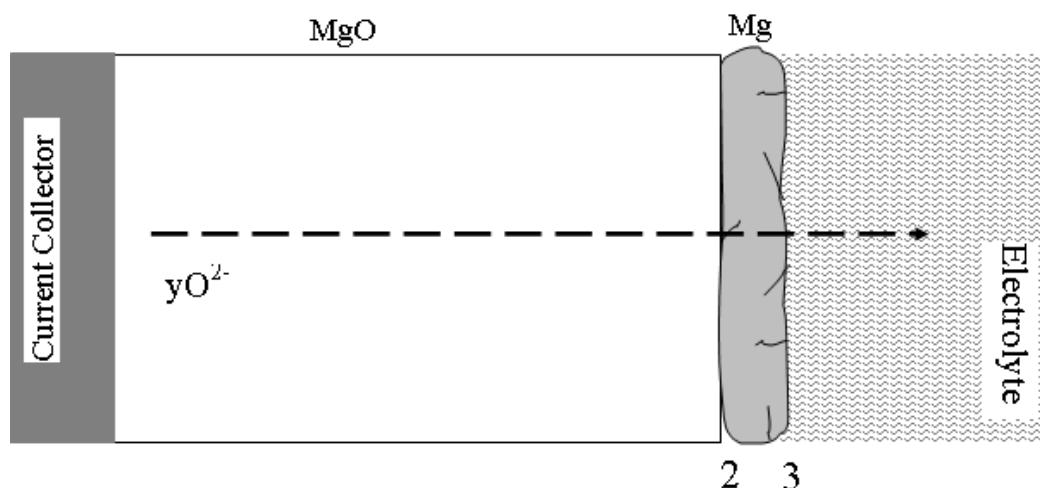


**Figure 5.6** Deoxidation of MgO. Note that Mg forms a blocking-layer between MgO and electrolyte.

Similar to transport in metallic Mg, transport of oxygen in MgO is also critical. Different values for oxygen transport in MgO were reported in the literature, i.e. diffusion coefficient values are between  $10^{-20} - 10^{-24} \text{ m}^2/\text{s}$  at  $900^\circ\text{C}$  (Harrop, 1968). Large ionic radius of oxygen ion makes the oxygen transport difficult to occur in MgO lattice at low temperatures. As a result, the rate of oxygen transfer from MgO to Mg is also very limited.

To sum up, since physical integrity of magnesium layer is maintained and oxygen permeability of Mg is extremely low, magnesium behaves as a blocking layer in deoxidation of MgO. The low reducibility of MgO is due to this blocking nature of Mg layer that could envelope MgO where it is in contact with electrolyte.

#### 5.4.3 Deoxidation of $\text{Fe}_2\text{O}_3$

As it is shown in Chapter 3, deoxidation of  $\text{Fe}_2\text{O}_3$  occurs rapidly. Metallic iron could be obtained within a few hours at  $900^\circ\text{C}$  when 3.2 V is applied between porous  $\text{Fe}_2\text{O}_3\text{-TiO}_2$  pellet and the graphite anode. This is in agreement with Qiu et al. (2006), who reported rapid formation of Fe from  $\text{Tb}_4\text{O}_7\text{-Fe}_2\text{O}_3$  mixtures.



Haarberg et al. (2009) examining the deoxidation of pure  $\text{Fe}_2\text{O}_3$  in  $\text{CaCl}_2\text{-CaO}$  electrolyte found that the deoxidation completed within a few hours.

Facile deoxidation of  $\text{Fe}_2\text{O}_3$  to form Fe could be attributed to low reduction voltage of  $\text{Fe}_2\text{O}_3$ . As it is mentioned in Chapter 2, reduction voltage of hematite is between zero and +0.17 V at 600 - 900 °C, respectively. Complete reduction of  $\text{Fe}_2\text{O}_3$  to Fe was reported even at applied voltages of as low as 1.0 V at 800 °C (Li et al, 2009).

As shown in Chapter 3, deoxidation of  $\text{Fe}_2\text{O}_3$  occurs in two steps: reduction to FeO and then the formation of Fe. It should be noted that while Ca-Fe-O system has many ternary compounds, i.e.  $\text{CaFe}_2\text{O}_4$ ,  $\text{Ca}_2\text{Fe}_2\text{O}_5$ ,  $\text{CaFe}_4\text{O}_7$ , they were not detected in partially reduced samples (Hillert et al., 1990). Li et al. (2009) conducted deoxidation experiments with pure  $\text{Fe}_2\text{O}_3$  and concluded the same for the reduction pathway.

The studies reported above imply that a semi-reduced  $\text{Fe}_2\text{O}_3$  oxide particle is composed of three layers:  $\text{Fe}_2\text{O}_3$  as unreacted part, FeO as reacted layer and Fe as metallic product. Rapid deoxidation of  $\text{Fe}_2\text{O}_3$  implies that metallic layer and reacted layer have non-blocking characteristics.

Normalized molar volumes of  $\text{Fe}_2\text{O}_3$ , FeO and Fe are given in Table 5.3. Table 5.3 demonstrates that both Fe and FeO have lower molar volume than  $\text{Fe}_2\text{O}_3$  has. As a result, some shrinkage is expected while  $\text{Fe}_2\text{O}_3$  is deoxidized to Fe.

In order to show volume change at each step of reduction, formation reactions of FeO and Fe and corresponding volume changes are given in Table 5.4. As it can be seen from the table, formation of FeO results in 18 % decrease in volume of the solid. The amount of shrinkage is more pronounced when FeO is reduced into Fe, i.e. 39 %.

**Table 5.3** Normalized molar volumes of  $Fe_2O_3$ ,  $FeO$  and  $Fe$ . The percent change in volume, when all oxygen is removed, is given in the last column.

| Material  | Molecular Weight<br>(g/mol) | Density<br>(g/cm <sup>3</sup> ) | Normalized<br>Molar Volume<br>(cm <sup>3</sup> /mol Fe) | %<br>Change |
|-----------|-----------------------------|---------------------------------|---|-------------|
| $Fe_2O_3$ | 159.69                      | 5.24                            | 15.24   | - 50.18     |
| $FeO$     | 71.84                       | 5.75                            | 12.49   | - 39.21     |
| $Fe$      | 55.85                       | 7.36                            | 7.59  | -           |

It is considered that shrinkage in  $FeO$  and  $Fe$  results in fragmentation of the solid. It is known that thin  $Fe-O$  scales may deform in a brittle manner at temperatures between 700 °C and 1000 °C (Hidika et al., 2003; Suarez et al., 2009). Thus, fragmentation of  $FeO$  phase is highly probable for 18 % shrinkage. The final reduction from  $FeO$  to  $Fe$  introduces high shrinkage in the solid, 39 %. This results in formation of  $Fe$  islands, leaving porosity between them.

The physical state of a  $Fe_2O_3$  particle during deoxidation is shown in Fig. 5.7. As seen in the figure, both reacted and metallic layers are porous networks of small particles. The porosity allows transport of electrolyte towards inner parts of the oxide particle. By this way, reactions given in Table 5.4 could proceed continuously at the surfaces of  $Fe_2O_3$  and  $FeO$ .

**Table 5.4** Volume change in solid state for stepwise reduction of  $Fe_2O_3$ . Note that the value is calculated for 1 mole of reactant.

| Reaction                                     | % Change |
|--|----------|
| $Fe_2O_{3(s)} + 4e^- = 2FeO_{(s)} + 2O^{2-}$ | - 18.05  |
| $FeO_{(s)} + 2e^- = Fe_{(s)} + O^{2-}$       | - 39.23  |

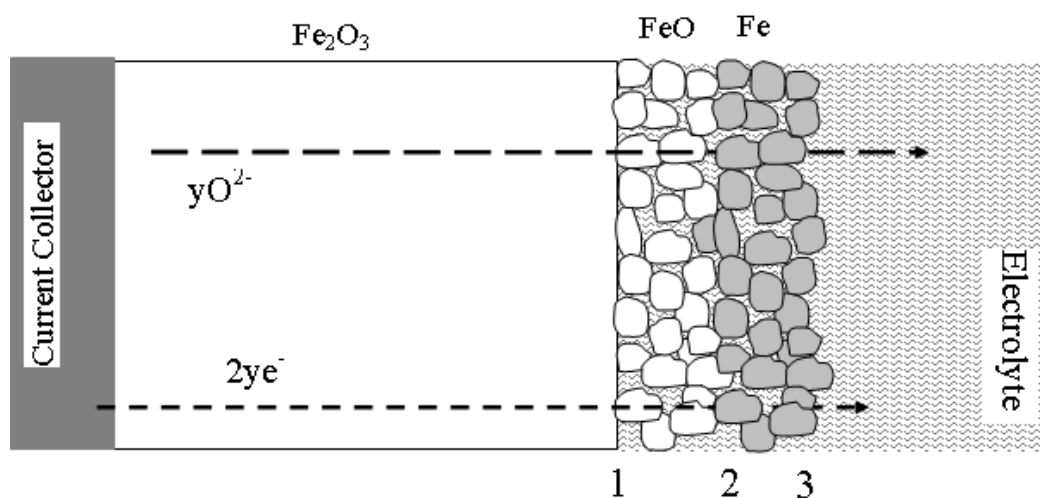


**Figure 5.7** *The schematic representation of deoxidation of  $\text{Fe}_2\text{O}_3$  particle.*

Fig. 5.8 shows the progress of electrodeoxidation in  $\text{Fe}_2\text{O}_3$  particle according to explanation given above. As it can be seen from the figure, both FeO and Fe form at the beginning of deoxidation while the amount of  $\text{Fe}_2\text{O}_3$  decreases with time. The non-blocking nature of both FeO and Fe layers allow transport of electrolyte through each layers and formation of new sites for oxygen removal. The reduction is completed with the full conversion of FeO to Fe.

It is known that  $\text{Fe}_2\text{O}_3$  is a stoichiometric oxide and solubility of oxygen in Fe is quite low. Thus, the diffusivity of oxygen in both phases is not a big concern. However, it is known that FeO has some oxygen solubility above 600 °C. Then, oxygen transport in the solid FeO could be crucial for deoxidation of FeO. According to Hembree and Wagner (1969), the diffusion coefficient of oxygen in  $\text{Fe}_{0.93}\text{O}$  lattice is nearly equal to  $5 \times 10^{-12} \text{ m}^2/\text{s}$  at 800 °C. Activation energy value for oxygen diffusion in the lattice is 326 kJ/mol (Ilschner et al., 1964). It should be noted that the reported diffusion coefficient value of oxygen in FeO is much higher than that in similar oxides, i.e. MgO and CoO. For the latter, values are between  $10^{-15}$  -  $10^{-24} \text{ m}^2/\text{s}$  at 900 °C (Harrop, 1968). Thus, high diffusion of oxygen in FeO allows facile oxygen removal from this phase.

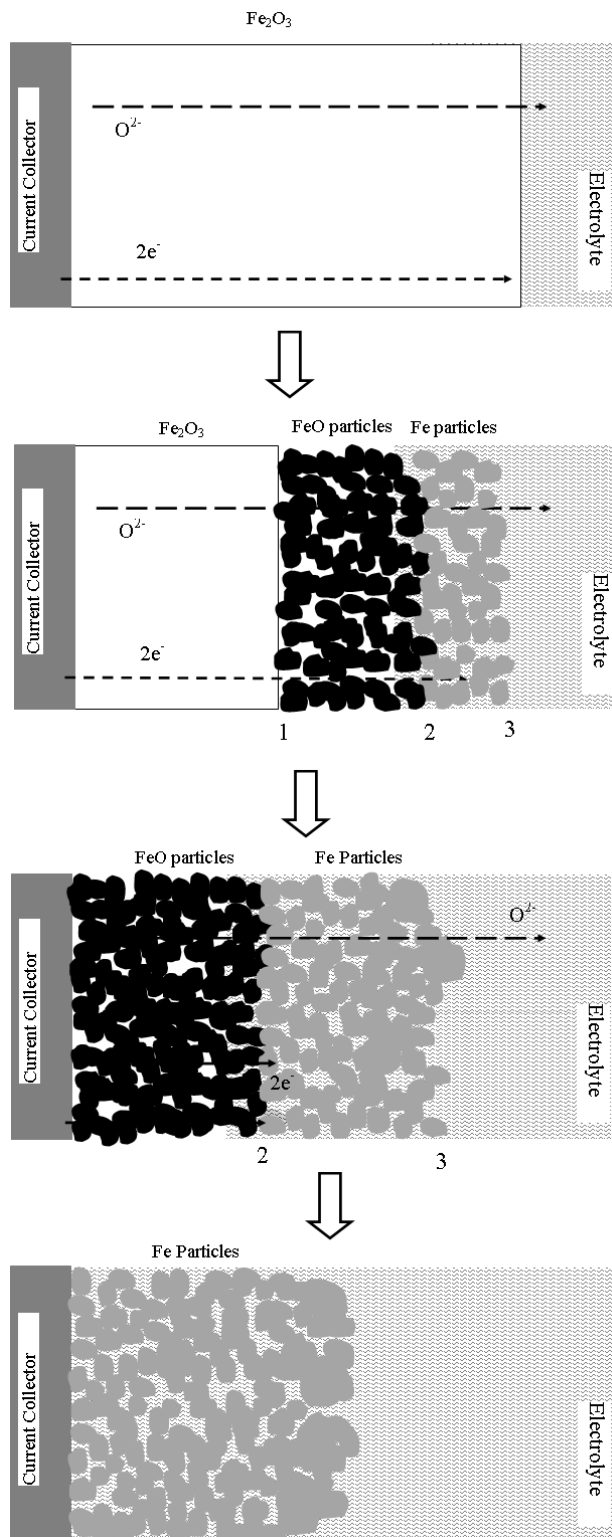


**Figure 5.8** The progress of deoxidation in  $\text{Fe}_2\text{O}_3$ . Note that  $\text{FeO}$  and  $\text{Fe}$  are non-blocking.

To sum up, extensive normalized molar volume change during the deoxidation of  $\text{Fe}_2\text{O}_3$  allows the rapid deoxidation of  $\text{Fe}_2\text{O}_3$ . Reacted layer, i.e.  $\text{FeO}$ , and metallic Fe do not impede deoxidation as they fragment into pieces at the deoxidation conditions. Meanwhile, comparatively fast transport of oxygen ions, i.e. high permeability of oxygen, in solid  $\text{FeO}$  is helpful to achieve rapid deoxidation.

#### **5.4.4 Deoxidation of $\text{TiO}_2$**

As shown in Chapter 3, deoxidation of  $\text{TiO}_2$  necessitates significantly long reduction times at 900 °C. One reason for this is the complexity of Ca-Ti-O and Ti-O systems and stepwise reduction of  $\text{TiO}_2$ .

The difficulty in deoxidation of  $\text{TiO}_2$  could be attributed to several reasons.  $\text{TiO}_2$  has many sub-oxides as Ti could possess many oxidation states. This forces the system to be reduced in a stepwise manner. According to Mohandas et al. (2004), oxygen removal from  $\text{TiO}_x$  becomes more and more difficult as the oxygen content (x) decreases, e.g. + 0.750V (vs.  $\text{Na}^+/\text{Na}$ ) and + 0.338V (vs.  $\text{Na}^+/\text{Na}$ ) for  $\text{TiO}_2$  and  $\text{TiO}$ , respectively. Meanwhile, these oxides may have completely different physical properties. For example,  $\text{TiO}$  is an electronic conductor while  $\text{TiO}_2$  is a semiconductor (Barsoum, 2002). Such variations in the oxide pellet also make  $\text{TiO}_2$  system difficult to examine.

As shown in Chapter 2, deoxidation of  $\text{TiO}_2$  does not occur directly but follows a complicated route. Formation of  $\text{CaTiO}_3$  is one indication of this. The complicated route in deoxidation of  $\text{TiO}_2$  was also shown in other studies (Wang and Lee, 2004; Dring et al., 2005). The most comprehensive study was performed by Alexander et al. (2006) demonstrating that reduction of  $\text{TiO}_2$  occurs step-wise manner through the formation of sub-oxides, i.e.  $\text{Ti}_4\text{O}_7$ ,  $\text{Ti}_3\text{O}_5$ ,  $\text{Ti}_2\text{O}_3$ ,  $\text{TiO}$  and finally  $\text{Ti(O)}$ .  $\text{CaTiO}_3$  and  $\text{CaTi}_2\text{O}_4$  also form during deoxidation.

Normalized molar volumes of each phase observed in the reduction of  $\text{TiO}_2$  are calculated and given in Table 5.5. As it can be seen from the table some phases, e.g.  $\text{CaTiO}_3$ ,  $\text{Ti}_4\text{O}_7$ , have larger molar volumes than  $\text{TiO}_2$  has while some others, e.g.  $\text{Ti}_3\text{O}_5$ ,  $\text{TiO}$ , have smaller molar volumes. Additionally, the percent change in volume, when all oxygen is removed from each phase, is also shown in the table. The normalized values show that the removal of oxygen results in volumetric shrinkage for each material which can be as large as 70 %.

In order to understand the volume changes in solid-state, a reaction-based analysis was performed. For this purpose, deoxidation route of  $\text{TiO}_2$  proposed by Alexander et al. (2006) is followed. The reaction sequence and related percent volume change are given in Table 5.6. It is seen from the table that expansion in solid occurs until the formation of  $\text{CaTi}_2\text{O}_4$ . It is already known that incorporation of  $\text{Ca}^{2+}$  ion into the solid-state results in expansion of the crystal structures. This expansion is apparent in the formation of Magneli phases. It may be noted that in formation of Magneli phases, there is no removal of oxygen from the solid-state.

Volume expansions associated with formation of Magneli phases varies between 3-15 %. These values are large enough to cause fragmentation of the phases involved, as they have only limited deformation capabilities, even at elevated temperatures (Li et al., 1996).

Formation of  $\text{TiO}$  occurs by disproportionation of  $\text{CaTi}_2\text{O}_4$ , see Table 5.6. The reaction brings about nearly 43 % volume shrinkage in the solid-state that is enough for  $\text{TiO}$  to break up into pieces. Thus, one can state that at this stage of reduction, gradual change in particle size and volume of the solid-state occur leading to the formation of significant amount of porosity in the structure.

Reduction from  $\text{TiO}$  to  $\text{Ti(O)}_x$  brings about 8 % decrease in volume. With the removal of oxygen atoms from the surface, the mismatch between volume of  $\text{Ti(O)}_x$  and  $\text{TiO}$  results in the development stress in the  $\text{Ti(O)}_x$  lattice.

**Table 5.5** Normalized molar volumes of materials observed in deoxidation of  $TiO_2$ . The percent change in volume, when all oxygen is removed, is given in the last column. The molecular weight and density of  $Ti(O)$  were calculated by assuming the material has 30 at % oxygen. Density of  $Ti(O)$  and  $Ti$  was calculated for 900 °C.

| Material    | Crystal Structure | Molecular Weight (g/mol) | Density (g/cm <sup>3</sup> ) | Normalized Molar Volume (cm <sup>3</sup> /mol Ti) | % Change |
|-------------|-------------------|--------------------------|------------------------------|---|----------|
| $TiO_2$     | Tetragonal        | 79.87                    | 4.25                         | 18.79   | - 40.72  |
| $CaTiO_3$   | Orthorhombic      | 135.94                   | 3.98                         | 34.15   | - 67.38  |
| $Ti_4O_7$   | Triclinic         | 303.47                   | 4.34                         | 17.48   | - 36.27  |
| $Ti_3O_5$   | Monoclinic        | 223.60                   | 4.35                         | 17.13   | - 34.98  |
| $Ti_2O_3$   | Hexagonal         | 143.73                   | 4.57                         | 15.72   | - 29.15  |
| $CaTi_2O_4$ | Orthorhombic      | 199.81                   | 4.37                         | 22.86   | - 51.04  |
| $TiO$       | Cubic             | 63.87                    | 4.95                         | 12.90   | - 13.66  |
| $Ti(O)$     | Hexagonal         | 52.67                    | 4.65                         | 11.87   | - 6.14   |
| $Ti$        | Hexagonal         | 47.87                    | 4.29                         | 11.14   | -        |

**Table 5.6** Volume change in solid state for stepwise reduction of  $TiO_2$ . Note that the value is calculated for 1 mole of solid reactant.

| Reaction  | % Change |
|---|----------|
| $5TiO_{2(s)} + Ca^{2+} + 2e^- = Ti_4O_{7(s)} + CaTiO_{3(s)}$    | + 10.76  |
| $4Ti_4O_{7(s)} + Ca^{2+} + 2e^- = 5Ti_3O_{5(s)} + CaTiO_{3(s)}$ | + 4.10   |
| $3Ti_3O_{5(s)} + Ca^{2+} + 2e^- = 4Ti_2O_{3(s)} + CaTiO_{3(s)}$ | + 3.30   |
| $2Ti_2O_{3(s)} + Ca^{2+} + 2e^- = 3TiO_{(s)} + CaTiO_{3(s)}$    | + 15.84  |
| $CaTiO_{3(s)} + TiO_{(s)} = CaTi_2O_{4(s)}$                     | - 3.28   |
| $CaTi_2O_4 + 2e^- = 2TiO_{(s)} + Ca^{2+} + O^{2-}$              | - 43.30  |
| $TiO_{(s)} + 2(1-x)e^- = Ti(O)_x + (1-x)O^{2-}$                 | - 8.00   |
| $Ti(O)_{x(s)} + 2xe^- = Ti_{(s)} + xO^{2-}$                     | - 6.14   |

Previous studies show that the plasticity of Ti decreases in the presence of interstitially dissolved atoms, i.e. oxygen, hydrogen and nitrogen (Wasz et al., 1996). It was reported that even a few percentage of oxygen in Ti results in brittle fracture of the metal upon deformation. Thus, the volume change causes fragmentation of  $\text{Ti(O)}_x$  layer in deoxidation. By this way, electrolyte reaches to new surfaces penetrates and the deoxidation progresses continuously.

Further purification of  $\text{Ti(O)}_x$  to Ti by removal of oxygen results in nearly 6 % decrease in volume. It should be noted that the decrease is gradual and plasticity increases in parallel with the increasing purity. Thus, there is a probability that at that stage Ti purification does not bring a refinement in the size of particles.

As discussed above, non-blocking phases form during the course of deoxidation process. This is schematically shown in Fig. 5.9. Here, the reacted layer has multiphase structure composed of  $\text{Ti}_4\text{O}_7$ ,  $\text{Ti}_3\text{O}_5$ ,  $\text{Ti}_2\text{O}_3$ ,  $\text{TiO}$ ,  $\text{CaTiO}_3$  and  $\text{CaTi}_2\text{O}_4$  and the metallic layer is simply  $\text{Ti(O)}_x$ .

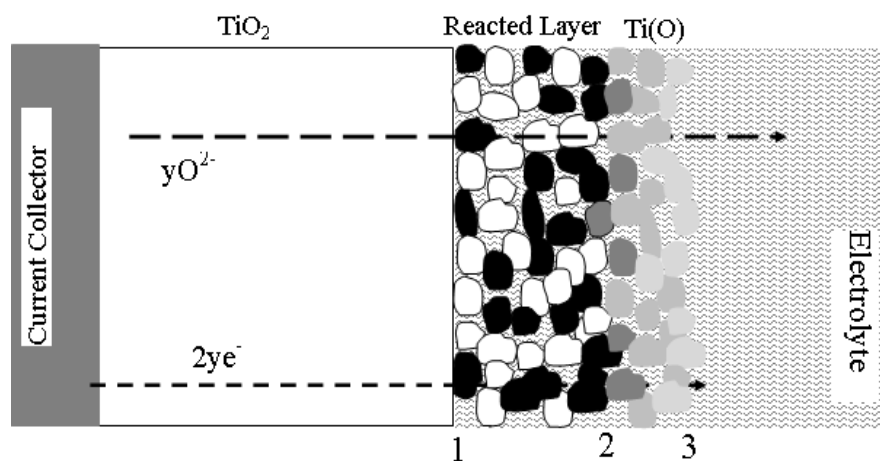


**Figure 5.9** The schematic view to  $\text{TiO}_2$  particle during deoxidation. The reacted layer is made out of  $\text{CaTiO}_3$  (black nodules) and different sub-oxides of  $\text{TiO}_2$  (white nodules). Metallic layer is  $\text{Ti(O)}$ , where metal with less oxygen is shown by lighter color.



The development of deoxidation in  $\text{TiO}_2$  particle is shown in Fig. 5.10. As stated above both reacted and metallic layers are porous and non-blocking. Continuous transport of electrolyte and  $\text{Ca}^{2+}$  ion is achieved through that porous structure. As a result, Magneli phases and  $\text{TiO}$  form continuously in the reacted layer. Metallic layer, which is made out of  $\text{Ti(O)}$ , grows continuously during deoxidation.

Regardless of the rate of the other electrochemical and solid state events, such as nucleation, oxygen transport in electrolyte, the study presented here demonstrates that volume change does not impede the reduction at any stage of deoxidation. Both reacted and  $\text{Ti}$  layers are porous and allow the transport of electrolyte into the necessary sites where the deoxidation proceeds.

Apparently, reduction of  $\text{TiO}_2$  involves many solid-state phenomena which could be rate limiting. For example, according to Alexander et al. (2006), chemical reaction in formation of  $\text{CaTi}_2\text{O}_4$  involves nucleation and growth processes which slow down the completion of the process.

One reason of slow deoxidation at later stages of reduction in  $\text{TiO}_2$  pellets is slow diffusivity of oxygen in  $\text{Ti(O)}_x$ . Reported diffusion coefficient values vary between  $10^{-6}$ -  $10^{-12}$   $\text{cm}^2/\text{sec}$  at  $900^\circ\text{C}$  (Stringer, 1960; Rosa, 1970). The permeability is probably moderately high due to high solubility of oxygen while the deoxidation proceeds slowly as the diffusion of oxygen is slow.

To sum up, change in volume in the solid state allows the progress of the deoxidation  $\text{TiO}_2$  pellets. Formation of Magneli phases expands the lattice; while with the formation of  $\text{CaTi}_2\text{O}_4$ , the shrinkage is expected. The amount of volume change is significant at almost all stages of the deoxidation resulting in flake of newly formed phases. In contrast to  $\text{Fe}_2\text{O}_3$  and  $\text{NiO}$ , the reduction of  $\text{TiO}_2$  yields  $\text{Ti}$  with extensive oxygen dissolves in it. The latter stages of deoxidation is spent to extract oxygen from  $\text{Ti}$  which has moderate oxygen permeability.

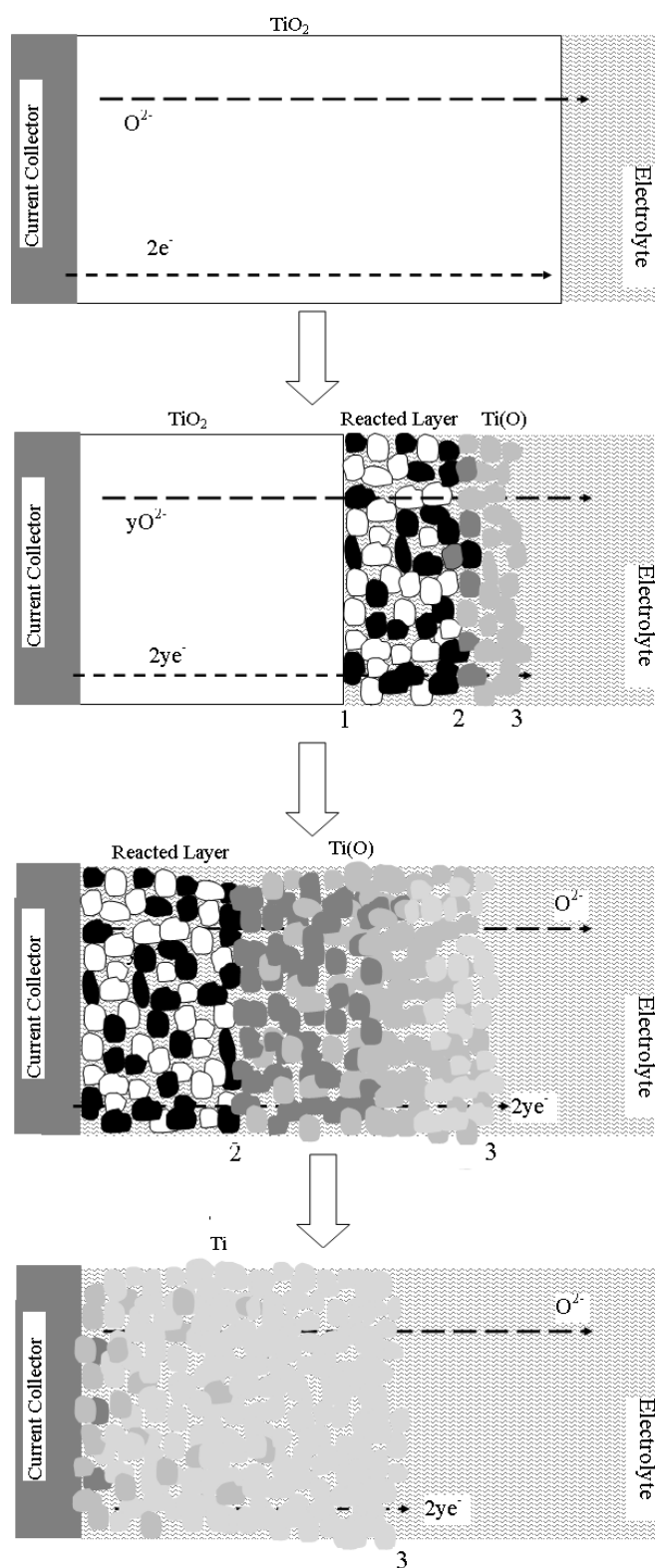


**Figure 5.10** The progress of deoxidation in  $\text{TiO}_2$ . Note that multi-phase reacted layer and metallic Ti are non-blocking.

## 5.5 Conclusion

A comparative study for electrodeoxidation of NiO, MgO, Fe<sub>2</sub>O<sub>3</sub> and TiO<sub>2</sub> based on oxygen permeability in solid state was carried out. It was concluded that deoxidation is continuous when the volume mismatch between product and reactant is high. In any case, i.e. contraction or expansion, the change must be large enough so that the product could not compensate the volumetric change by mechanism other than fragmentation. Equally importantly, the oxygen permeability of the resultant metallic phase and intermediate phases are important. In cases where the volume mismatch is low, the oxygen permeability of the solid phases must be high enough to carry on deoxidation process. Low oxygen permeability in solid phases may impede the progress of deoxidation.

The approach successfully explains why solid MgO particle could not be reduced at ordinary deoxidation conditions. It appears that either the expansion of Mg is compensated by volume expansion towards electrolyte or the volume is maintained constant by inducing local stresses around Mg nuclei. This local stress may hinder oxygen transport from MgO to electrolyte and may retard the progress of reduction on the surface of MgO. Once the surface is covered with Mg layer, Mg may block the oxygen transport between MgO and electrolyte since it has very low oxygen permeability.

## CHAPTER 6

### CONCLUSION

In this study, two hydrogen storage compounds, FeTi and Mg<sub>2</sub>Ni, were synthesized by electro-deoxidation technique from oxide mixtures, i.e. Fe<sub>2</sub>O<sub>3</sub>-TiO<sub>2</sub> and MgO-NiO, respectively. Experiments showed that synthesis of compounds necessitates adjustment of pellet properties and optimization of processing conditions.

Fe<sub>2</sub>O<sub>3</sub> and TiO<sub>2</sub> were sintered at temperatures between 900 °C to 1300 °C. The reduction of oxide pellets were conducted at 900 °C. The reduction of oxide pellets conducted at 3.2 V showed that sintering temperature has profound effect on the synthesis of FeTi. Pellets sintered at 900 °C yield mainly Fe with minor amount of FeTi and Fe<sub>2</sub>Ti. In contrast, the use of sintering temperatures close to or above 1100 °C leads to the formation of target composition FeTi in substantial amounts. This is attributed to two-phase structure of the pellets, Fe<sub>2</sub>TiO<sub>5</sub> and TiO<sub>2</sub>, sintered at high temperatures allowing uniform distribution of Fe and Ti atoms in a smallest scale. Interrupted experiments showed that Fe rapidly forms in the first 6 hours of deoxidation, while reduction of Ti-bearing oxides and formation of FeTi occurs at the later stages of reduction.

Deoxidation of MgO-NiO mixtures (in molar ratio of 2:1 and 1:2) as well as pure MgO and NiO were conducted in eutectic mixture of CaCl<sub>2</sub>-NaCl electrolyte at temperatures between 600 °C – 900 °C. It was observed that reduction of pure NiO and NiO-rich oxide mixture yield target compositions, i.e. Ni and MgNi<sub>2</sub>, successfully at applied potential of 3.2 V. However, pure MgO and MgO-rich

mixture are difficult to reduce via electro-deoxidation.  $\text{Mg}_2\text{Ni}$  hydrogen storage compound was obtained only at 5.0 V, which formed together with  $\text{MgNi}_2$ .

The difficulties in reduction of  $\text{MgO}$  are attributed to many reasons. High reduction voltage of  $\text{MgO}$  puts a significant barrier for deoxidation of  $\text{MgO}$ . Low conductivity of  $\text{MgO}$  is also responsible for the difficulty in deoxidation. The study showed that these two inherent properties of  $\text{MgO}$  can be favored by increasing deoxidation temperature, while low melting point of  $\text{Mg}$  limits the temperature at which the deoxidation is carried out. It was also shown that the low oxygen permeability of  $\text{Mg}$  inferiorly affects the progress of deoxidation in  $\text{MgO}$ . Calculations point out that metallic magnesium covers the surface of  $\text{MgO}$  and probably remains there without fragmentation during deoxidation. The deoxidation of  $\text{MgO}$  is then prevented by this  $\text{Mg}$  layer as there is no direct contact between  $\text{MgO}$ /electrolyte and oxygen permeability of  $\text{Mg}$  is extremely low.

## REFERENCES

- Abdelkader A.M., Daher A., Abdelkareem A. and El-Kashif “*Preparation of Zirconium Metal by the Electrochemical Reduction of Zirconium Oxide.*” E. Metall. Mater. Trans. B 38 (2007): 35-44.
- Abdelkader A.M., Hyslop D.J.S., Cox A. and Fray D.J., J. “*Electrochemical synthesis and characterization of a NdCo<sub>5</sub> permanent magnet*” Mater. Chem. 20 (2010): 6039-6049.
- Abiko T., Park I. and Okabe T.H. “*Reduction of Titanium Oxide in Molten Salt Medium*” Proceedings of 10th World Conference on Titanium, Wiley VCH (2004): 13-18.
- Akyidiz H., Ozturk T. “*Hydrogen sorption in crystalline and amorphous Mg–Cu thin films*” J. Alloys Compd. 492 (2010): 745-750
- Alexander D.T.L., Schwandt C. and Fray D.J. “*Microstructural kinetics of phase transformations during electrochemical reduction of titanium dioxide in molten calcium chloride*” Acta Mater. 54 (2006): 2933-2944.
- Antolini E. “*Formation of Li<sub>x</sub>Ni<sub>1-x</sub>O solid solution from mixtures*” Mater. Lett. 16 (1993): 286-290.
- Ashby M.F. “*A first report on deformation-mechanism maps*” Acta. Mater. 20 (1972): 887-897.
- Assadi H. “*Phase-field modelling of electro-deoxidation in molten salt*” Modelling Simul. Mater. Sci. Eng. 14 (2006): 963-974.
- Avedesian M.M., Baker H., “*Magnesium and Magnesium Alloys*” ASM Int. Handbook, 1999.
- Bale C.W., Chartrand P., Degterov S.A., Eriksson G., Hack K., Mahfoud R. B., Melançon J., Pelton A.D. and Petersen S. “*FactSage thermochemical software and databases*” Calphad 26 (2002): 189-228.
- Barin I., Knacke O. and Kubaschewski O., “*Thermochemical Properties of Inorganic Substances*”, 2<sup>nd</sup> ed., Springer-Verlag, Berlin, 1973.
- Barnett R., Kilby K.T. and Fray D. J. “*Reduction of Tantalum Pentoxide Using Graphite and Tin-Oxide-Based Anodes via the FFC-Cambridge Process*” Metall. Mater. Trans. B 40 (2009): 150-157.

Barsoum M.W., “*Fundamentals of Ceramics*”, 1<sup>st</sup> ed., Taylor and Francis, Bristol, 2002.

Bérube V., Radtke G., Dresselhaus M. and Chen G.Z. “*Size effects on the hydrogen storage properties of nanostructured metal hydrides: A review*” Int. J. Energy Res. 31 (2007): 637-663.

Bhagat R., Jackson M., Inman D. and Dashwood R. “*The Production of Ti–Mo Alloys from Mixed Oxide Precursors via the FFC Cambridge Process*” J Electrochem. Soc. 155 (2008): E63-E69.

Chen X., Xia T., Liu X., Liu T. and Zhao W. “*Mechanism of combustion synthesis of  $Mg_2Ni$* ” J. Alloy. Comp. 426 (2006): 123-130.

Chen G. Z., Fray D. J. and Farthing T. W. “*Direct electrochemical reduction of titanium dioxide to titanium in molten calcium chloride*” Nature 407 (2000): 361-364.

Chen G.Z. and Fray D.J. “*Cathodic refining in molten salts: Removal of oxygen, sulfur and selenium from static and flowing molten copper*” J. Appl. Electrochem. 31 (2001): 155-164.

Chen G.Z. and Fray D.J. “*Voltammetric Studies of the Oxygen-Titanium Binary System in Molten Calcium Chloride*” J. Electrochem. Soc. 149 (2002): E455-E467.

Chen G.Z. and Fray D.J., “*Light Metals*”, ed. Anjier J.L., Warrandale, PA, TMS (2001): 1147-1151.

Chen G.Z. “*Solid State Electro-reduction in Liquid Salts*” ECS Trans. 16 (2009): 205-210.

Chen G.Z., Fray D.J. and Farthing T.W. “*Cathodic deoxygenation of the alpha case on titanium and alloys in molten calcium chloride*” Metall. Mater. Trans. B 32 (2001): 1041-1052.

Chen G.Z., Gordo E., Fray D.J. “*Direct electrolytic preparation of chromium powder*” Metall. Mater. Trans. B35 (2004): 223-233.

Chen P., Zhu M. “*Recent progress in hydrogen storage*” Mater. Today 11 (2008): 36-43.

Cox A. and Fray D.J., “*Production of Aluminum, Magnesium and Aluminum Magnesium Alloys by Direct Electrochemical Reduction of Their Solid Oxides*” Electrochem. Soc. Proc. 19 (2002): 745-757.

Deng Y., Wang D., Xiao W., Jin X., Hu X., Chen G.Z. “*Electrochemistry at Conductor/Insulator/Electrolyte Three-Phase Interlines: A Thin Layer Model*” J.Phys. Chem. 109 (2005): 14043-14051.

Dring K., Bhagat R., Jackson M., Dashwood R. and Inman D. “*Direct electrochemical production of Ti-10W alloys from mixed oxide preform precursors*” J. Alloys Compd. 419 (2006): 103-109.

Dring K., Dashwood R. and Inman D. “*Predominance Diagrams for Electrochemical Reduction of Titanium Oxides in Molten CaCl<sub>2</sub>*” J. Electrochem. Soc. 152 (2005): D184-D190.

Dubois C., Monty C., Philibert J. “*Influence of oxygen pressure on oxygen self-diffusion in NiO*” Solid. State Ionics 12 (1984): 75-78.

F\*A\*C\*T, Collection of Phase Diagrams, available from: <http://www.crct.polymtl.ca/fact/> (last visited on 16/02/2011)

Fenn A.J., Cooley G., Fray D.J. and Smith L. “*Exploiting the FFC Cambridge Process*” Adv. Mater. Proc. 162 (2004): 51-53.

Fray D.J. and Chen G.Z. “*Reduction of titanium and other metal oxides using electrodeoxidation*” Mater. Sci. and Tech. 20 (2004): 295-300.

Fray D.J. “*Emerging molten salt technologies for metals production*” JOM 53 (2001): 27-31.

Fray D.J., “*Aspects of technology transfer*” Metall. Mater. Trans. B 31 (2000): 1153-1162.

Gao P., Jin X.B., Wang D.H., Hu X.H. and Chen G.Z. “*A quartz sealed Ag/AgCl reference electrode for CaCl<sub>2</sub> based molten salts*” J. Electroanal. Chem. 579 (2005): 321-328.

Glowacki B.A., Yan X.Y., Fray D.J., Chen G.Z., Majoros M. and Shi Y. “*Niobium based intermetallics as a source of high-current/high magnetic field superconductors*” Physica C:Superconductivity 372-376 (2003): 1315-1320.

Gordo W., Chen G.Z., Fray D.J. “*Toward optimisation of electrolytic reduction of solid chromium oxide to chromium powder in molten chloride salts*” Electrochim. Acta 49 (2004): 2195-2208.

Haarberg. G.M., Burheim O., Fray D.J., Male S., “*Electrodeoxidation of Solid Fe<sub>2</sub>O<sub>3</sub> in Molten CaCl<sub>2</sub> to Produce Iron*” Proceedings of the 8<sup>th</sup> International Conference on Molten Slags, Fluxes and Salts (2009):152.



Harrop P.J. “*Self-diffusion in simple oxides (A bibliography)*” J.Mat.Sci. 3 (1968): 206-222.

Hembree P., Wagner JBJR “*Diffusion of Fe<sup>55</sup> IN Wustite as a function of composition at 1000 °C*” Trans. Met. Soc. AIME 245 (1969): 1547-1552.

Hidika Y., Anraku T. and Otsuka N. “*Tensile Deformation of Iron Oxides at 600–1250 °C*” Oxidation of Metals 58 (2002): 469-485.

Hillert M., Selleby M., Sundman B. “*An assessment of the Ca-Fe-O system*” Metall.Trans. A. 21 (1990): 2759-2776.

Hirota K., Okabe T. H., Saito F., Waseda Y. and Jacob K. T. “*Electrochemical deoxidation of RE–O (RE=Gd, Tb, Dy, Er) solid solutions*” J. Alloy. Comp. 282 (1999): 101-108

Hongyan M., Wang M., Wu W., J. “*Oxygen permeation behaviors and hardening effect of Titanium alloys at high temperatures*” Mater. Sci. Technol. 20 (2004): 719-723

Honig E. P., Ketelaar J. A. A. “*Electromigration and self-diffusion in ionic melts*” Trans. Faraday Soc. 62 (1966): 190-197.

Hu X. F. and Xu Q. “*Preparation of Tantalum by Electro-deoxidation in a CaCl<sub>2</sub>-NaCl melt*” Acta Metall. Sin. 42 (2006) 285-289.

Hur J.M., Seo C.S., Hong S.S., Kang D.S., Park S.W. “*Metallization of U<sub>3</sub>O<sub>8</sub> via catalytic electrochemical reduction with Li<sub>2</sub>O in LiCl molten salt*” React. Kinet. Catal. Lett. 80 (2003): 217-226.

Hyslop D. J. S., Abdelkader A. M., Cox A. and Fray D.J. “*Electrochemical synthesis of a biomedically important Co-Cr alloy*” Acta. Mat. 58 (2010): 3124-3130.

Ikeda Y., Ohmori T. “*Study on chemical synthetic method to prepare Mg<sub>2</sub>Ni hydrogen absorbing alloy*” Int. J. Hydrogen Energ. 34 (2009): 5439-5443.

İlschner B., Reppich B., Riecke E. “*High-temperature steady-state creep and atomic disorder in iron<sup>II</sup> oxide*” Discuss. Faraday Soc. 38 (1964): 243-250.

Jackson B., Jackson M., Dye D., Inman D. and Dashwood R. “*Production of NiTi via the FFC Cambridge Process*” J. Electrochem. Soc. 155 (2008): E171-E177.

Jackson B., Inman D. Jackson M., Dye D. and Dashwood R., “*NiTi Production via the FFC Cambridge Process: Refinement of Process Parameters*” J. Electrochem. Soc. 157 (2010): E36-E43.

Jeong S.M., Jung J.Y., Seo C.S., Park S.W. “*Characteristics of an electrochemical reduction of Ta<sub>2</sub>O<sub>5</sub> for the preparation of metallic tantalum in a LiCl–Li<sub>2</sub>O molten salt*” J. Alloy. Comp. 440 (2007): 210-215

Jeong S.M., Yoo H.Y., Hur J.M. and Seo C.S. “*Preparation of metallic niobium from niobium pentoxide by an indirect electrochemical reduction in a LiCl–Li<sub>2</sub>O molten salt*” J. Alloy. Comp. 452 (2008): 27-31.

Jiang K., Hu X. H., Ma M., Wang D. H., Qiu G. H., Jin X. B. and Chen G. Z. “*Perovskitization*”-Assisted Electrochemical Reduction of Solid TiO<sub>2</sub> in Molten CaCl<sub>2</sub>” Angew. Chem. Int. Edit. 45 (2006) 442-446.

Jin X. B., Gao P. Wang D. H., Hu X. H. and Chen G. Z. “*Electrochemical Preparation of Silicon and Its Alloys from Solid Oxides in Molten Calcium Chloride*” Angew. Chem. Int. Ed. 43 (2004): 733-736.

Kang X., Xu Q., Yang X. and Song Q. S. “*Electrochemical synthesis of CeNi<sub>4</sub>Cu alloy from the mixed oxides and in situ heat treatment in a eutectic LiCl–KCl melt*” Materials Chemistry 64 (2010) 2258-2260.

Kar P., Evans J.W. “*Determination of kinetic parameters by modeling of voltammograms for electrochemical reduction of titanium dioxide*” Electrochem. Com. 8 (2006): 1397-1403.

Kar P., Evans J.W. “*A shrinking core model for the electro-deoxidation of metal oxides in molten halide salts*” Electrochim. Acta. 53 (2008): 5260-5265.

Karakaya İ. and Thompson W. T. “*A Thermodynamic Study of the System MgCl<sub>2</sub>-NaCl–CaCl<sub>2</sub>*” Can. Met. Quart. 25 (1986): 307-317.

Karen P., J. “*Nonstoichiometry in oxides and its control*” Solid State Chem. 179 (2006): 3167-3183

Kassner M. E. and Prado P. M. T. “*Fundamentals of Creep in Metals and Alloys*”, Elsevier B.V., Amsterdam, 2004.

Keefe M., Moore J.M. “*Diffusion of oxygen in single crystal nickel oxide*” J. Phys. Chem. 65 (1961): 1438-1439.

Khanna A. S. “*Introduction to High Temperature Oxidation and Corrosion*”, ASM International, Ohio, 2002.

Kharton V.V., Tsipis E.V., Kolotygin V.A., Avdeev M., Viskup A.P., Waerenborgh J.C., Frade J.R. “*Mixed conductivity and stability in CaFe<sub>2</sub>O<sub>4-x</sub>*” J. Electrochem. Soc., 155 (2008): P13-P20.

Kim B. C., Lee J. H. and Kim J. J. “*Rapid rate sintering of nanocrystalline indium tin oxide ceramics: particle size effect*” Mater. Lett. 52 (2002): 114.

Kofstad P., Norby T., “*Lecture notes on Defects and Transport in Crystalline Solid*”, Univ. of Oslo, 2007.

Kofstad P. K., “*Nonstoichiometry, Diffusion and Electrical Conductivity in Binary Metal Oxides*”, JWS, New York, 1972.

Korinek S.L., Dupau F. “*Grain boundary behavior in superplastic Mg-doped alumina with yttria codoping*” Acta Metall. Mater. 42 (1994): 293-302.

Lee M, “*Ionic Conductivity Measurement in  $MgAl_2O_4$  Spinel and Solid State Galvanic Cell with  $MgAl_2O_4$  Electrolyte*”, Ph.D. Thesis, Univ. of Colorado, 2007.

Lewis T. J. and Wright A. J. “*The electrical conductivity of magnesium oxide at low temperatures*” Brit. J. Appl. Phys. D 1 (1968): 441-447.

Li Q., Liu J., Liu Y., Chou K. “*Comparative study on the controlled hydriding combustion synthesis and the microwave synthesis to prepare  $Mg_2Ni$  from micro-particles*” Int. J. Hydrogen Energ. 35 (2010) 3129-3135.

Li W., Jin X., Huang F. and Chen G. Z. “*Metal-to-Oxide Molar Volume Ratio: The Overlooked Barrier to Solid-State Electroreduction and a “Green” Bypass through Recyclable  $NH_4HCO_3$* ” Angew. Chem. Int. Ed. 49 (2010): 3203-3206.

Li G., Wang D., Chen G.Z. “*Direct Reduction of Solid  $Fe_2O_3$  in Molten  $CaCl_2$  by Potentially Green Process*” J. Mater. Sci. Technol. 25 (2009): 767-771.

Li P., Karato S. and Wang Z. “*High-temperature creep in fine-grained polycrystalline  $CaTiO_3$ , an analogue material of  $(Mg, Fe)SiO_3$  perovskite*” Phys. Earth and Plan. Inter. 95 (1996): 19-36.

Liao X., Xie H., Zhai Y. and Zhang Y. “*Preparation of  $Al_3Sc$  Intermetallic Compound by FFC Method*” J. Mater. Sci. Technol. 25 (2009): 717-720.

Lutterotti L., Matthies S. and Wenk H.R., Maud: a friendly java program for materials analysis using diffraction, Int. U. Crystallogr. Comm. Powder Diffraction Newslett. 21 (1999) 14. MAUD Version 2.072, 2008, <http://www.ing.unitn.it/luttero/maud> (last visited on 16/02/2011)

Ma M., Wang D., Hu X., Jin X. and Chen G. Z. “*A Direct Electrochemical Route from Ilmenite to Hydrogen-Storage Ferrotitanium Alloys*” Chem-Eur. J., 12 (2006): 5075-5081.

Ma M., Wang D., Wang W., Hu X., Jin X. and Chen G.Z. “*Extraction of titanium from different titania precursors by the FFC Cambridge process*” J. Alloy. Comp. 420 (2006): 37-45

Martin M. “*Diffusion in Condensed Matter: Methods, Materials, Models*”, ed. Heitjans P. and Karger J., Chapter 5, Springer, Berlin, 2004.

Masset P., Guidotti R.A. “*Thermal activated (thermal) battery technology: Part II. molten salt electrolytes*” J. Pow. Sour. 164 (2007): 397-414.

MetalYSIS®, <http://www.metalYSIS.com/> (last visited on 16/02/2011)

Mishra B., Olson D. L. “*Molten salt applications in materials processing*” J. Phys. Chem. Solids 66 (2005): 396-401.

Mitoff S. P. “*Electrical Conductivity and Thermodynamic Equilibrium in Nickel Oxide*” J. Chem. Phys., 35 (1961): 882-889.

Mohandas K.S., Fray D.J. “*Electrochemical Deoxidation of Solid Zirconium Dioxide in Molten Calcium Chloride*” Metall. Mater. Trans. B 40 (2009): 685-699.

Mohandas K.S., Fray D.J. “*FFC Cambridge process and removal of oxygen from metal-oxygen system by molten salt electrolysis:an overview*” Trans. Indian Inst. Met. 57 (2004) 579

Nagehs C.R. and Ramachandran C.S. “*Electrochemical process of titanium extraction*” Trans. Nonferrous Met. Soc. China 17 (2007) 429-433.

Nohira T., Yasuda K. and Ito Y. “*Pinpoint and bulk electrochemical reduction of insulating silicon dioxide to silicon*” Nat. Mater. 2 (2003): 397-401.

Okabe T. H., Deura T., Oishi T., Ono K. and Sadoway D. R., J. “*Electrochemical deoxidation of yttrium-oxygen solid solutions*” Alloy. Comp. 237 (1996): 150-154.

Okabe T.H., Hirota K., Kasai E., Saito F., Waseda Y. and Jacob K.T. “*Thermodynamic properties of oxygen in RE–O (RE=Gd, Tb, Dy, Er) solid solutions*” J. Alloy. Comp. 279 (1998): 184-191.

Okabe T.H., Oishi T. and Ono K., “*Preparation and characterization of extra-low-oxygen titanium*” J. Alloy. Comp. 184 (1992): 43-56.

Okabe T. H., Oishi T. and Ono K., “*Deoxidation of titanium aluminide by Ca-Al alloy under controlled aluminum activity*” Metall. Mater. Trans. B 23 (1992): 583-590

Okabe T. H., Oishi T. and Ono K. “*Electrochemical deoxidation of titanium*” Metall. Mater. Trans. B 24 (1993): 449-455.

Ono K. and Suzuki R.O. “*A new concept for producing Ti sponge: Calciothermic reduction*” JOM 54 (2002): 59-61.

Ors T., Tan S., Öztürk T. and İ. Karakaya, “Synthesis of Fe–4.6 wt% B alloy via electro-deoxidation of mixed oxides” J. Mater. Sci. 44 (2009): 3514-3519

Park J.W., Altstetter J. “*The Diffusion and Solubility of Oxygen in Solid Nickel*” Metall. Trans. A 18 (1987): 43-50.

Peng J., Jiang K., Xiao W., Wang D., Jin X. and Chen G. Z. “*Electrochemical Conversion of Oxide Precursors to Consolidated Zr and Zr–2.5Nb Tubes*” Chem. Mater. 20 (2008): 7274-7280.

Peng J., Zhu Y., Wang D., Jin X. and Chen G.Z. “*Direct and low energy electrolytic co-reduction of mixed oxides to zirconium-based multi-phase hydrogen storage alloys in molten salts*” J. Mater. Chem. 19 (2009): 2803-2809.

Peng J. J., Li G., Chen H., Wang D., Jin X. and Chen G. Z., J. Electrochem. Soc., 157, (2010) F1-F9.

Pirovano M. V. G., Hofmann A. “*Oxygen vacancies in transition metal and rare earth oxides: Current state of understanding and remaining challenges*” Sauer J., Surface Sci. Rep. 62 (2007): 219-270

Qiu G., Feng X., Liu M., Tan W. and Liu F. “*Investigation on electrochemical reduction process of Nb<sub>2</sub>O<sub>5</sub> powder in molten CaCl<sub>2</sub> with metallic cavity electrode*” Electrochim. Acta 53 (2008): 4074-4081.

Qiu G., Ma M., Wang D., Jin X., Hu X. and Chen G.Z. “*Metallic Cavity Electrodes for Investigation of Powders*” J. Electrochem. Soc. 152 (2005) E328-E336

Qiu G., Wang D., Ma M., Jin X. and Chen G.Z. “*Electrolytic synthesis of TbFe<sub>2</sub> from Tb<sub>4</sub>O<sub>7</sub> and Fe<sub>2</sub>O<sub>3</sub> powders in molten CaCl<sub>2</sub>*” J. Electroanal. Chem. 589 (2006): 139-147.

Qui G., Wang D., Jin X. and Chen G.Z. “*A direct electrochemical route from oxide precursors to the terbium–nickel intermetallic compound TbNi<sub>5</sub>*” Electrochim. Acta 51 (2006): 5785-5793.

Reilly J. and Wiswall R. “*Formation and properties of iron titanium hydride*” Inorg. Chem. 13 (1974): 218-222.

Rosa C. “Oxygen diffusion in alpha and beta titanium in the temperature range of 932° to 1142 °C” Metal. Trans. 1 (1970): 2517.

Sadoway D. R. “Inert anodes for the Hall-Héroult cell: The ultimate materials challenge” JOM 53 (2001) 34-35.

Sakamura Y., Kurata M., Inoue T. “Electrochemical Reduction of  $UO_2$  in Molten  $CaCl_2$  or  $LiCl$ ” J. Electrochem. Soc. 153 (2006): D31-D39.

Sakintuna B., Lamari-Darkim F., Hirscher M. “Metal hydride materials for solid hydrogen storage: A review” Int. J. Hydrogen Energ. 32 (2007) 1121-1140

Sanchez R. L., Gray D. J. and Chen G. Z. “Study on the reduction of highly porous  $TiO_2$  precursors and thin  $TiO_2$  layers by the FFC-Cambridge process” J. Mater. Sci. 42 (2007): 7494-7501

Schwandt C. and Fray D.J. “Determination of the kinetic pathway in the electrochemical reduction of titanium dioxide in molten calcium chloride” Electrochimica Acta 51 (2005): 66-76

Seo C.S., Jeong S.M., Park S.B., Jung J.Y., Park S.W. and Kim S.H. “Preparation of Tantalum Powder from  $Ta_2O_5$  by an Electrochemical Reduction in an  $LiCl-Li_2O$  Molten Salt System” J. Chem. Eng. Japan 39 (2006): 77-82.

Song Q., Xu Q., Kang X., Du J. and Xi Z. “Mechanistic insight of electrochemical reduction of  $Ta_2O_5$  to tantalum in a eutectic  $CaCl_2-NaCl$  molten salt” J. Alloys Compd. 490 (2010) 241-246.

Stankic S., Sterrer M., Hoffman P., Bernardi J., Diwald O., Knozinger E. “Novel Optical Surface Properties of  $Ca^{2+}$ -Doped  $MgO$  Nanocrystals” Nano Lett. 5 (2005):1889-1893.

Stringer J. “The oxidation of titanium in oxygen at high temperatures” Acta Metall. 8 (1960): 758-766.

Suarez L., Houbaert Y., Eynde X. V. and Colas R.”High temperature deformation of oxide scales” Corr. Sci. 51 (2009): 309-315.

Suzuki R. O. “Calciothermic reduction of  $TiO_2$  and in situ electrolysis of  $CaO$  in the molten  $CaCl_2$ ” J. Phys. Chem. Solids 66 (2005): 461-465.

Suzuki R.O., Tatemoto K. and Kitagawa H. “Direct synthesis of the hydrogen storage V-Ti alloy powder from the oxides by calcium co-reduction” J. Alloys Compd. 385 (2004): 173–180.

- Tan S., Örs T., Aydinol M.K., Öztürk T. and Karakaya İ. “*Synthesis of FeTi from mixed oxide precursors*” J. Alloys Compd. 475 (2009): 368-372.
- Toaz M. W. and Ripling E. J. “*Flow and Fracture Characteristics of Binary Wrought Magnesium-Lithium Alloys*” J. of Metals (1956): 936.
- Tripathy P.K., Gauthier M., Fray D.J. “*Electrochemical Deoxidation of Titanium Foam in Molten Calcium Chloride*” Metall. Mater. Trans. B 38 (2007): 893-900.
- Varin R.A. and Czujko T. “*Overview of processing of nanocrystalline hydrogen storage intermetallics by mechanical alloying/milling*” Mater. Manuf. Process 17 (2002): 129-156.
- Wang C. C., Akbar S. A., Chen W., Patton V. D. “*Review Electrical properties of high-temperature oxides, borides, carbides, and nitrides*” J. Mat. Sci. 30 (1995): 1627-1641
- Wang D., Jin X., Chen G. Z., “*Solid state reactions: an electrochemical approach in molten salts*” Annu. Rep. Prog. Chem. Sect. C 104 (2008): 189-234.
- Wang D., Qiu G., Jin X., Hu X. and Chen G. Z. “*Electrochemical Metallization of Solid Terbium Oxide*” Angew. Chem. Int. Ed. 45 (2006): 2384-2388.
- Wang S.L., Li Y. “*Reaction mechanism of direct electro-reduction of titanium dioxide in molten calcium chloride*” J. Electroanal. Chem. 571 (2004): 37-42
- Wang S.L., Xue Y., Sun H. “*Electrochemical study on the electrodeoxidation of Nb<sub>2</sub>O<sub>5</sub> in equimolar CaCl<sub>2</sub> and NaCl melt*” J. Electronal. Chem. 595 (2006): 109-114.
- Ward R.G. and Hoar T.P. “*The Electrolytic removal of oxygen, sulphur, selenium and tellurium from molten copper,*” J. Inst Met., 90 (1961) 6-12.
- Wasz M. L., Brotzen F. R., McLellan R. B., Griffin, A. J. “*Effect of oxygen and hydrogen on mechanical properties of commercial purity titanium*” Inter. Mat. Rev. 41 (1996): 1-12.
- Wood A.J.M., Copcutt R.C., Chen G.Z. and Fray D.J. “*Electrochemical Fabrication of Nickel Manganese Gallium Alloy Powder*” Adv. Eng. Mat. 5 (2003): 650-653.
- Wu T., Jin X., Xiao W., Hu X., Wang D. and Chen G. Z. “*Thin Pellets: Fast Electrochemical Preparation of Capacitor Tantalum Powders*” Chem. Mater. 19 (2007): 153-160.

Wu T., Xiao W., Jin X., Liu C., Wang D. and Chen G. Z. “Computer-aided control of electrolysis of solid  $Nb_2O_5$  in molten  $CaCl_2$ ” *Phys. Chem. Chem. Phys.* 10 (2008): 1809-1818.

Xiao W., Jin X., Deng Y., Wang D., Hu X. and Chen G. Z. “Three-Phase Interlines Electrochemically Driven into Insulator Compounds: A Penetration Model and Its Verification by Electroreduction of Solid  $AgCl$ ” *Chem. Eur. J.* 13 (2007): 604-612.

Xiao W., Jin X., Deng Y., Wang D., Hu X. and Chen G. Z. “Electrochemically Driven Three-Phase Interlines into Insulator Compounds: Electroreduction of Solid  $SiO_2$  in Molten  $CaCl_2$ ” *Chem. Phys. Chem.* 7 (2006) 1750-1758.

Xie H., Zhang H., Zhai Y., Wang J. and Li C. “Al Preparation from Solid  $Al_2O_3$  by Direct Electrochemical Deoxidation in Molten  $CaCl_2$ - $NaCl$  at  $550^\circ C$ ” *J. Mater. Sci. Technol.* 25 (2009): 459-461.

Xu Q., Deng L., Wu Y. and Ma T. “A study of cathode improvement for electro-deoxidation of  $Nb_2O_5$  in a eutectic  $CaCl_2$ - $NaCl$  melt at  $1073\text{ K}$ ” *J. Alloy. Comp.* 396 (2005): 288-294

Yan X. Y. and Fray D. J. “Electrochemical studies on reduction of solid  $Nb_2O_5$  in molten  $CaCl_2$ - $NaCl$  eutectic. I. Factors affecting electrodeoxidation of solid  $Nb_2O_5$  to niobium” *J. Electrochem. Soc.* 152 (2005): D12-D21.

Yan X. Y. and Fray D. J. “Electrochemical studies on reduction of solid  $Nb_2O_5$  in molten  $CaCl_2$ - $NaCl$  eutectic. II. Cathodic processes in electrodeoxidation of solid  $Nb_2O_5$ ” *J. Electrochem. Soc.* 152 (2005): E308-E318.

Yan X.Y. and Fray D. J. “Direct electrolytic reduction of solid alumina using molten calcium chloride-alkali chloride electrolytes” *J. Appl. Electrochem.* 39 (2009): 1349-1360.

Yan X.Y. and Fray D.J. “Electrosynthesis of  $NbTi$  and  $Nb_3Sn$  Superconductors from Oxide Precursors in  $CaCl_2$ -Based Melts” *Adv. Func. Mater.* 15 (2005): 1757-1761

Yan X.Y. and Fray D.J. “Synthesis of niobium aluminides by electro-deoxidation of oxides” *J. Alloy. Comp.* 486 (2009): 154-161.

Yan X.Y. “Chemical and Electrochemical Processing of Aluminum Dross Using Molten Salts” *Metall. Mater. Trans. B* 39 (2008): 348-363.

Yan X. Y., Pownceby M. I., Cooksey M. A. and Lanyon M. R. “Preparation of  $TiC$  powders and coatings by electrodeoxidation of solid  $TiO_2$  in molten salts” *Trans. Inst. Metal.* C 118 (2009): 23-34.



Yasuda K., Nohira T., Hagiwara R. and Ogata Y. H. “*Diagrammatic Representation of Direct Electrolytic Reduction of SiO<sub>2</sub> in Molten CaCl<sub>2</sub>*” J. Electrochem. Soc. 154 (2007): E95-E101.

Yasuda K., Nohira T., Hagiwara R., Ogata Y. “*Direct electrolytic reduction of solid SiO<sub>2</sub> in molten CaCl<sub>2</sub> for the production of solar grade silicon*” Electrochem. Acta 53 (2007): 106-110.

Yasuda K., Nohira T., Ito Y. “*Effect of electrolysis potential on reduction of solid silicon dioxide in molten CaCl<sub>2</sub>*” J Phys. Chem. Solids 66 (2005): 443-447.

Yasuda N., Wakabayashi R., Sasaki S., Okinaka N., Akiyama T. “*Self-ignition combustion synthesis of TiFe<sub>1-x</sub>Mn<sub>x</sub> hydrogen storage alloy*” Int. J. Hydrogen Energ. 34 (2009) 9122-9127.

Yong Z., Meng M., Dihua W., Kai J., Xiaohong H., Xianbo J. and Chen G.Z. “*Electrolytic reduction of mixed solid oxides in molten salts for energy efficient production of the TiNi alloy*” Chin. Sci. Bull. 51 (2006): 2535-2540.

Zaluski L., Zaluska A. and Stromolsen J.O. “*Hydrogen absorption in nanocrystalline Mg<sub>2</sub>Ni formed by mechanical alloying*” J. Alloys Compd. 217 (1995): 245-249.

Zhao X. and Ma L. “*Recent progress in hydrogen storage alloys for nickel/metal hydride secondary batteries*” Int. J. Hydrogen Energ. 34 (2009): 4788-4796.

Zhu Y., Wang D., Ma M. Hu X., Jin X and Chen G.Z. “*More affordable electrolytic LaNi<sub>5</sub>-type hydrogen storage powders*” Chem. Commun. 24 (2007): 2515-2517.

## APPENDIX A

### ELECTRODEOXIDATION SET-UP

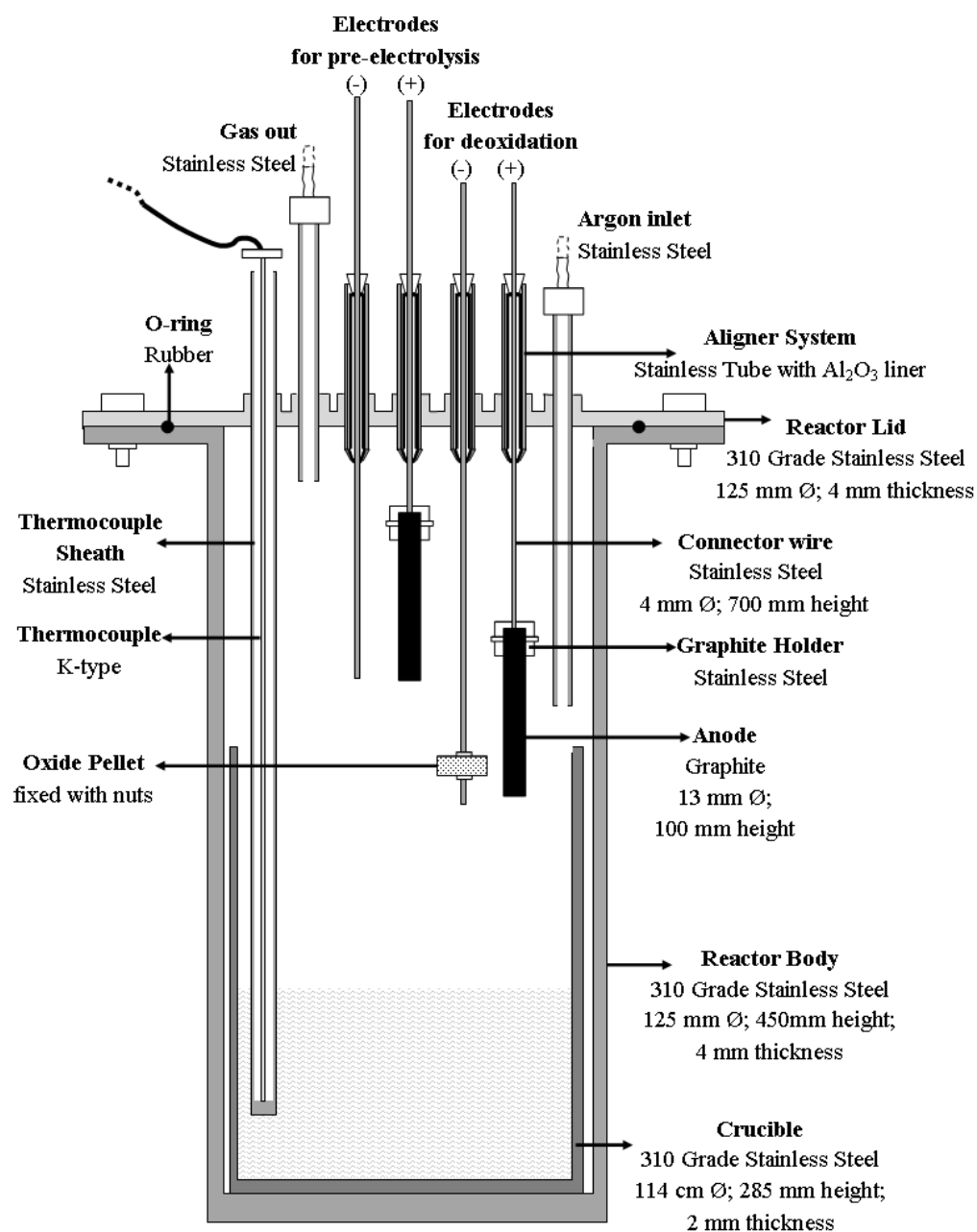


**Figure A.1** Schematic drawing of deoxidation set-up used in the study

## APPENDIX B

### PHASE DIAGRAMS

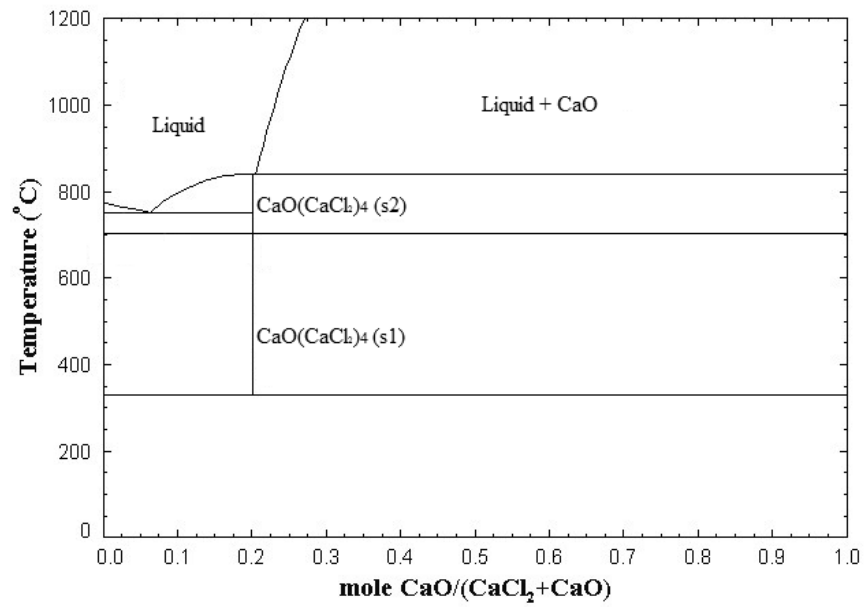


**Figure B.1**  $\text{CaCl}_2$ - $\text{CaO}$  system ( $F^*A^*C^*T$ )

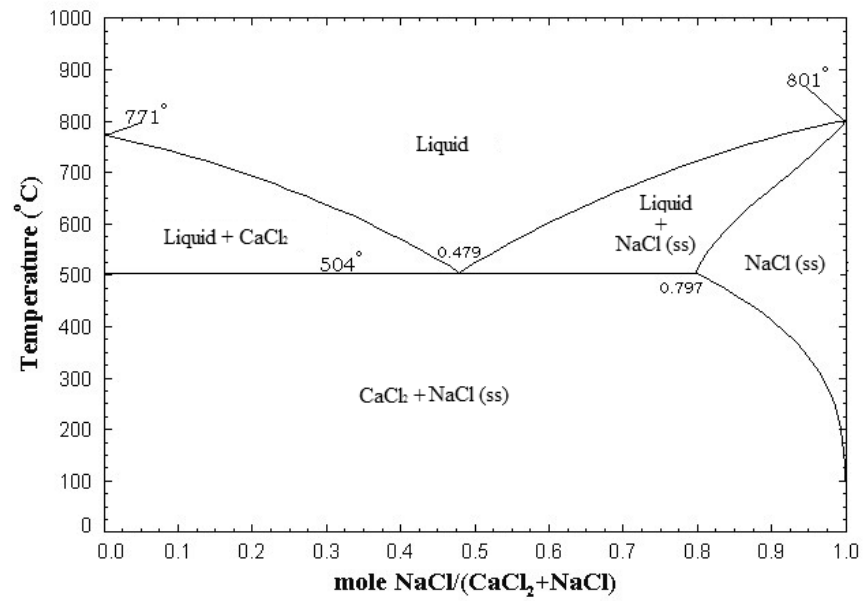


**Figure B.2**  $\text{CaCl}_2$ - $\text{NaCl}$  system ( $F^*A^*C^*T$ )

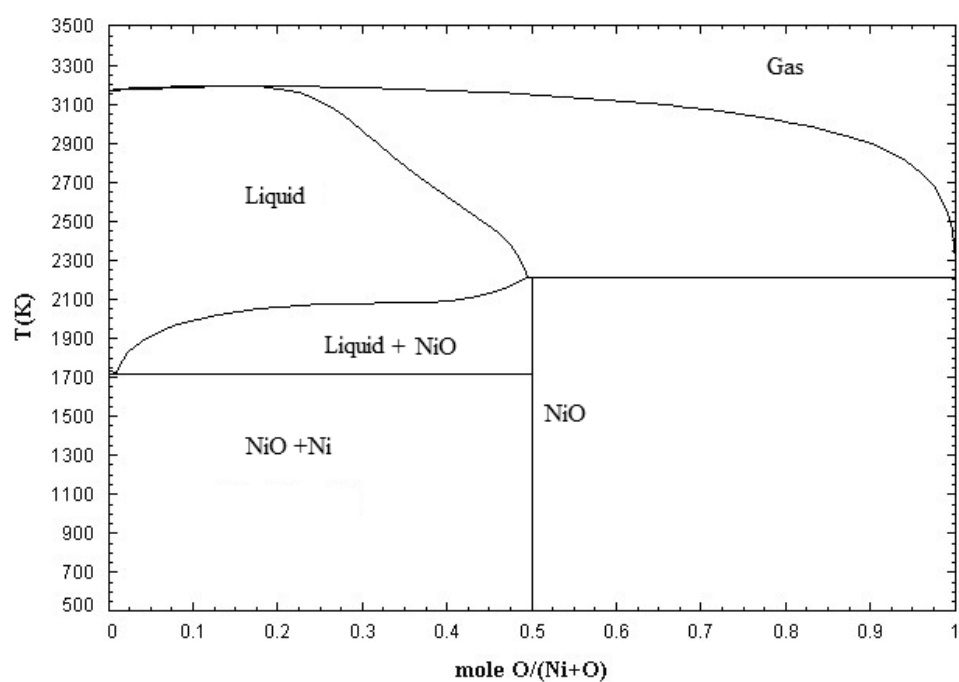


**Figure B.3** *Ni-O system ( $F^*A^*C^*T$ )*

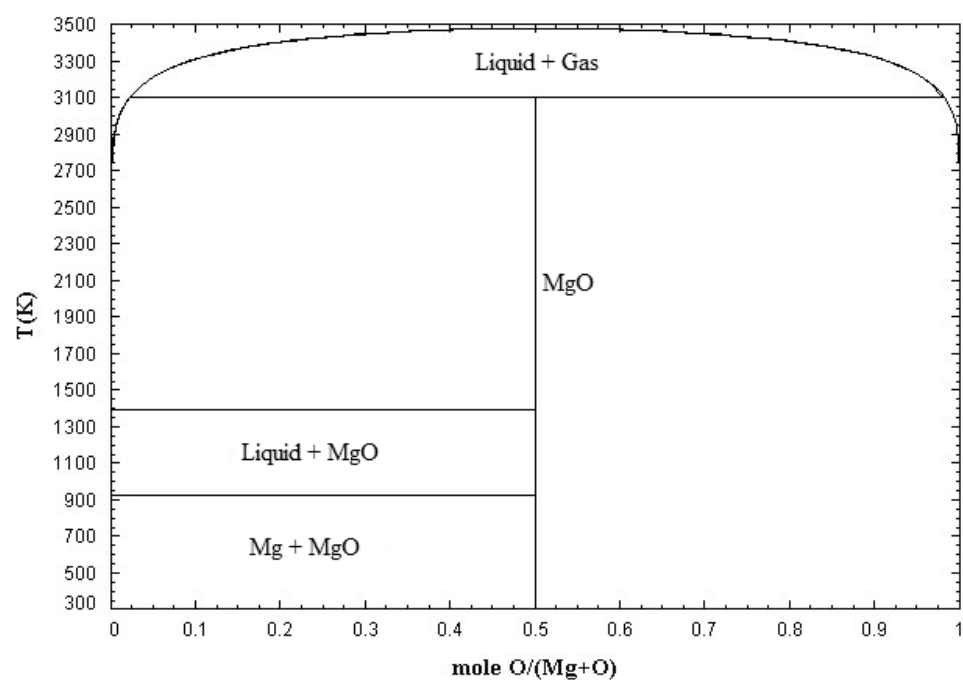


**Figure B.4** *Mg-O system ( $F^*A^*C^*T$ )*

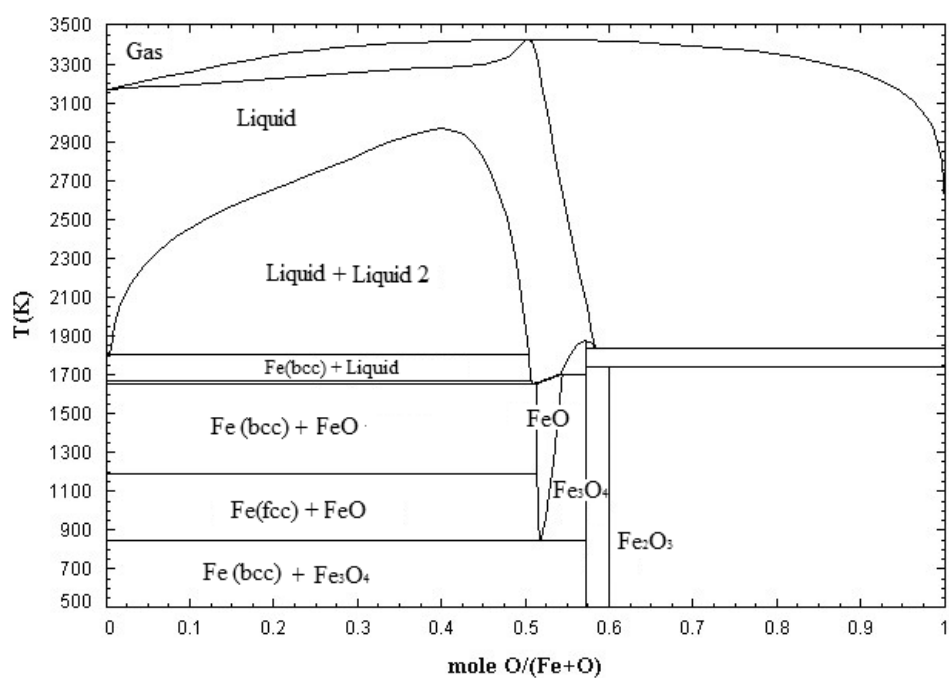


**Figure B.5** *Fe-O system ( $F^*A^*C^*T$ )*

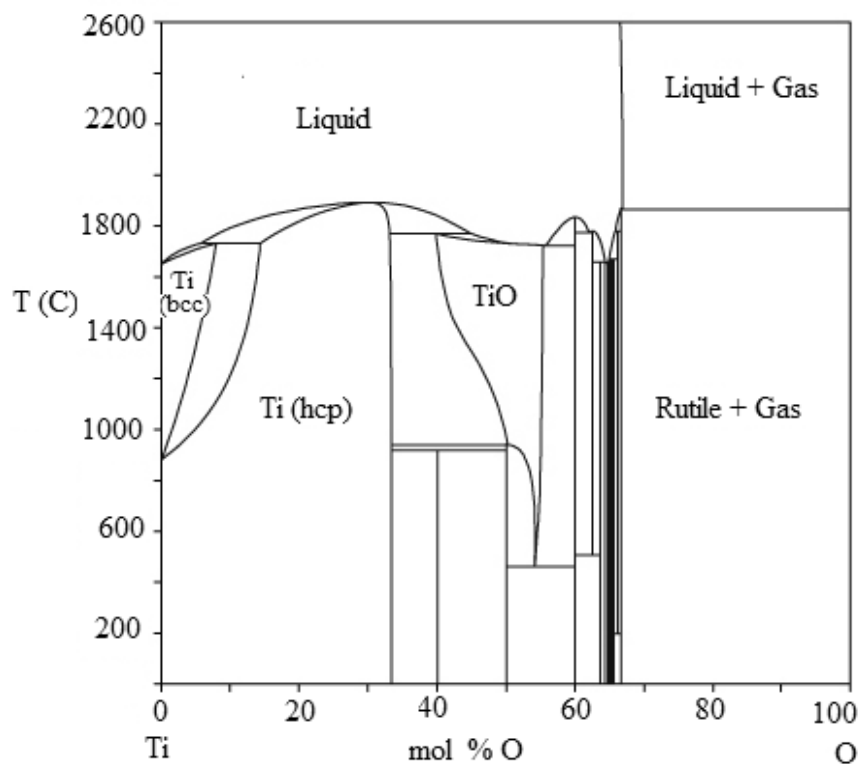


**Figure B.6** *Ti-O system ( $F^*A^*C^*T$ )*

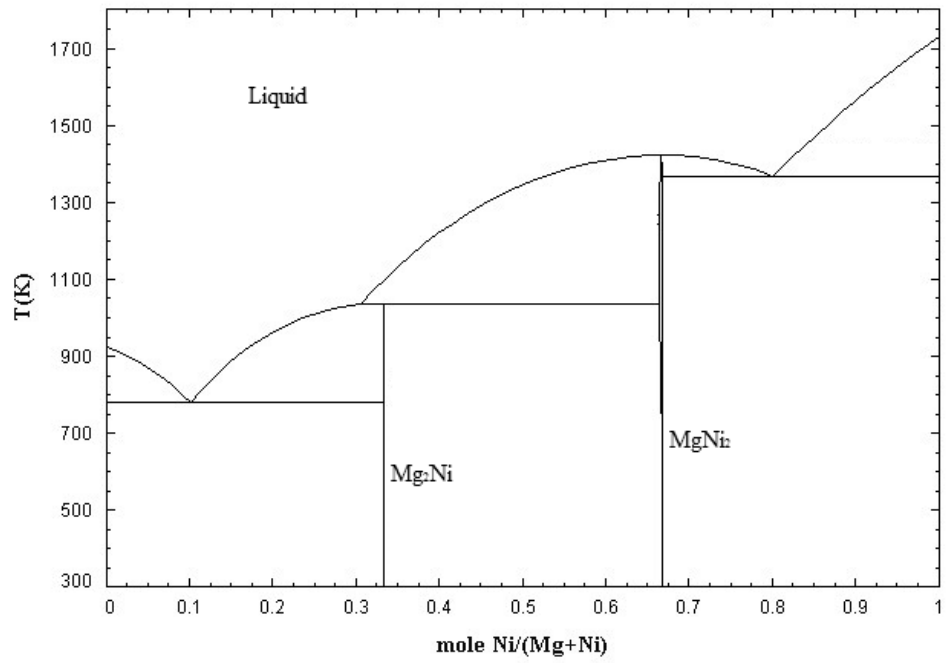


**Figure B.7** *Mg-Ni system ( $F^*A^*C^*T$ )*

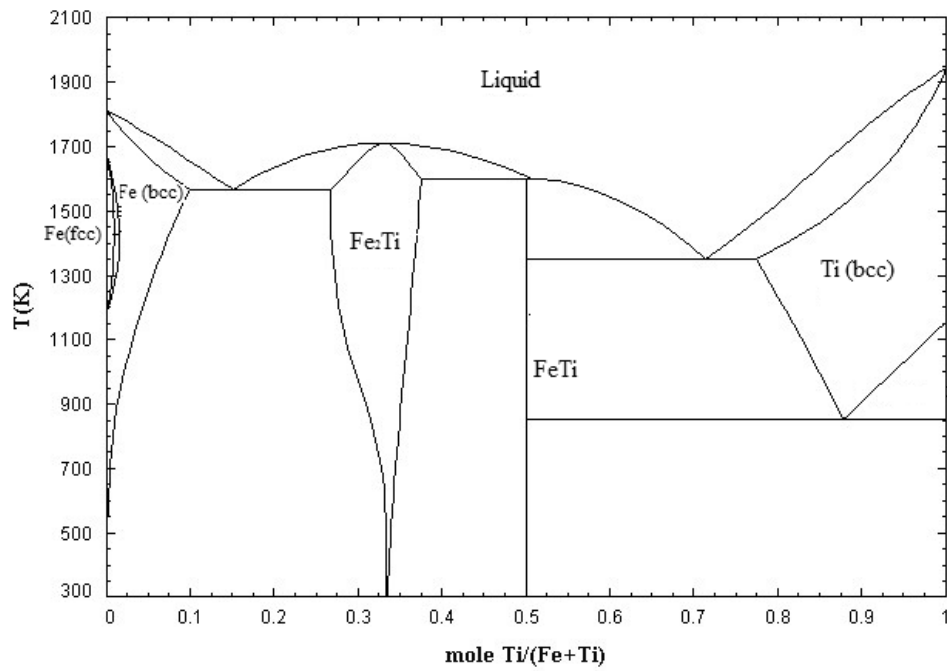


**Figure B.8** *Fe-Ti system ( $F^*A^*C^*T$ )*

## CURRICULUM VITAE

**Serdar Tan**

06/19/1977, Ankara



### **Education :**

- Ph.D.** Middle East Technical University (METU),  
Metallurgical & Materials Engineering, February 2011, CGPA : 3.43 /4.00
- M.S.** Middle East Technical University (METU),  
Metallurgical & Materials Engineering, June 2003, CGPA : 3.57 /4.00  
Thesis: Optimization of Macrostructure in Aluminium Foams
- B.S.** Middle East Technical University (METU),  
Metallurgical & Materials Engineering, June 2000, CGPA : 3.03 /4.00

### **Work Experience :**

- 2010-2011** Visiting Researcher,  
Uppsala University, Ångström Advanced Battery Centre
- 2000-2011** Research Assistant,  
METU, Department of Metallurgical & Materials Engineering

### **Journal Publications :**

1. *“Direct synthesis of Mg-Ni compounds from their oxides”*, S. Tan, K. Aydınol, T. Öztürk, İ. Karakaya, J. Alloys and Comp., 504 (2010) 134.
2. *“Synthesis of Fe-4.6 wt% B alloy via electro-deoxidation of mixed oxides”*, T. Örs, S. Tan, T. Öztürk, İ. Karakaya, J. Mater. Sci. 44 (2009) 3514.
3. *“Synthesis of FeTi from mixed oxide precursors”*, S. Tan, T. Örs, T. Öztürk, K. Aydınol, İ. Karakaya, J. Alloys and Comp., 475 (2009) 368.
4. *“A screening method for hydrogen storage alloys”*, Akyıldız H., Çakmak G., Tan S., Öztürk T., Turkish J. Eng. Env. Sci., 31 (2007) 1.

### **Conference Proceedings :**

1. ***“Scaling up the Synthesis of  $\text{Li}_2\text{FeSiO}_4$  for LIB Cathodes”***, S. Tan, A. Liivat, T. Gustafsson, J. Thomas, MRS 2010 Fall Meeting, Boston, USA.
2. ***“Inexpensive Synthesis of  $\text{Li}_2\text{FeSiO}_4$  for up-scaled LIB Cathodes”***, S. Tan, K. Kam, J. Thomas, T. Gustafsson, IMLB 2010 - The 15th International Meeting on Lithium Batteries, Montreal, Canada 2010.
3. ***“Synthesis and Electrochemical Properties of  $\text{LiCr}_{0.2}\text{Ni}_{0.4}\text{Mn}_{1.4}\text{O}_4$  Spinel as 5V Cathode Material”***, S. Tan, S. Malmgren and S. Tan, The 15<sup>th</sup> International Meeting on Lithium Batteries, Montreal, Canada 2010.
4. ***“Synthesis of Mg-Ni Compounds from Their Oxides via Electrodeoxidation”***, S. Tan, T. Ozturk, M. K. Aydinol, I. Karakaya, ECS 211<sup>th</sup> Meeting, Chicago USA, 6-10 May 2007.
5. ***“Synthesis of FeTi Hydrogen Storage Alloys for Stationary Applications”***, Serdar Tan, Taylan Örs, Hasan Akyıldız, A. Ferdi Kalcıoğlu and Tayfur Öztürk, Proceedings of 2<sup>nd</sup> International Hydrogen Energy and Congress, Istanbul Türkiye, 13-15 July 2007.
6. ***“Mg-Ni Metallerarası Bileşiklerin Elektrodoksidasyon Yöntemi ile Oksitlerinden Doğrudan Sentezi”***, Tan S., Öztürk T., Aydınol K., Karakaya İ., 13<sup>th</sup> International Metallurgy-Materials Congress, İstanbul Türkiye, 09-12 November 2006.
7. ***“Aluminyum Köpüklerin Toz Metalurjisi Yöntemi ile Üretimi ve Sürecin Modellenmesi”***, Kubilay C., Ölmez R., Tan S., Öztürk T. , 12<sup>th</sup> International Metallurgy-Materials Congress, İstanbul Türkiye, 28 September- 02 October 2005.
8. ***“A Rapid Method to Assess Hydrogen Storage Potentials in Binary or Multi-Component Systems”***, Akyıldız H., Çakmak G., Tan S., Öztürk T., International Symposium on Metal Hydrogen Systems: Fundamentals & Applications, Poland, Cracow, 5-10 September 2004.
9. ***“Foaming of Aluminium with and without  $\text{TiO}_2$  Addition”***, Tan. S., Öztürk T., Proceedings of 3<sup>rd</sup> Balkan Metallurgy Conference, 2003, 191.

### **Memberships :**

Electrochemical Society (ECS)

International Society of Electrochemistry (ISE)

Turkish Chamber of Metallurgical Engineers

METU Alumni Association